Study of material cracking in tube compression beading (Coolant Spigots)

Gustavo Nuno Reis Ferreira

Dissertação de Mestrado

Orientador na FEUP: Prof. Dr. José Ferreira Duarte

Orientador na Empresa: Eng.º Pedro Espinheira Rio

U.PORTO
FEUP FACULDADE DE ENGENHARIA
UNIVERSIDADE DO PORTO

Mestrado Integrado em Engenharia Mecânica

2016-07-04

À minha família

Abstract

This project has been developed within the company BorgWarner (BWES) Emissions Systems Portugal, a company belonging to the automobile industry and situated in Viana do Castelo. The aim of this assignment is to provide the company with a deeper understanding of tube compression beading operation and define design guidelines that will make the manufacturing process easier and guarantee higher quality of the bead geometries, with a focus on material cracking defects. As it is not possible to detect the beginning of cracking and its propagation by visual inspection alone, cracking defects are, in fact, a serious concern. Furthermore, it is also considered a major defect because the induced stress to the bead geometry during service is difficult to predict thus the cracking propagation cannot be predicted during part lifetime neither can its influence on the performance and durability of the exhaust gas recirculation (EGR) cooler.

The work includes the following procedures: a study on the constraining effects of the weld and HAZ material on the stainless steel welded tubes formability; the effect of cold forming on material properties; analyses of the coolant spigot parts that are currently in production; experimental tests and finite element analysis in order to identify the parameters that govern the tube compression operation and understand the deformation mechanism and formability limits regarding quality defects in the bead geometry, with focus on material cracking. Based on the experimental results, a standard design that determines the bead dimension and geometry is defined according to the achieved manufacturing and material formability limits. Some improvements to the manufacturing process are also proposed, since they can lead to higher production rates and lower manufacturing defects.

In conclusion, the weld and HAZ material, despite having lower formability limits regarding the fact that they present higher Vickers micro hardness, do not present any major influence on material flow or defects regarding the tube compression beading operation. The material cracking, detected in both studied coolant spigot parts references, shows that it occurs when the formability limit of the material is almost exceeded. Therefore, to overcome this, basing the bead dimensioning on the minimum sheet bending radius theory is proposed. The experimental results showed no material cracking for specimens which respect the defined minimum bead height dimension, based on the minimum sheet bending radius theory. The numerical results revealed that a higher bead makes it possible to achieve larger bead widths without compromising the inner radius of the bead, and consequently preventing material cracking. The influence of major manufacturing parameters on bead geometry has been addressed and design guidelines have been established.

The developed design guidelines will certainly have a positive impact on the quality of the coolant spigot parts, efficiency of the design and manufacturing development process and consequently on the productivity in the coolant spigots production lines.

Estudo de fissuras no processo de compressão axial de tubo (*Coolant Spigots*)

Resumo

Este projeto foi desenvolvido na empresa BorgWarner Emissions Systems (BWES) Portugal, inserida na indústria automóvel e localizada em Viana do Castelo. O objetivo deste trabalho é fornecer à empresa uma maior compreensão sobre o processo de compressão axial de tubo e definir diretrizes de design que facilitem o processo de fabrico e garantam maior qualidade do produto, com foco nos defeitos relativos à fissuração de material. A fissuração é um defeito preocupante uma vez que pode conduzir a uma fratura inesperada do material, uma vez que a iniciação e propagação de fissuras, não é possível detetar por inspeção visual. A presença deste tipo de defeitos, na peça em estudo, revela-se também de demais importância pois os esforços induzidos durante o serviço são de difícil previsão, como resultado, não é possível prever a influência de tais fissuras sobre o desempenho e durabilidade do *cooler EGR*.

O trabalho seguiu a seguinte metodologia: estudo sobre os efeitos da soldadura e zona afetada pelo calor (HAZ) na formabilidade de tubos soldados; efeito da deformação plástica nas propriedades mecânicas do material; análise dos defeitos presentes em *coolant spigots* atualmente em produção; testes experimentais e análise numérica, a fim de identificar os parâmetros que regem o processo, o mecanismo de deformação e limites de formabilidade do processo relativos à fissuração de material. Com base nos resultados experimentais e numéricos, foram definidas directrizes de design que definem as dimensões e geometria do "bordeado" de acordo com os limites de formabilidade do material. Algumas melhorias ao processo de fabrico são propostas, uma vez que podem potenciar maior produtividade e eficiência do processo.

Em conclusão, a soldadura e HAZ, apesar de apresentarem limites de formabilidade inferiores pois apresentam valores de microdureza superior, não apresentam uma influência significativa sobre o fluxo de material ou defeitos inerentes ao processo em estudo. Em ambas as referências estudadas foram detetadas fissuras, sendo que a análise efetuada revelou que ocorrem devido à deformação plástica imposta quase transpor os limites de formabilidade do material.

A solução proposta baseia-se no dimensionamento do "bordeado" com base na teoria do raio interno mínimo referente a conformação de chapas metálicas. Os resultados experimentais mostraram que as amostras dimensionadas de acordo com o design proposto, que se baseia na imposição de uma altura mínima de bordeado, não apresentaram fissuras. Os resultados numéricos revelam que uma altura de bordeado superior permitem também alcançar diâmetros de bordeado maiores sem que seja comprometido o raio interno do "bordeado" e consequentemente uma menor probabilidade de ocorrência de fissuração do material. A influência dos parâmetros do fabrico na geometria de "bordeado" obtido foi também estabelecida.

As directrizes de design estabelecidas irão certamente ter um impacto positivo na qualidade dos *coolant spigots*, na eficiência do processo de desenvolvimento de novas referências e consequentemente aumentar a produtividade das linhas de produtivas.

Acknowledgements

I would like to take this opportunity to thank BorgWarner Portugal, and all my working colleagues who, although not being directly involved, were important to the conclusion of the thesis by welcoming and integrating me in the company and for making this journey even more pleasant.

I would especially like to thank Eng. º Pedro Espinheira Rio, for the opportunity to develop this Master's Dissertation project, for being always ready to help me and for the unconditional support provided to me through the course of the project.

I must thank my supervisor at FEUP, Prof. Dr. José Ferreira Duarte, for his support during this project from the first moment, and for his encouragement and guiding advice.

I would like to thank Eng. º Rémi Ferreira, for his readiness to respond to my needs and for sharing is knowledge.

I would also like to thank Mrs. Armanda for her help when performing the metallographic tests.

I want to thank my friends from FEUP who accompanied me during these last five years, for all the support and good moments that we have experienced during this path.

I would like to thank my girlfriend, Bé Lima, for her love and ever-present support and encouragement.

Finally, I would like to thank my family for their unwavering support through my academic path and because they are responsible for the opportunity of graduating and doing this master thesis.

Contents

List of Symbols

A	Bead height;
Al	Elongation;
BWES	BorgWarner Emissions Systems;
Cr	Chromium;
D	Bead diameter;
d	Mean length of the indentation diagonal;
D_0	Tube reference diameter:
E	Young's modulus;
EGR	Exhaust gas recirculation.
F_a	Axial force;
FEA	Finite elements analyses;
F_q	Counter force;
h	Straight length of the die;
H	Bead width;
HAZ	Heat affected zone;
H_b	Die height;
HV	Vickers microhardness;
l	Reference length of the tube;
L	Distance between the bend and the bead;
l_0	Initial unsupported height of the upper tube;
L_0	Tube reference length;
Lc	Depth of the die;
L_{gap}	Initial gap height;
l_i	Initial unsupported height of the lower tube;
L_{pe}	Distance between the edge and the bulge;
Mn	Manganese;
Mo	Molybdenum;
n	Strain hardening exponent;
Ni	Nickel.
P	Load force;
Pi	Internal pressure;
r	Anisotropy coefficient;

R	Concordance radius;
r_0	Tube reference radius;
R_c	Corner radius of the die;
r_{cd}	Fillet radius of the die;
r_d	Radius of reduction;
R_e	Fillet radius of the die;
R_m	Tensile strength;
Rmin	Minimum bending radius;
r_p	Radius of expansion;
$Rp_{0.2}$	0.2% proof strength;
$Rp_{1.0}$	1.0% proof strength;
t_0	Tube reference thickness;
α	Angle of the die/punch;
α_0	Angle of the chamfered tube ends.
ε	True deformation;
ν	Poisson's Coefficient.
σ	True stress.

List of Figures

List of Tables

1 Introduction

Automotive product development is all about efficiency, productivity and time-to-market. Therefore, it is necessary to develop tools that allow Research and Development Engineers to create a high-quality product in the shortest time and at the lowest possible cost. This means that companies have to be continuously looking for new concepts and improvements that increase efficiency and productivity.

The design phase is one of the most complex and time consuming of the overall development process. In fact, during this phase not only the design requirements have to be evaluated and taken into account but also it is essential to develop a design for manufacturing in order to ensure that the product is easy to manufacture at an economical cost and with the required quality. Design for manufacture requires a multi-disciplinary team in order to evaluate design and manufacture requirements thoroughly, and is based on two main aspects: parts standardisation and parts reduction.

Parts standardisation or geometries standardisation is one the most effective methods to increase efficiency and productivity, by reducing the design and manufacture development time, quality defects, and part lifecycle cost.

To develop a design standard or design guidelines, it is necessary a deeper understanding on part or geometry requirements (aesthetics, quality, function, etc.) and on the manufacturing process to determine the feasibility intervals and the final achievable geometries in terms of the major process parameters.

Concerning tube compression beading, there is a lack of knowledge on the major process parameters and their influence on the achievable bead geometry. Regarding the major quality defects, the available studies have been focused only on successful and unsuccessful modes of deformation not taking into account other quality defects that usually occur during manufacturing, such as dimensional or geometry asymmetries and material cracking. These defects also play an important role for tubular part manufacturers, therefore there is a need to develop design guidelines that take into account an overall assessement of the bead geometry quality. These design guidelines, as mentioned above, will permit to develop designs not only focused on design requirements but also on the manufacturing process limitations, which allows to achieve higher efficiency both in design and manufacture phase.

In this chapter both the company and the scope of this project will be contextualized being therefore easier to comprehend the real problem, the proposed solution and the adopted methodology.

1.1 Thesis motivation

The project evolved within the company BorgWarner Emissions Systems Portugal (BWES), more specifically in the Applications Engineering Department, responsible for developing new products, according to engine manufacturer’s specifications, prototypes and support

product industrialization. The Manufacturing Department also supported the development of this project, mainly during the design of new forming tools.

The theme of this thesis is **Study of Material Cracking in Tube Compression Beading Operation (Coolant Spigots)**, a tube end-forming manufacturing operation. This project was proposed by BWES Portugal, regarding the need of the company to improve the coolant spigots (part) quality and standardize the design parameters of the bead geometry applied in nearly any spigot.

That project is then, based in the continuous improvement mindset of BorgWarner and focused on increasing the efficiency and quality of the design and manufacturing operations. Being expected to achieve a higher quality in the produced parts and time savings in the design and manufacturing process development. Moreover, it is essential to ensure that the spigot parts are free of defects as it can compromise the performance and durability of the product. Even if the defects do not have a high impact in the final product, it can lead to customers' complaints as the parts are not according to quality specifications.

An overall study of other important tube end forming operations was also developed in order to get a deeper understanding in tube forming mechanics and, also because these operations are widely used at BWES shop floor.

1.2 The company

BorgWarner is a global and well known automotive components and parts supplier (Tier 1) being product leader in powertrain solutions. The mission of BorgWarner is to deliver innovative powertrain solutions that improve fuel economy, emissions and performance to contribute for "*A Clean, Energy-Efficient World*".

Nowadays, BorgWarner it is operating in 74 locations across 19 countries, including United States, Canada, Europe and Asia, with almost 30000 employees worldwide. (BorgWarner)

Figure 1 - Logo of BorgWarner.

BorgWarner, is divided in two main groups: Engine Group and Drivetrain Group. The Engine Group is responsible for the research and development of air management strategies and products, as exhaust gas recirculation systems (EGR), turbochargers and boosting systems, and cooling engine systems. The fundamental core business of Drivetrain Group its automotive transmission and power drive systems, being specialize in automated transmission components and interactive control systems for all types of torque management. (BorgWarner)

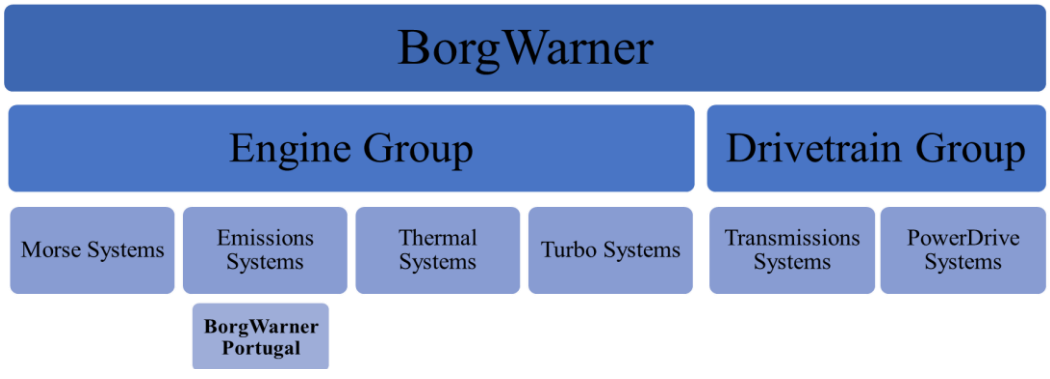

Figure 2 - BorgWarner Portugal inside BorgWarner Group.

BorgWarner Emissions Systems Portugal is part of BorgWarner Engine Group since 2010. The plant is located in Parque Empresarial de Lanheses, Viana do Castelo and was inaugurated in 2014.

BorgWarner Portugal is responsible for the development, industrialization and manufacturing of products such as:

- EGR Coolers, EGR tubes and EGR modules;
- Glow plug control modules.

Figure 3 - EGR module. (BorgWarner)

The main objective of Exhaust Gas Recirculation (EGR) system is to reduce oxides of nitrogen (NOx) emissions. This system, basically, involves recirculating a controllable proportion of the engine's exhaust, at a reduced temperature, back into the combustion chamber. Being the percentage of exhaust gas intake controlled by a valve. As a consequence of this air displacement, lower amount of oxygen in the intake mixture is available for combustion. This effective reduction in air–fuel ratio (AFR) affects exhaust emissions substantially. In addition, a mixture of exhaust gases and air increases the specific heat of intake mixture, which results in the reduction of flame temperature and peak cylinder temperature. Thus, the combination of lower oxygen quantity in the intake air and reduced flame temperature reduces the formation of NOx. However, the application of EGR presents some disadvantages such as higher hydrocarbons, carbon monoxide and particulate matter emissions. These emissions increase can be reduced by using exhaust after-treatment techniques, such as diesel oxidation catalysts (DOCs). (Hussain et al. 2012)

The main manufacturing processes used to produce the EGR parts are sheet and tube metal forming (tube bending, tube end-forming, hydroforming, etc.), soldering and brazing.

The totality of the produced parts are targeted at the automotive industry, supplying several customers as BMW, General Motors, Nissan, Jaguar Land Rover and Ford.

1.3 Thesis objectives

The aim this project is to create design guidelines which limits or eliminates the material cracking defects in the bead geometry applied on coolant spigot parts by defining the bead dimensions and tolerances, manufacturing process operations, quality and measurement control parameters and restrict other identified parameters that can lead to the occurrence of defects. The design standard apart from limiting the occurrence of defects, it is also a powerful tool that can improve the design and manufacturing development process. The technical drawing of the studied coolant spigot parts are presented in (Annex A1.1, 1.2, 1.3).

To achieve this main objective, it was defined as sub-goals the study of the influence of material properties, design and manufacturing parameters that can lead to material cracking or other identified defects.

- Raw material properties

  Identify the mechanical and dimensional properties of the welded tube (raw material) that have a direct influence on the formability limits on tube compression beading operation with focuses on the constraining effects of the weld on material mechanical properties and consequent impact on the dimensions and defects on the bead geometry;

- Design parameters

Understanding the relation between the design parameters of the bead according to the manufacturing process and establishing basic design guidelines according to material and tube compression beading operation formability limits in order to successfully achieve a bead geometry free of defects;

- Manufacturing parameters

Understanding the mechanism of deformation of tube compression beading applied to welded tubes and address the influence of the major manufacturing parameters on the formability limits of the process and final bead dimensions and geometry.

The project was developed by means of a comprehensive investigation based on bibliography, finite element modelling and experimentation analyses.

It was defined as an extra-objective, the study of the constraining effects of the tube bends in the material properties and resulting impact on the bead design (the beading operation is performed after the bending operation). This objective, as agreed with BorgWarner, will only be studied if the first proposed objectives have been successfully achieved.

1.4 Thesis layout

This thesis is organized by chapters that address different topics that are connected to the main goal of developing design guidelines for bead geometries applied to welded tubes.

Chapter 2 presents the state of the art in tube forming processes. Different topics are addressed, including the influence of the major manufacturing parameters, material properties and a review on formability limits and failure, regarding each presented tube forming process.

Chapter 3 describes the main properties related to each stainless steel grade, and reviewed the main influence of the alloying elements.

Chapter 4 presents the parts that will be in study, by describing its function and geometry and addressed the quality defects previously detected by BorgWarner. It is also reviewed the current manufacturing process, quality tests and control tools in use, and presented the production line capacity and scrap rates.

In Chapter 5 is made an analysis of the influence of the weld and HAZ material on the material mechanical properties and on bead geometry defects. It is analyzed two coolant spigot parts references, currently in production, in order to assess the occurrence of material cracking and understand why it is occurring.

Chapter 6 presents the numerical analyses approach and the developed experimental procedure. It is discussed the experimental and numerical results, and addressed a first final conclusion.

Lastly, in Chapter 7, the main conclusions regarding the work carried out during this thesis and some follow-up work are presented.

2 State of art

2.1 Tube end-forming

The term ‘end forming of tubes’ usually refers to the production of a wide variety of shapes and profiles, by uniaxial compression, such as inversions, flares, expansions, reductions, beads and noses by means of single or multiple metal forming operations (Figure 4). The different shapes are accomplished by forcing a dedicated punch (or die) into the tube end, and then retracting the punch (or die) back off after achieving the desired shape (Alves et al. 2006).

Allowing manufacturing of complex profiles by using only simple tools and small press machines.

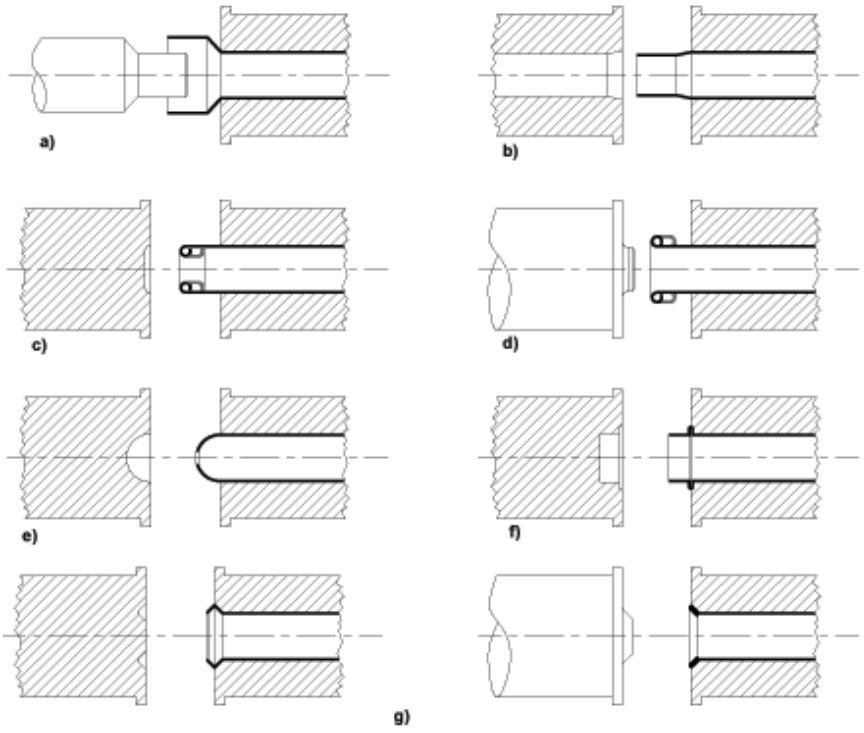

Figure 4 - Tube end forming processes: (a) expansion, (b) reduction, (c) internal inversion, (d) external inversion, (e) nosing, (f) compression beading and (g) flaring. (Alves, Medeiros, and Martins 2011)

Plastic deformation is the result of three different mechanisms in tube expansion, reduction, inversion and nosing (Schaeffer and Brito 2007):

- Bending/Unbending;
- Stretching or compression (along the circumferential direction);
- Friction.

In tube compression beading the plastic deformation and material flow is the result of local buckling, a mode of plastic instability characterized by two fundamental modes of deformation:

- Global buckling;
- Local buckling.

Global buckling takes place when a tube fails as a whole (like a column) and it is expected to occur when the tube is long and has relatively thick walls. Local buckling leads to the development of axisymmetric wrinkles or compression beads, along the tube and usually takes place when a tube has thin walls. (Alves and Martins 2012)

Tube end-forming profiles are used not only for building up applications for pneumatic, hydraulic and exhaust systems of machines, transportation vehicles and appliances but also to interconnecting individual tubular parts and tubular parts to sheets. (Almeida et al. 2006) The use of end tubes profiles to join tube to tube profiles and/or tube profiles to sheet panels are also an effective and environmentally friendly joining solution, which ensure economic and time savings, and lighter structures. Being a suitable alternative to usual joining technologies based on mechanical fixing, welding and adhesive bonding.

Although the range of application is huge and polyvalent, however, basic design rules of tube end forming using a die are mainly derived from the accumulated experience of manufacturers of tubular parts, being error procedures commonly utilized to determine the formability limits and the final achievable geometry. (Gouveia et al. 2006b)

These topics are crucial for a deeper comprehension of the mechanics in tube end forming, understanding the studying problem and to successfully organize an experimental procedure and testing plan.

2.1.1 Expansion and reduction of tubes

Expansion and reduction of thin walled tubes are the most common end forming operations, as they are simple and significantly easy to achieve even by error procedures. These shapes are accomplished by forcing a dedicated conical punch/die into the tube end, as represented in Figure 5.

The expansion punch is dedicated to an outside radius, r_p, and a required length of expansion while the reduction die is dedicated to an inside radius, r_d, and a required length of reduction. The lengths of expansion and reduction are a function of the angle of inclination, α, and the design of each tool is limited to the specific initial reference radius, r_0, of the tube. (Almeida et al. 2006)

Therefore the main process parameters that rule expansion and reduction operations of thin-walled tubes using a die are (Almeida et al. 2006):

- The ratios r_p / r_0 (for expansion), r_d / r_0 (for reduction);
- The ratio t_0 / r_0 ;
- The angle α of the conical surface of the punch/die;
- Material properties;
- Lubrication.

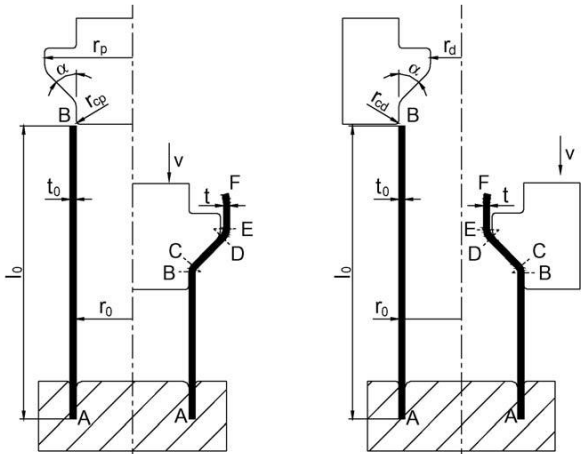

Figure 5 - Schematic representation of the expansion (a) and reduction (b) operations. (Almeida et al. 2006)

Different authors have confirmed by experimental work, on tube expansion and reduction, the existence of three different modes of deformation, by analyzing load-displacement curves related to the mentioned operations.

Tubes bending takes place at point B, where the tube first contacts the punch/die, while unbending takes place at point D, where the tube leaves contact with the punch/die. Stretching/compression develops while the tube gradually deforms over the punch or against the die along the length CD. The influence of friction predominantly occurs between points B and D although, some minor restraint, is also likely to take place at the entrance of the punch/die. (Alves et al. 2006)

On tube expansion, for large ratios of r_p/r_0 and high values of α (small lengths of expansion/reduction) formability is limited by the occurrence of local buckling, while for larger lengths of expansion restrictions are normally set by ductile damage in the regions that are highly stretched in the circumferential direction. While on tube reduction, for small values of r_d/r_0 and high values of the angle α formability is mainly limited by the development of local buckling due to the increase of the slenderness ratio, while for larger lengths of reduction restrictions are normally set by excessive thickening of the tube wall and by the occurrence of wrinkling at the conical wall. (Gouveia et al. 2006a)

As well, some studies have been carried out in order to understand the influence of the wall thickness in formability limit. A non-successful mode of deformation was obtained for the thinnest walls, on tube reduction, due to the occurrence of wrinkling at the upper region of the tube caused by high compressive values of the circumferential stress, acting at the unsupported conical wall of the tubes. As reduction induces compressive stresses at the conical section of the tube, the minimum r_d/r_0 that can be taken in a single operation is limited not only by the axial collapse of the tube but also by the occurrence of wrinkles. (Gouveia et al. 2006a)

Concluding, for small values of t_0/r_0 restrictions are generally set by excessive thickening of the tube wall and, therefore, by the occurrence of wrinkling.

In expansion, reduction and almost tube end forming operations the energy is dissipated in two different ways: one by friction at the contact interface between the tooling and the tube, and the other by the work done in deforming the tube.

As well, the influence of lubrication has been studied, and as concluded from the observation of Figure 6, a successful tube reduction can easily be replaced by a non-successful mode of deformation simply by changing the lubrication regime.

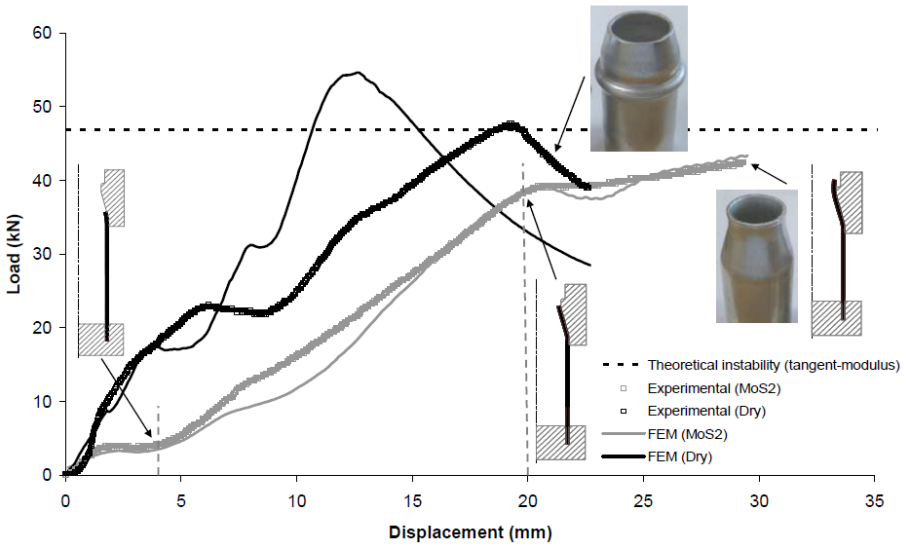

Figure 6 - Theoretical and experimental evolutions of the load-displacement curve for tube reduction. (Almeida et al. 2006)

The forming load, Pf, in steady-state conditions is approximately constant, however in the non-lubricated case the tube develops an instability before its leading edge reaches the end of the die. This is due to a much higher rate of load grow owing to the increase of friction and to a peak value of the forming load above the critical instability load. (Gouveia et al. 2006a) Showing the importance and direct influence of lubrication conditions in the formability limit.

The key of success for designing sound expanded or reduced tubular components is to change the ratios r_d/r_0 and t_0/r_0, the angle α of the conical section of the tube and the lubrication regime so that strain-paths will not approach any of the forming limits imposed by fracture, local buckling and wrinkling. (Almeida et al. 2006)

2.1.2 External and internal inversion of tubes

Invert-forming of tubes is a metal forming process in which a tube, when subjected to axial compression, will undergo inside-out inversion or vice-versa to form a double-walled tubular component that is difficult to produce by any other manufacturing process. (Rosa, Rodrigues, and Martins 2004)

The Figure 7 presents a scheme of the evolution of the inversion operation from the beginning of the operation until a certain displacement of the die.

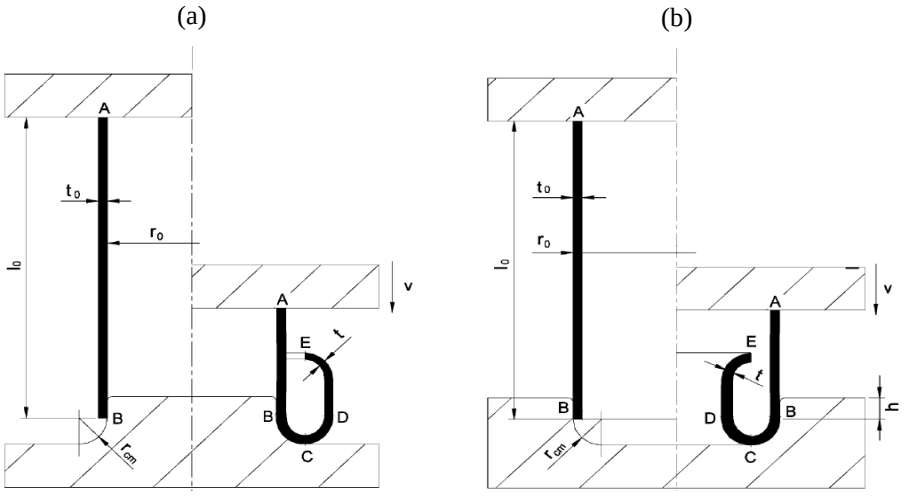

Figure 7 - Schematic representation of the invert-forming operations. (a) External inversion, (b) internal inversion. (Rosa, Rodrigues, and Martins 2004)

During the external inversion operation, bending occurs at point B, where the tubes have the first contact with the die and at point D where the unbending takes place. Stretching occurs along the circumferential direction while the tube is deformed against the die radius, from point B to D. The friction exerts influence from point B to C where there is contact between the tube and the tool. The internal inversion process runs in an analogous form to external inversion. The only difference is that the tube is compressed between points B and D, instead of being stretched. (Schaeffer and Brito 2007)

The main process parameters that govern the internal inversion of tubes using a die are (Rosa, Rodrigues, and Martins 2004):

- The ratio, r_{cd}/r_0, between the fillet radius of the die and the outer radius of the tube;
- The ratio t_0/r_0;
- Lubrication;
- The height, h, of the straight part of the die.

In the external and internal inversion process, for small values of the die radius (r_{cd}) formability is limited by the occurrence of plastic instability (local buckling), due to the increase of friction along the contact interface between the tube and the die, creating higher resistance to deformation. As a consequence, the resulting forming load is higher than the critical instability load and the tube buckles. (Gouveia et al. 2006a)

For large die radius the formability is limited by excessive thickening of the tube wall and consequently the occurrence of wrinkling due to high values of the tangential compressive stresses, acting at the unsupported curved wall of the tubes.
The development of wrinkles and the thickening of the wall at the free curved end of the tubes also increases the forming load that is necessary to apply for the material to continue to flow, which can overcome the critical instability load and causes subsequent development of local buckling at the undeformed portion of the tube. (Rosa, Rodrigues, and Martins 2004)

The range of formability is, also, strongly influenced by frictional boundary conditions. In fact, lubrication plays an important role on the overall success of the invert-forming operation. The height of the straight part of the die also influences the formability of the process since it influences the alignment between the undeformed part of the tube and the die during the initial stages of the process. (Rosa, Rodrigues, and Martins 2004). The Figure 8 shows successful and unsuccessful modes of deformation of invert formed parts.

Figure 8 - Specimens of successful and unsuccessful invert-formed tubular parts. (Alves, Medeiros, and Martins 2011)

2.1.3 Tube compression beading and nosing

Compression beading is accomplished by the compression of a tube while leaving a gap opening in-between the dies that hold the tube ends (L_{gap} refers to the initial gap height). As the upper die compresses the tube it collapses at the gap opening creating the required bead. (Gouveia et al. 2006b)

In the first stage the load increases steeply and the thickness of the tube increases uniformly until reaching the critical instability load where the plastic instability (local buckling) starts to occur. With the continuous movement of the die the material flows radially creating a well-defined bead. This behaviour is shown in Figure 10.

The dies are dedicated to a specific reference radius, r_0, of the tube and their geometry, together with the initial gap opening between them, is responsible for defining the shape and position of the beads (Figure 9.a). Nosing is also performed by axial pressing the open end of a tube with a contour die and then retracting the die back off after achieving the desired shape. Each die is dedicated to a specific nosing contour (specific radius, r_d, in case of the hemispherical shaped dies) and reference radius of the tube (Figure 9.b). (Gouveia et al. 2006b)
The most important process parameters that govern compression beading and nosing operations are (Gouveia et al. 2006b):

- The ratio between the initial gap height and the reference radius of the tube (L_{gap}/r_0) (in case of compression beading);
- The ratio between the radius of the upper die and the reference radius of the tube (r_d/r_0) (in case of tube nosing);
- The ratio between the reference radius and the thickness of the tube wall (r_0/t_0);
- Lubrication (in case of tube nosing).

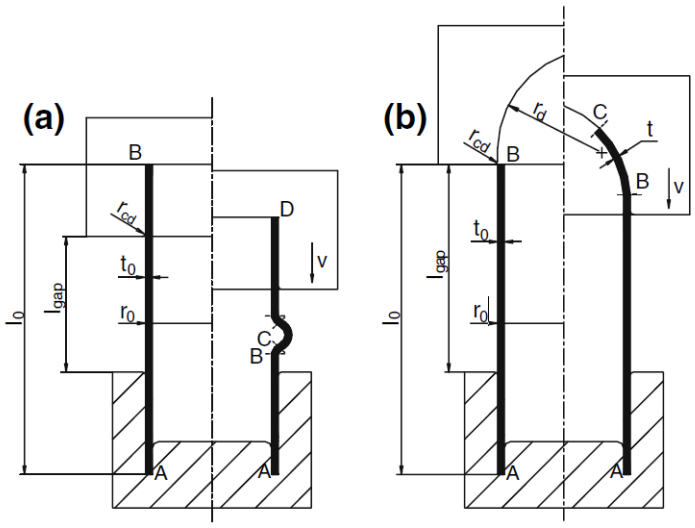

Figure 9 - Schematic representation of the compression beading (a) and nosing (b) operation. (Gouveia et al. 2006b)

In tube compression beading the influence of friction does not have considerable importance as the contact between the tube and tools does not exist in the area where material plastic deformation occurs.

Compression beading is based on a local buckling collapse mechanism, as explained in Chapter 2.1, which involves material to flow inward and outward during successive compressive instability waves. Experimental works, show that by varying the ratio between the reference radius and the thickness of the tube wall (r_0/t_0), it is possible to divide material

flow into two different groups. For high values of r_0/t_0, tube beads are formed both outward and inward, and for decreasing values of r_0/t_0, material flow gradually changes to became outward dominant and, as a consequence, tube beads start to be formed mainly outward. ((Gouveia et al. 2006b); (Alves, Silva, and Martins 2014))

The flow of material inward is not desired as it gives rise to defects (geometrical depression) on the surface of the tube placed immediately above and below the bead and to non-acceptable variation, for most of the applications, in the inner diameter of the tube. The material flow can be controlled by the utilization of an inside mandrel which can avoid geometrical depression and guarantee the dimension tolerance of the inner diameter of the tube. (Alves and Martins 2012)

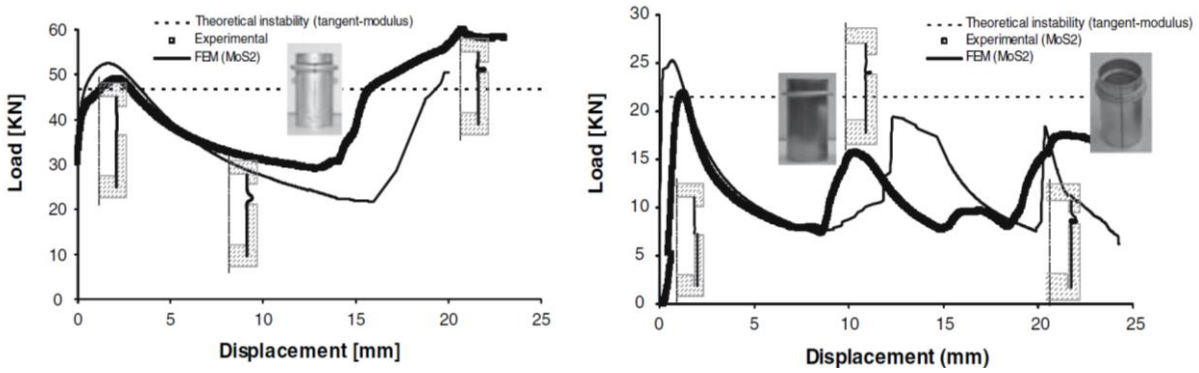

Figure 10 - Theoretical and experimental evolution of the load-displacement curve for tube compression beading. (Gouveia et al. 2006b)

Also, experimental work concluded that the number of tube beads increases with the initial gap height and decreases with the wall thickness. Consequently it was possible to define the number of tube beads for each combination of process parameters (L_{gap}/r_0 and r_0/t_0), as represented in Figure 11.

The width of the beads is also significantly influenced by the slenderness ratio, L_{gap}/r_0, and can be made larger or smaller by changing the initial gap opening between the upper and lower dies.

If the slenderness ratio, L_{gap}/r_0, is below a minimum threshold, the unsupported free length of the tube is not capable of ensuring local buckling and, therefore, the thickness of the tube increases uniformly and no compression bead is formed. (Alves and Martins 2012)

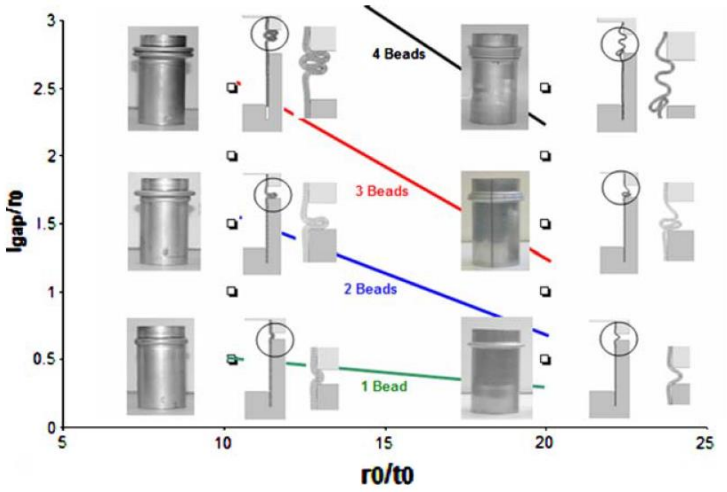

Figure 11 - Formability diagram for tube compression beading operation. (Gouveia et al. 2006b)

Experimentally two types of failure has been observed in tube compression beading. One caused by cracking along the meridional direction, as presented in Figure 12.a, and is attributed to high values of ductile damage at the equatorial plane of the specimens. The other is caused by cracking along the circumferential direction, as shown in Figure 12.b, and is attributed to meridional stresses emerging from the asymmetric propagation of compression beads whenever the initial gap opening is very large. (Tekkaya et al. 2014)

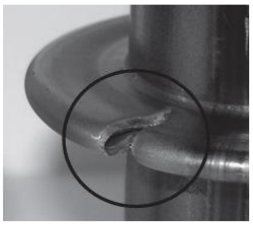

(a)

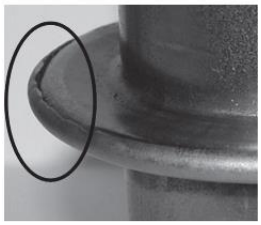

(b)

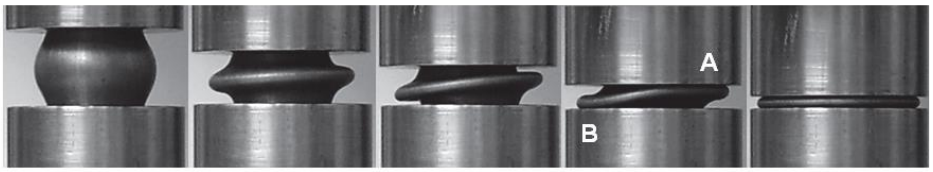

(c)

Figure 12 - (a) Failure by cracking along the meridional direction, (b) failure by cracking along the circumferential direction, (c) evolution of the compression bead. (Tekkaya et al. 2014)

In tube nosing the occurrence of an unsuccessful mode of deformation (local buckling) is found to happen when the peak value of the forming load reaches the critical instability load. Therefore, the value of the forming load must be regarded as a necessary, but not a sufficient, condition for the occurrence of local buckling during tube nosing operations. However, as during experiments some specimens grow high above the critical instability load without promoting the development of an unsuccessful mode of deformation, the initial gap height also has to play an important role in the overall success of the tube nosing operation, as it controls the amount of free space for the tube to buckle. Experimental work also demonstrates that the evolution of the load with the displacement depends on the die radius, where larger values of the ratio r_d/r_0 promote lower growing rates of the forming load, thereby, increasing the total amount of tube nosing. (Gouveia et al. 2006b)

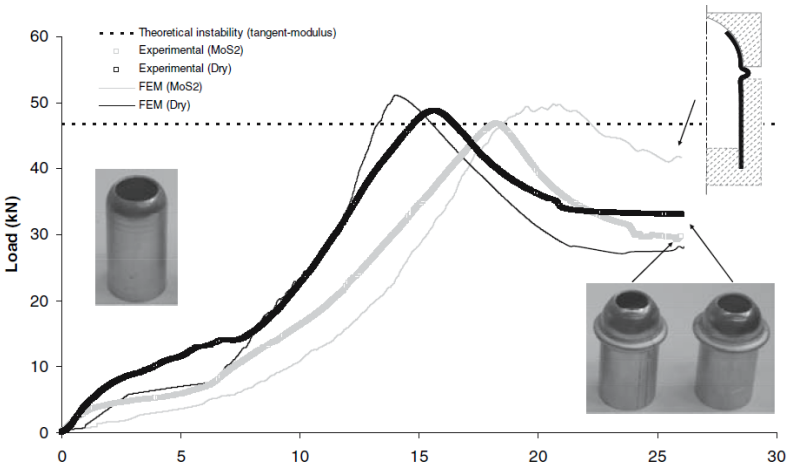

Figure 13 - Theoretical and experimental evolution of the load-displacement curve for tube nosing. (Gouveia et al. 2006b)

According to Figure 13, the influence of lubrication is depicted as the increase of friction leads to a higher forming load which reaches a peak value equal to the critical instability load, and thereby a smaller amount of nosing. Being easily concluded that good lubrication will provide lower forming loads and higher degree of formability.

Concluding, the number, dimensions and material flow of tube beads depends mainly on process parameters related to the wall thickness, reference radius and initial gap height.

As well, the formability limits in nosing is strongly influenced by the initial gap height, wall thickness, reference radius and radius of the die.

2.1.4 Tube-tube and tube-sheet joining processes

The most common solutions/technologies for end-to-end tube and tube to sheet joining makes use of mechanical fixing, welding or brazing, and structural adhesive bonding (Alves, Silva, and Martins 2014). Although these joints are very different from one another, their universe of applicability is limited by aesthetic, physical, chemical and mechanical requirements.

The utilization of mechanical fasteners usually suffers from unwanted aesthetic features, corrosion problems or functional difficulties related to the maximum effort that nuts, bolts and rivets can support safely. Although the use of welding and brazing is widespread it has similar problems to those mentioned for mechanical fasteners plus specific difficulties related to the heat-cooling cycles, to the weldability of dissimilar materials and the high temperatures required in welding, which may reduce the quality, accuracy and reliability of joined parts. (Mori et al. 2013)

In Figure 14 and 15 it is presented the most used solution for joining tubes to tubes and sheets to tubes, respectively.

Structural adhesive bonding offers engineers the possibility of joining different types of materials while improving aesthetics by avoiding rivets and bolt heads. However, adhesives require careful preparation of the surfaces where they are to be applied and may experience significant decrease in performance over time, mainly in the presence of hostile environmental conditions. (Alves, Dias, and Martins 2011)

Also, the growing need of strong, special purpose joints made of dissimilar materials in large batch sizes, the increasing environmental concerns in case of welding and adhesives, and the competitive necessity of reducing set-up and production run times make the mentioned technologies not sufficiently efficient as required by industry. (Alves and Martins 2013)

Concerning the joining of dissimilar materials a relevant example is the demand in automotive for joints of high strength steel and aluminium sheets in some current car models, to allow weight reduction. (Mori et al. 2013)

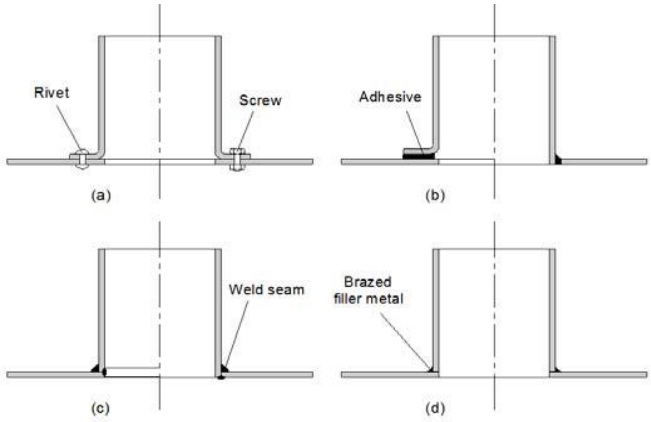

Figure 14 - Conventional tube-sheet joints obtained by means of (a) fasteners, (b) adhesives, (c) welding and (d) brazing. (Alves, Silva, and Martins 2015)

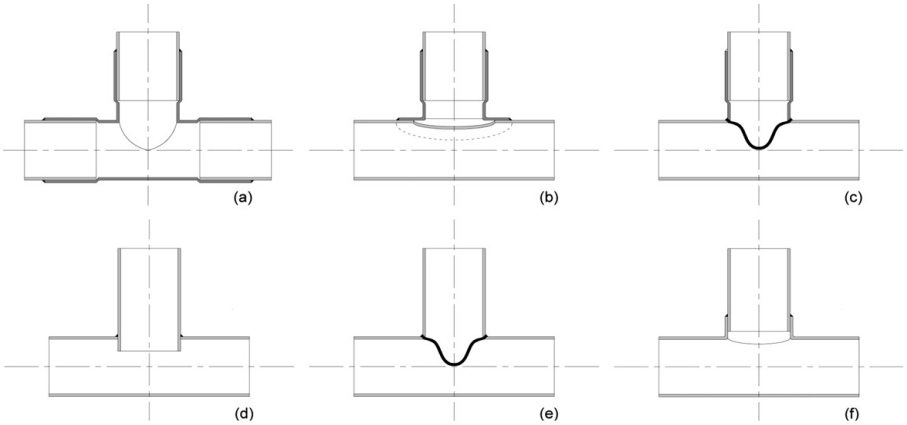

Figure 15 - Conventional tube to tube joining methods by means of (a) tee fittings, (b) saddle adapters, (c) weld-o-lets, (d) nozzle-welds, (e) nozzle-welds and (f) spin-forming. (Alves and Martins 2012)

This leads to a need of developing and evaluating innovative technologies for mass joining of sheet panels to tubes and tubes to tubes that can simultaneously cope with the growing agile manufacturing trends and sustainability issues. New progresses in tube forming and joining, can ensure the same joining quality as the conventional solutions which allows replacing it with increased flexible, eco-friendly and cost effective solutions that are based on the fundamental modes of deformation of tube end forming. ((Alves, Dias, and Martins 2011); (Alves and Martins 2013)) This technology for connecting tubes and tubes to sheets by plastic deformation, is built upon asymmetric compression beading, followed by tube end flaring in some cases, as represented in Figure 16 and 17.

The basis of this tube joining technology is the use of two opposite asymmetric compression beads, which allows connecting tubes with perpendicular or inclined axis by plastic deformation, at room temperature, following the same collapse mechanism as tube compression beading, presented in chapter 2.1.3. If the connection between tubes has to be performed at the tube end, in order to guarantee that any unsupported length is left inside the tube, the asymmetric compression beading is combined with tube end flaring/external inversion. This joining mechanism is schematically represented in Figure 16.

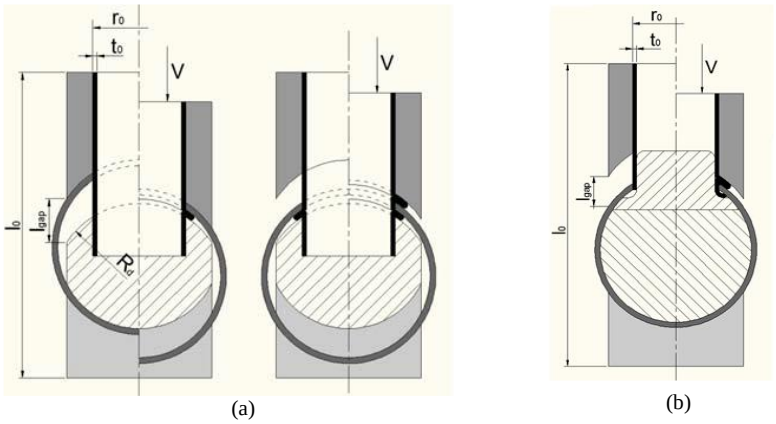

Figure 16 - Schematic representation of the process. (a) Two-stage asymmetric compression beading and (b) asymmetric compression beading followed by tube end flaring. (Alves, Silva, and Martins 2015)

By compression beading it is also possible locking both tubes by their ends, referred as end to end joining of tubes. The joining is accomplished in one stroke, by a sequence of two elementary tube end forming operations: expansion and compression beading (Alves, Silva, and Martins 2014). As schematically shown in Figure 17.

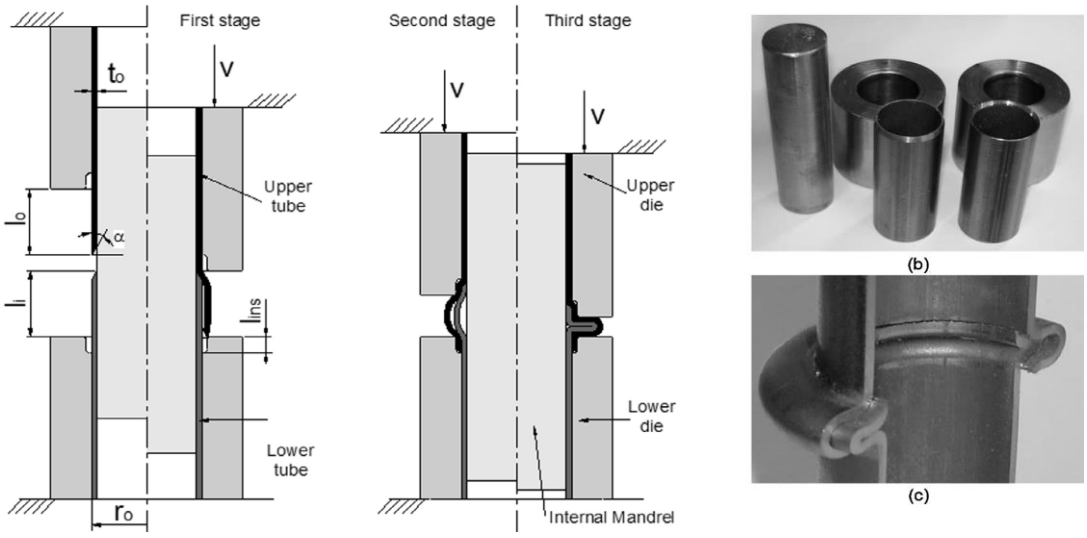

Figure 17 - End-to-end joining of tubes by plastic instability. (a) Schematic representation of the process, (b) forming tools, (c) detail of the cross section of two tubes connected by their ends.(Alves, Silva, and Martins 2014)

Initially, expansion is performed by forcing the upper tube against the chamfered end of the lower tube in order to enlarge the unsupported height, l_0, of the upper tube radially in order to get contiguous surfaces between the two tubes. During this stage of the joining process the lower tube acts like a tapered punch and the angle the chamfered edge plays a key role in the overall feasibility of the process. Once the unsupported height, l_0, of the upper tube gets into contact with the lower die, there is a change in the overall kinematics of the process. Expansion is replaced by plastic instability (local buckling) and locking is accomplished by simultaneous compression beading of the two tubes. The main process parameters are represented in Figure 17 as (Alves, Silva, and Martins 2014):

(i) The initial unsupported height, l_o, of the upper tube;

(ii) The initial unsupported height, l_i, of the lower tube;

(iii)The angle, α_0, of the chamfered tube ends.

The main process parameters of this joining process related to the second stage of it (plastic instability-local buckling) are the same and has almost the same influence as in compression beading operation. The initial gap opening ($L_{gap}= l_o+ l_i$) between the upper and lower dies controls the number and width of the compression beads, whereas the ratio l_o/l_i tubes controls the possibility of the plastic instability waves to occur simultaneously. Values of the ratio $l_o/l_i\approx1$ are recommended in order to ensure that plastic instability beads occur at the same time in both tubes. The angle of the chamfered tube edges also plays a role in the deformation mechanics, during the first stage of the joining process, as referred before.

Figure 18 shows successful and unsuccessful joining of tubes by their ends, according to different chamfered angles.

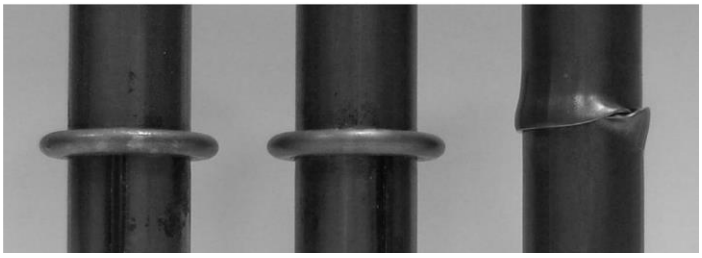

Figure 18 - End-to-end joining of tubes by plastic instability using an inclination of the chamfered tube edge equal to 25◦, 45◦and 90◦. (Alves, Silva, and Martins 2014)

The inclination angle of the chamfered edges is recommended not to take values close to 90º because of potential risk of the expansion of the upper tube being replaced by local buckling. Experimental work shows that inclination angles between 25º and 45º are the most appropriate. (Alves, Silva, and Martins 2014)

The joining process of sheet panels to tubes follows the same mechanisms as the tube to tube joining process, described above. The process allows sheets to be locked perpendicularly or inclined to the tube axis by combining axisymmetric or asymmetric compression beads, respectively, followed by tube end flaring/external inversion in a second stage.

The tools system is exactly the same as used during the tube compression beading and external inversion operation presented on chapters 2.1.3 and 2.1.2, respectively. The overall process is schematically presented in Figure 19.

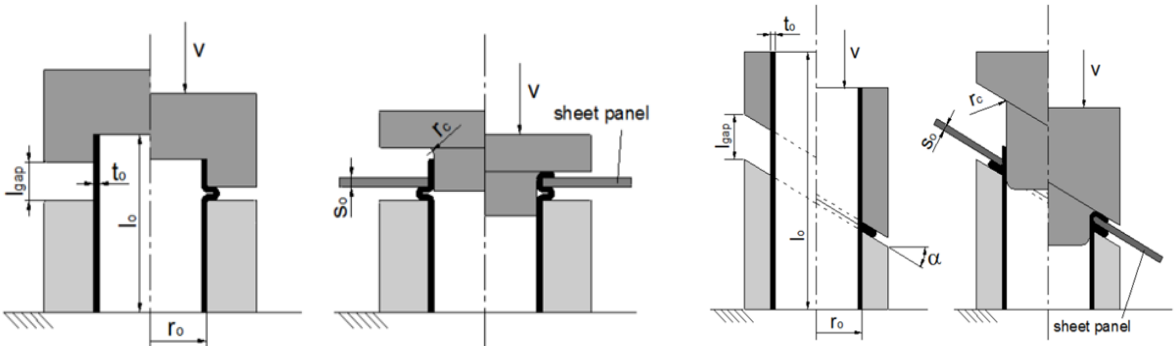

Figure 19 - Schematic representation of the joining process of sheet panels to tubes. (a) Sheets fixed perpendicular to the tube axis, (b) sheets fixed inclined to the tube axis. (Alves, Dias, and Martins 2011)

Obviously, the process parameters and their influence, in the overall process, are the same as in compression beading and external inversion operation, respectively. In case the sheet is inclined to the tube axis, there is another parameter involved which is the angle, α, of the lower and upper dies. The development of sound compression beads by asymmetric local buckling is greatly reduced as, the angle α, increases from 0º to 60º. Being the maximum practicable angle 45º, as for higher angles no beads can be found or do not have enough width. The use of internal mandrels in the beading operation is mandatory as the inward material flow becomes more significant with the increasing of the angle α. (Gonçalves 2013)

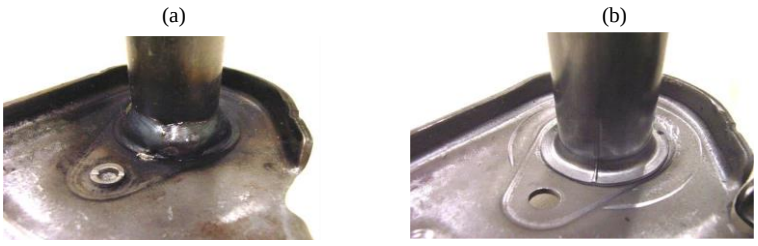

Figure 20 - (a) Joining by soldering, (b) joining by plastic deformation. (Alves, Dias, and Martins 2011)

Figure 20 shows the visually observed differences between a joining by soldering and plastic deformation, applied to a part of an automotive braking system. The presented joining processes, based on tube end forming, compared with conventional technologies show the following main advantages (Alves, Silva, and Martins 2015):

- Flexible process capable of handling small, medium or large batch sizes with different geometries and high levels of repeatability in production line;
- Environmentally friendly process that allows savings in raw material and eliminates filler materials and shielding gases;

- Energy saving process that eliminates heat-cooling cycles as well as heat affected zones and residuals stresses in the regions of the sheet panels and tubes that are joined together;
- Value added process that is capable of joining dissimilar materials;
- Cost-efficient process that requires low amount of capital investment because it can be designed to operate with existing tube end forming machine-tools.

Table 1 - Summary of the main features of joining by forming and by welding. (Alves, Silva, and Martins 2015)

	Joining by forming	**Joining by welding**
Mechanism	Plastic deformation	Melting
Shape of the connections	Arbitrary geometries	Limited
Operating temperature	Ambient	Melting
Heat-affected zone	No	Yes
Shielding gases	No	Yes
Materials	Metals and polymers	Metals (similar)
Coated materials	Possible	Very difficult or impossible
Energy consumption	Less	More
Productivity	More	Less
Cost	Less	More
Environmental friendliness	More	Less

Nowadays, the presented joining technologies are able to be implemented in industry and some automotive companies have already made use of them. However, it is now emerging and the range of applications is huge, and certainly it will shortly be a common technology. In Figure 21, is presented a summary of the types of joints previously reviewed and some possible applications of this technology.

Figure 21 - Examples of possible applications of cold joining technologies based on tube end forming. (Leitão 2013)

2.2 Tube hydroforming

Tube hydroforming (THF) is one of the most popular and well-known metal forming technologies and widely used to form various tubular components it has become, during the last years, an economic and efficient alternative to various stamping processes.

Main applications of tube hydroforming can be found in the automotive and the aircraft industries in exhaust system parts, chassis parts, engine and power train components and body and safety parts. Due to this process, many companies in the automotive sector could reduce parts weight, overall costs, and the number of parts per vehicle. (Alaswad, Benyounis, and Olabi 2012)

The main advantages of THF when compared with conventional manufacturing methods are (Alaswad, Benyounis, and Olabi 2012):

- Better part quality (tighter tolerances, weight reduction through more efficient section design, improved structural strength and stiffness, and enhanced surface finish);
- Lower manufacturing costs resulting from reduced number of forming and assembly operations and lower overall tooling cost due to fewer parts.

However, THF also has some drawbacks such as low cycle time and expensive equipment since it requires secondary operations that cannot be performed by THF (bending, flaring, etc.) and more developed and complex tools (presses/clamping devices, pressure systems, hydraulic cylinders and punches/dies).

The forming shapes in tube hydroforming, are basically achieved by the application of internal pressure (high pressure liquid) and two axial forces (plungers), acting simultaneously to improve the material forming capabilities. The internal pressure can also be applied, in some cases, by an elastomer (rubber or polyurethane), or a soft metal (lead). For some basic shapes, the tube can be formed by the increasing internal pressure only, without feeding material into the expansion zone. However, the axial forces acting on the tube ends must exceed the sealing limit force, in order to avoid leakage. (Ahmetoglu and Altan 2000) The process sequence of the THF process is shown in Figure 22.

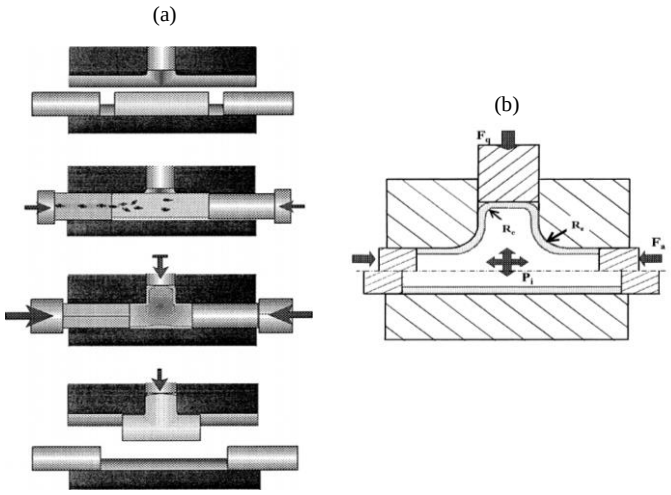

Figure 22 - (a) Tube hydroforming process, (b) elements of a typical THF process: (Fa) axial force, (Fq) counter force, (Pi) internal pressure, (Rc) corner radius, (Re) fillet radius. (Ahmetoglu and Altan 2000)

During the free forming stage, where the material flow is not restricted by the die geometry, the axial force and internal pressure increase proportionally, however at the end of the THF process, during calibration stage, the tube is forced to the die corners and small corner radius which requires large pressures, as it is achieved by stretching the material at the corner by

increasing the internal pressure only, which leads to wall thinning. At this stage, since the internal pressure is very large, it is not possible to push additional material into the deformation zone due to large frictional forces. (Ahmetoglu and Altan 2000)
The graph Internal Pressure vs Axial Force during the different stages is presented in Figure 23.

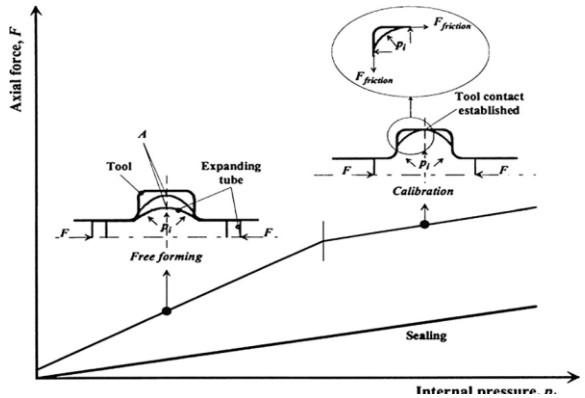

Figure 23 - Stages of tube hydroforming. (Alaswad, Benyounis, and Olabi 2012)

The material properties, the die and tube geometry, process parameters (internal pressure, axial force) and friction play an important role in the success of THF process and they have to be addressed during the process development stage.

Material properties such as material composition, weld type, yield strength, ultimate tensile strength, percent elongation, anisotropy and dimensions (diameter, thickness, shape) of the tube must be determined based on the final part requirements and closely monitored during the manufacturing process.

The basic required characteristics of tubular materials for quality and easier THF applications are(Ahmetoglu and Altan 2000):

- High and uniform elongation;
- High strain-hardening exponent;
- Low anisotropy;
- Close mechanical and surface properties of weld line to the base material;
- Good surface quality;
- Close dimensional tolerances (thickness, diameter and shape);
- Tube edges perpendicular to the longitudinal axis.

The strain hardening exponent (*n*) and anisotropy coefficient (*r*) play an important role in the forming limits, as demonstrated in various studies. Increasing the strain hardening exponent leads to a uniform thickness variation along the tube wall, which resulted in a decrease of corner thinning during expansion of a circular tube. It also decreases the required internal pressure to form a certain bulge height, which permits to achieve a higher critical expansion limit. Regarding anisotropy coefficients, the longitudinal coefficient is reported to have a significant effect on thinning ratio and the critical expansion limit, while anisotropy in hoop direction affects the internal pressure requirement. (Alaswad, Benyounis, and Olabi 2012) These conclusions can be notice from Figure 24.

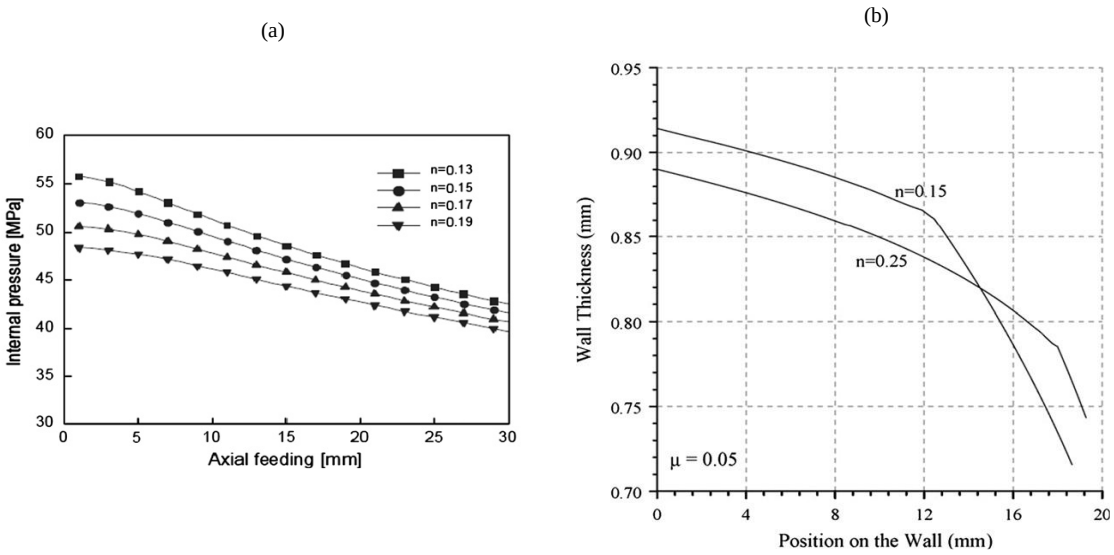

Figure 24 - Effect of the strain hardening coefficient on (a) busting pressure, and (b) wall thickness. (Alaswad, Benyounis, and Olabi 2012)

Concluding, higher values of strain-hardening and anisotropy coefficients favor a larger critical expansion limit (small radii, higher bulge) due to a more uniform distribution of strains, lower corner thinning ratio, internal pressures and axial forces.

The geometry of the tube and die also have an important influence on THF process success. The starting tube geometry for hydroforming may be straight or it may have a pre-bent/formed shape depending on the complexity of the final product to be manufactured. The parts that require excessively tight bends no wrinkles and buckles can be tolerated in the bend region, as these defects could limit the formability of the tube during the THF process. As well, the wall thinning at the outside of the bend and ovality must be kept to minimum and surface marks and scratches must be avoided. (Ahmetoglu and Altan 2000) Another important factor is the position of the weld line due to the inhomogeneous properties of the weld bead and heat affected zone. Therefore, it has to be taken into account during the process development being necessary defining the positioning where the constraining effects are the lower in order to guarantee a minimum effect in the formability limit.

Regarding the tool design and geometrical parameters in the formability limits/bulge height, the most influential is the distance between the edge and the bulge (L_{pe}). Experimental works has concluded that a shorter L_{pe} distance leads to higher bulge heights with less thinning. As well, it was noticed that lower heights resulted from increasing the die corner fillet radius (R_e) and the larger the perimeter of the initial tube is, a more uniform wall thickness distribution is achieved. (Alaswad, Benyounis, and Olabi 2012)

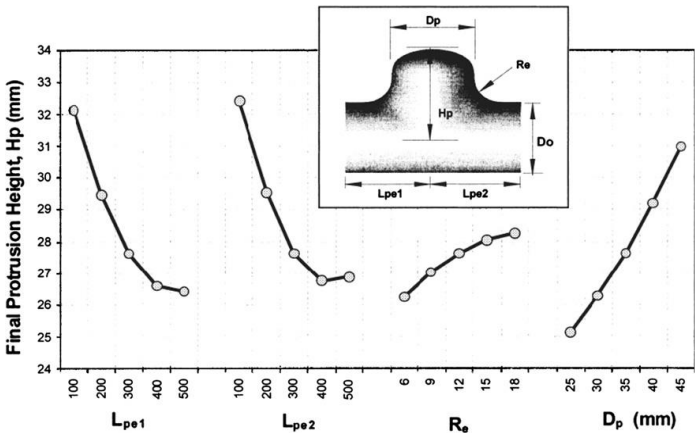

Figure 25 - Effect of geometrical factors on the bulge height. (Alaswad, Benyounis, and Olabi 2012)

From the experimental work results, the bulge height was modeled as a function of geometrical parameters and plotted for the corresponding levels of the factors, as shown in Figure 25.

As far as process parameters are concerned, in all investigated cases it has been found that the axial feed has a significant role in avoiding cracks and thinning ratio by achieving a better wall thickness uniformity for the hydroformed part. However, along with the axial feed increase, it is required a raise of the internal pressure to form the part to its desired shape. Therefore, an accurate coordination between internal pressure and axial feeding during the process time essential, since these process parameters are dependent and have to be applied synchronously. A pressure predominant path gives smoother deformation while a predominant axial load path may result in buckling or wrinkling.

3 Stainless steel

In this Chapter it is presented the main properties related to each stainless steel grade, and reviewed the main influence of the alloying elements. This review proves to be important since the parts that are being studied are manufacture from stainless steel tubes.

Iron and the most common iron alloy, steel, are from a corrosion viewpoint relatively poor materials. In spite of this there is a group of iron-base alloys, the iron-chromium (Fe-Cr) alloys, often with nickel (Ni) additions, known as stainless steels. Stainless steel is the name given to a family of corrosion and heat resistant steels containing a minimum of 10.5% chromium, which are distinguished for having excellent corrosion resistance combined with good mechanical properties and manufacturing characteristics.(*Handbook of Stainless Steel* 2013) Carbon is normally present in amounts ranging from less than 0.03% to over 1.0% in certain martensitic grades.

With chromium content above 10.5% and in the presence of air or any other oxidising environment, a transparent and tightly adherent layer of chromium-rich oxide forms spontaneously on the surface of the steel. If the film is damaged, by scratching or cutting, it will reform immediately in the presence of oxygen. Although the film is very thin (about 5×10^{-6} mm), it is both stable and non-porous, thus preventing the steel from reacting further with the atmosphere. For this reason, it is called a passive layer. The stability of this passive layer depends on the composition of the steel, its surface treatment and the corrosive nature of its environment. (Badoo and Burgan 2012)

Inside the stainless steel family there are a variety of grades results from the controlled addition of alloying elements, each offering specific attributes in respect of strength and ability to resist different environments. To achieve the optimum economic benefit from using stainless steel, it is important to select a grade of steel, which is adequate for the application without being unnecessarily highly alloyed and costly. (Badoo and Burgan 2012)

It presents engineers with many possibilities of shape, colour, form and reliability which can be used in different environments. It is this remarkably unique and universal usefulness of stainless steels the reason for its huge importance in several industries and thus explains the growth in the use of this material in the last decades. (Baddoo 2008)

3.1.1 Applications

Stainless steels are used in a wide variety of applications, but it is dominated by a few major areas:

- Catering, food and beverage
- Automotive and transportation
- Energy industry
- Architecture, building and infrastructure

Most of the structural applications occur in the chemical and power engineering industries, which account for more than a third of the market for stainless steel products. These applications include an extremely diversified range of uses, including nuclear reactor vessels, heat exchangers, components for chemical processing, furnace parts, and boilers used in fossil fuel electric power plants. ("Introduction to Stainless Steels" 1994)

3.1.2 Stainless steel grades

There are a large number of stainless steels with widely varying chemical compositions, however stainless steels have traditionally been divided into grades based on their metallurgical structure at room temperature, which gives a rough division in terms of both composition and properties. (*Handbook of Stainless Steel* 2013) In addition, a fifth grade, the precipitation-hardenable stainless steels, is based on the type of heat treatment used rather than the microstructure. ("Introduction to Stainless Steels" 1994)

The different grades are standardized by two relevant standards, EN 10088-1 and ASTM A240, and classified into the following five basic categories:

- Austenitic Stainless Steels
- Ferritic Stainless Steels
- Martensitic Stainless Steels
- Precipitation Hardened stainless Steels
- Duplex (austenitic-ferritic) Stainless Steels

The relationship, related to chemical composition, between the different stainless steel grades is as shown in Figure 26.

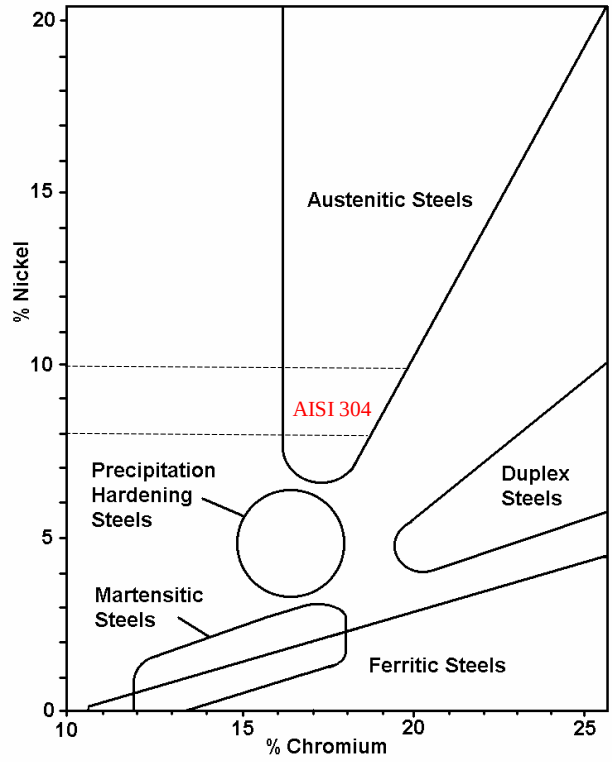

Figure 26 - Chemical composition of stainless steel grades.

The first and most important step toward successful use of a stainless steel is selection of a type that is appropriate for the application. There are a large number of standard types that differ from one another in composition, corrosion resistance, physical properties, and

mechanical properties. The selection of the optimum type for a specific application is the key to satisfactory performance at minimum total cost. This may be based on corrosion resistance, fabrication characteristics, availability, mechanical properties in specific temperature ranges and product cost. However, corrosion resistance and mechanical properties are usually the most important factors in selecting a grade for a given application. (S.D. and G. 1990)

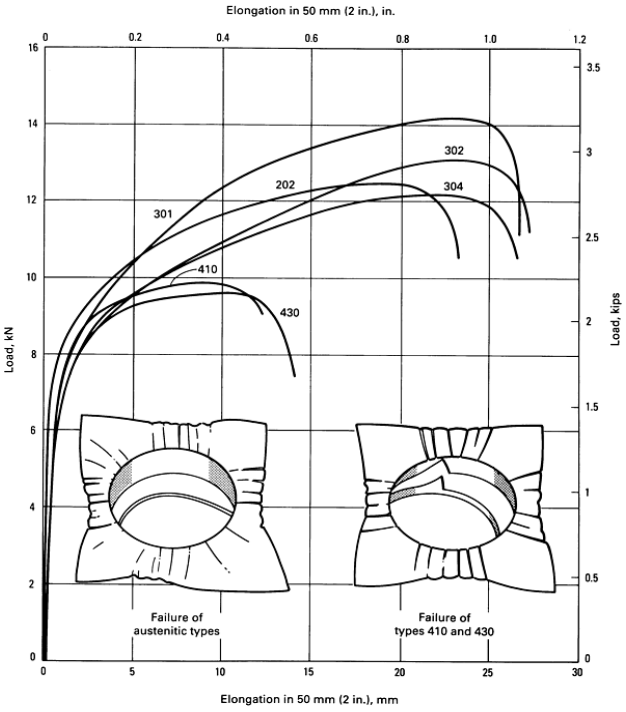

Figure 27 - Comparison of ductility of six stainless steels and of the types of failure resulting from deep drawing. (Joseph 1988)

In terms of mechanical properties, stainless steels have similar properties within each grade. Figure 27 shows stress-strain curves for six types of stainless steel: four austenitic (AISI 202, 301, 302, and 304), one martensitic (AISI 410), and one ferritic (AISI 430). The Figure 27 also shows that the type of failure in deep drawing of the austenitic types was different from that of types 410 and 430. The austenitic types broke in a fairly clean line near the punch nose radius, however types 410 and 430 broke in the sidewall, as a result of a higher strain hardening coefficient and lower elongation. (Joseph 1988)

Austenitic stainless steels

The austenitic grades, contain at least 16% chromium and 6% nickel, and are the largest and most widely used types of stainless steels, and can be divided into five sub-groups, Cr-Mn grades, Cr-Ni grades, Cr-Ni-Mo grades, high performance austenitic grades and high temperature austenitic grades. (Badoo and Burgan 2012)

The most commonly used grades, typically referred to as the standard austenitic grades, are 1.4301 (AISI 304) and 1.4401 (AISI 316), which contains about 17-18% chromium and 8-11% nickel.

Austenitic grades have good to excellent corrosion resistance (can be further enhanced by additions of molybdenum), good formability and weldability. They also have significantly high toughness over high and cryogenic temperatures, compared with standard structural grades. (Badoo and Burgan 2012) Generally, they have a relatively low proof of strength and are characterized by strong work hardening. The type AISI 301 has the lowest nickel and chromium contents of the standard austenitic types and consequently the highest tensile strength. The extremely high rate of work hardening of type 301 results in appreciable increases in tensile strength and yield strength with each increase in the amount of cold working. On the other hand, types 304, 304L have a lower rate of work hardening and are usually use for deep-drawing applications. In general, the austenitic alloys are more difficult to form as the nickel content or both the nickel and the chromium contents are lowered. (Joseph 1988)

These steels are essentially nonmagnetic in the annealed condition and can be hardened only by cold working while retaining good ductility and toughness. (S.D. and G. 1990)

Ferritic stainless steels

The chromium content of the most popular ferritic stainless steels is between 10.5 and 18%, some non-usual ferritic stainless steel can achieve 30%. Small amounts of ferrite stabilizers, such as aluminum, niobium, and titanium make part of their composition too. ("Introduction to Stainless Steels" 1994)

Ferritic stainless steels contain less nickel than austenitic grades and the atomic structure is the same as structural carbon steels (c.c.c). As a result, they are generally less ductile, less formable, less weldable and less corrosion resistant than austenitic stainless steels. (Badoo and Burgan 2012)

However, the low nickel content of the ferritic grades make them cheaper and more price stable as nickel is one of the most expensive alloying elements. (*Handbook of Stainless Steel* 2013)

Like the austenitic grades they only can be strengthened by cold working, but to a more limited degree than the austenitic grades.

Although, ferritic steels can have good ductility and formability, high-temperature strengths are relatively poor compared to the austenitic grades.(S.D. and G. 1990) They are not as corrosion resistant as austenitic stainless steels. However, the superferritic grade grades containing higher chromium (up to 30%), molybdenum (up to 4%), and nickel (up to 2%), have an excellent resistance to stress-corrosion cracking (SCC). ("Introduction to Stainless Steels" 1994)

Ferritic stainless steels can be used for structural applications, as well as such traditional applications as kitchen sinks, automotive parts, and luggage trim which require good resistance to corrosion and bright, highly polished finishes.

Duplex stainless steels

Duplex stainless steels are supplied with a microstructure of approximately equal amounts of austenite and ferrite. These alloys contain roughly 22 to 25% Cr, 5 to 7% Ni, up to 4% Mo, as well as additions of copper and nitrogen. Some of the more highly alloyed, corrosion-resistant grades are referred to as superduplex stainless steels.

Compared to the austenitic and ferritic steels, they offer the combination of relatively high strength and good corrosion performance. These grades have very good resistance to the form of corrosion known as stress corrosion cracking, compared with the austenitic grades. (*Handbook of Stainless Steel* 2013)

Although duplex stainless steels have good ductility, their higher strength results in more restricted formability, compared to the austenitic grades.

They can also be strengthened by cold working, but, like the austenitic and ferritics on which they are based, they cannot be strengthened by heat treatment.

Duplex steels should generally be used when a material has to withstand high mechanical stresses under severe corrosion conditions.

Martensitic stainless steels

Martensitic stainless steels are distinguished for having a higher carbon content (> 0.08%) and lower chromium to permit hardening by heat treatment. These contents are balanced to ensure a martensitic structure after hardening, which gives steel good hardness and high toughness. (Barralis and Maeder 2005)

The corrosion resistance of martensitic stainless steels is similar to that of ferritic grades, however their ductility is more limited than the ferritic, austenitic and duplex grades. (Badoo and Burgan 2012)

Most martensitic stainless steels have poor weldability but it can be overcome by pre-heat treatment and post weld heat treatments or by adding some nickel and reducing the carbon content to improve corrosion resistance in some media and to improve toughness.(S.D. and G. 1990) Although they are cheaper than austenitic and ferritic steels, their low corrosion resistance and poor weldability limits the range of suitable applications, being mainly used where hardness, strength, and wear resistance are required. (*Handbook of Stainless Steel* 2013)

Precipitation hardened steels

Precipitation-hardening stainless steels are chromium-nickel alloys containing precipitation-hardening elements such as copper, aluminium, or titanium. (S.D. and G. 1990)

They can be strengthened by heat treatment, like martensitic stainless steel, to very high strengths. However the strengthening mechanism is different due to the lower carbon levels. The heat treatment consists in a hyper-quenching, which produce a saturated solid solution, follow by a tempering where happens the precipitation of the intermetallic compound. (Barralis and Maeder 2005)

The strength after heat treatment of precipitation hardened steels is generally not as high as in the martensitic grades, but the tensile strength and toughness can be expected to be better.

These steels are not normally used in welded fabrication. Another advantage, is the corrosion resistance of these steels, which is generally better than the martensitic or ferritic grades and is similar to the 18% chromium, 8% nickel austenitic grades.

3.1.3 The effects of alloying elements

Chromium is the most important alloying element as it gives stainless steels their basic corrosion resistance. It also increases the resistance to oxidation at high temperatures and promotes a ferritic microstructure, as described before, the chromium content in ferritic steels can achieve 30%. Nickel and molybdenum also have influence in corrosion resistance, the first reduces the corrosion rate and increases the corrosion resistance especially in acid environments. The second, significantly increases the resistance to both uniformed and localized corrosion, promotes a ferritic microstructure and increases the mechanical strength (especially in ferritic grades). However, the main reason for the nickel addition is to promote an austenitic microstructure, and it gives to the austenitic steels their high ductility and good weldability. (*Handbook of Stainless Steel* 2013)

The Silicon and aluminum improves oxidation resistance and mechanical resistance. Carbon is a strong austenite former that also significantly increases the mechanical strength. However, it also reduces the resistance to intergranular corrosion. In ferritic steels carbon will strongly reduce both toughness and corrosion resistance, this is why the carbon content is maintaining in low levels. In the martensitic steels carbon increases hardness and strength, but decreases the toughness. Titanium is added to austenitic steels with increased carbon content in order to lower the effect of carbon in the corrosion resistance and also to improve the mechanical strength. Copper and sulphur are mainly added to improve machinability. (*Handbook of Stainless Steel* 2013)

Other alloying elements are added with very particular effects.

4 Problem statement

In this chapter, it is described the function and geometry of the parts that have been studied and addressed as a result of quality problems detected by BorgWarner. Therefore, in this Chapter, is described the current manufacturing processes, dimensional control parameters, quality tests, and presented the production line capacity and scrap rates.

The studied part is designated as coolant spigot at BorgWarner, and its function is to connect the EGR cooler, which it is integrated in the engine of the vehicle, to the engine cooling system. In Figure 28 it is presented an EGR cooler module, being identified the positioning of the coolant spigot.

Figure 28 - EGR Cooler assembly. (1) Bead related to the outer shell of the EGR cooler, (2) bead related to the outer shell of the engine cooler. (BorgWarner)

BorgWarner produces several references of coolant spigots and most of them have a similar geometry and manufacturing process. Therefore, the present study focused in the references manufactured in the production line with highest production rates and where BorgWarner detected few defects. Some coolant spigots are also purchased to external suppliers and in these the final quality (dimensional tolerances and visual inspection) is secured by suppliers and checked by BWES.

BorgWarner want to avoid all the possible defects in coolant spigots, and understand why they are occurring and how it can be avoided in order to establish an internal design standard, which defines the design and manufacturing process parameters, to guarantee the highest quality of the final product and also to speed up the design and manufacturing development process of new references.

The internal coolant spigots references produced, in the studied production line, are the following:

- E1 (⌀16x0.5 mm) (Annex A1.1)
- E2 (⌀16x0.5 mm) (Annex A1.2)
- E3 (⌀18x1 mm) (Annex A1.3)

The bead is often designed at the spigot end, as the main function of it is acting as a mechanical stopper and positioner between the coolant spigot and the cooler housing during the joining operation (brazing), and as interface with the engine refrigerator.

To the reference part E1 is applied two beads, at the tube ends of the tube and referred as “bead cooler side” (E 1.1) and “bead engine side” (E 1.2). The bead design related to the cooler side is developed by BWES and the bead applied in the engine side defined by the customer. In Figure 28 is also represented the both referred beads.

The detected defects occurred in the reference E1.1 (cooler side), which consists of cracks in the inner zone of the compression bead, presented in the metallographic section in Figure 29. These types of defects are difficult to control as it is needed a metallography test to verify its occurrence. Also due to this, cracks are considered a worrying defect as can lead to an unexpected fracture as it is not possible to detect the cracking initiation and propagation by visual inspection.

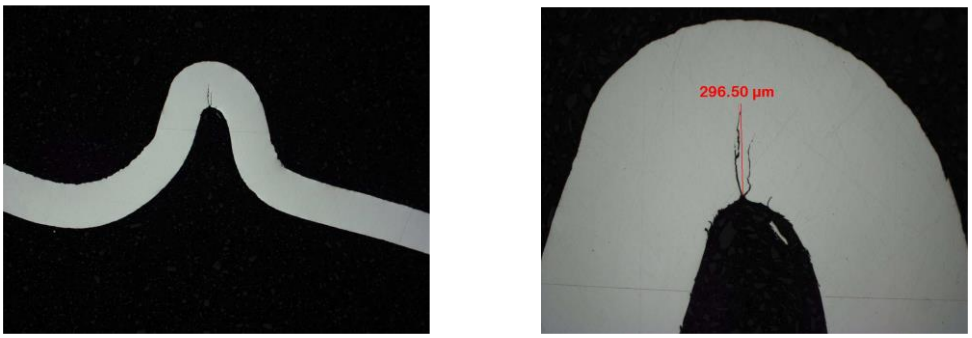

Figure 29 - Metallographic section of reference E1.

As the cracks are only appearing in the compression bead region, this work will be focused in the design and manufacturing operations parameters related to this geometry. However the influence of earlier processes, on the compression bead, will be also analysed.

Currently, the compression bead design does not follow any design rule or internal standard norm, being the engineer in charge responsible for defining the geometry and dimensions of the bead geometry during the development of the coolant spigot design. Also, the manufacturing process parameters and tools design are not internally specified, and are defined by the manufacturing engineer based on his and tools supplier’s experience. This also leads to obstacles during the prototyping stage, being difficult to accomplish the technical dimensional and geometry requirements, as for spigots which make use of the same raw material properties and reference dimensions the geometry of the bead differs.

The coolant spigots are produced from austenitic stainless steel (AISI 304/304 L) welded tubes, currently purchased to an external supplier. Should be noted that each raw material package has different chemical, physical and mechanical properties but always according to standard norms specifications.

The manufacturing process of spigots is based on two main operations which are always performed in the same sequence. The first operation consists on tube bending followed by cutting and tube end forming which can include tube expansion, nosing and compression beading operations, according to the geometry of the desired bead. During the bending operation, the initial positioning of the tube is random, consequently the weld bead line does not have a defined position. In tube end operations the tube is always positioned in the same position, as it is supported by a JIG tool.

The tools for tube end forming operations consists of a die (or punch), an internal mandrel (linked to the die/punch) and a JIG tool, and are manufactured in a horizontal press machine (Figure 30).

(a) (b) (c)

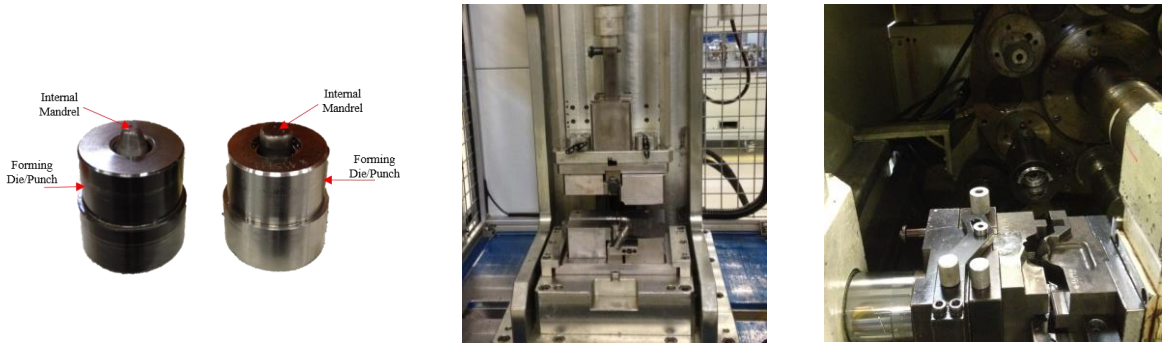

Figure 30 - (a) Forming tools, (b) cutting machine, (c) horizontal press machine and JIG tool.

The compression bead related to the reference E3, is produced in three operations, after the bending operation, in the following sequence:

1. Calibration: This first operation makes sure that the tube end has the minimal admissible diameter and is correctly aligned with the die. This operation is essential as if the tube has a diameter lower than the diameter of the internal mandrel it will lead to defects due to the contact between the tube wall and the inner mandrel.
2. Tube compression beading (Figure 9.a)
3. Tube nosing (Figure 9.b)

The bead geometry of the reference parts E1 (cooler side) and E2 has the same dimensions, so it follows the same manufacturing operations:

1. Tube expansion: As the tube end requires a diameter larger than the reference tube diameter, the first performed operation is tube expansion to achieve the desired diameter of the tube end. This operation also guarantees the calibration of the tube. (Figure 5.a)
2. Tube compression beading (Figure 9.a)
3. Tube nosing (Figure 9.b)

The tube nosing operation is not performed at the tube end related to the engine side of the reference E1 being only executed the calibration and tube beading operation.

During the manufacturing process the geometry and dimensions are controlled in dimensional/geometry control jigs. The first control is performed after the bending operation, to ensure this operation was successfully performed before moving on to the tube end forming operations. At the end of the tube end forming operations, the relevant dimensions of the bead are reviewed and the part geometry is once again controlled. The dimensional and geometry control instructions are presented in Annex A2.1, A2.2 and A2.3, and will also be reviewed during this work, in order to ensure that that tools are being used correctly and efficiently.

It is important to refer, that the bead geometry of the parts E1 and E2, which makes use of the same raw material and have the same dimensions, are not fully defined in the technical drawing as the bead height dimension is not specified.

The parts are also visually inspected and to be acceptable have to be free from wrinkles, buckles and scratches. If any of the parts is not according to all of the mentioned specifications it is rejected and considered scrap. Concerning the cracking defects, a quality strategy is defined, currently, it is performed a metallography test for each batch produced that enable review the occurrence of material cracking.

That production line can works three to 8-hours shifts in a row according to the internal client demand. The capacity of the production line per shift is presented in Table 2.

Table 2 - Production capacity of the production line.

Reference Part	Cycle Time (second/part)	Shift Capacity (7,5hours)
E1	39.52s	683
E2	27.83s	970
E3	27.83s	970

The total number of produced parts and scrap parts, during the month of April, is presented in Table 3 and the scrap causes quantified in Figure 31. As concluded from the bar graph one of the main causes of scrap are due to NOK bead, which represents dimensional bead defects, evident asymmetry of the bead or material failure. The references which had a highest scrap relative frequency are E1 and E2 as due to the thickness of the raw material, the manufacturing operations are more demanding. The reference E1 has a much higher scrap rate due to bead defects, because this part has two different beads.

It is important to point out that the scrap rates due to other defects are related to the bending operation (wrinkling, fracture, tool calibration, etc.) therefore the tube beading was not performed in these parts.

Table 3 - Production data related to April.

	E1	E2	E3	**Total**
No. of OK produced parts	2699	2856	4427	**9982**
No. of parts considered scrap	356	208	44	**608**
Scrap percentage [%]	11.7	6.8	1.0	**5.7**

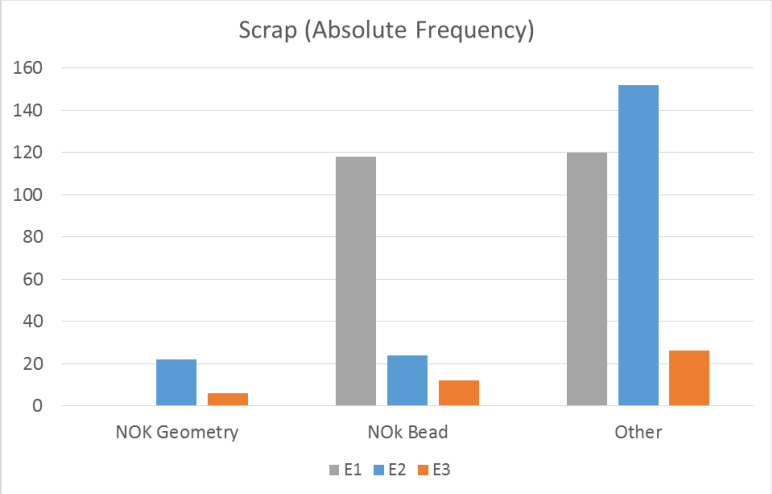

Figure 31 - Scrap causes related to April.

With this project it is expected to identify improvements to the coolant spigot manufacturing process, however the main objective is focused in the creation of a design standard, in order to eliminate the cracking defects and, improve and reduce the design and manufacturing development time.

5 Analyses of the coolant spigot parts

5.1 Raw material analysis

The welded tube consists of different material zones, such as weld, heat affected zone (HAZ) and parent material, and each of these zones possesses individual mechanical properties, which cause a complicated material nonlinearity. (Ren et al. 2012)

Knowledge of the raw material mechanical properties, dimensional tolerances, composition and considering the weld bead and HAZ is essential for a correct and reliable design of shapes, manufacturing tools and parameters in forming of welded tubes. As, many researchers have shown that there are obvious differences in the microstructure, microhardness, yield stress, tensile stress, and elongation of the weld bead, HAZ, and parent metal. Therefore, from the perspective of plastic forming, welded tube plastic forming belongs to the category of inhomogeneous materials forming. (Zhan, Guo, and Yang 2016)

Due to the non-uniform effect of heating in the HAZ the microstructure has different arrangements which make the mechanical properties not constant over its width, and this indicates that the HAZ should be divided into zones for a complete and accurate formability characterization of the weld joint. (Ren et al. 2012) However, for the present study it was not needed define and characterize the different zones of the HAZ in order to get accurate and reliable results, as the differences on the mechanical properties between the different zones are almost insignificant. So, the HAZ was not divided in different zones but treated as just one area of the weld joint.

All these differences in the material properties are closely related to the welding process and related parameters as speed, temperature, extrusion force and thickness of the tube. ((Zhan, Guo, and Yang 2016); (Zhan et al. 2010)) As it leads to weld seams and HAZs with different appearances, sizes and mechanical properties.

Several types of discontinuities may occur in welds or HAZ. Welds may contain porosity, inclusions or cracks, however, cracks are the most detrimental. Most forms of cracking result from the solidification, cooling and stresses developed due to weld shrinkage. Due to this is it essential to guarantee that the weld is free of cracks or other defects, as these defects easily propagate during forming processes.

One of the most important mechanical properties of a material is the material elongation, it is defined as the extent to which a material can be deformed in a specific forming process without a ductile fracture. If ductility of the material is high the material can be mechanically worked with ease and therefore presents higher formability limits. In forming processes this mechanical property plays an important role, however the material mechanical properties has to be analysed as a group.

Concluding, it is essential to perform a complete and accurate characterization of the weld bead, HAZ and parent material of welded tubes by a range of experimental tests as tensile, microhardness and metallography tests. Standard norms which specifies different parameters

and the standard quality of welded tubes, are also reviewed as it defines several important characteristics.

5.1.1 Experimental procedure

Metallography test

The specimen is mounted in plastic or epoxy resin to convenience in handling and to protect the edges of the specimen being prepared.

After mounted, the specimens are wet grinded by electrical disks using silicon carbide paper with a grain size of 80, 180, 320, 600 and a velocity of 300rpm.

At the end of the grinding operation, the specimen must:

- Be free from scratches, stains and others imperfections which tend to mark the surface;
- Be free from all traces of disturbed metal.

After grinding the specimen, polishing is performed on a diamond paste with a grain size of three and one micron, and a velocity of 150rpm.

Finally, the surfaces of specimens are etched with a solution of picric and hydrochloric acid and alcohol liquid during about 20 seconds and then placed under an optical microscope for observation and photography.

Microhardness test

The microhardness is performed by a Microhardness Tester Shimadzu Type M, using a diamond indenter at room temperature and the Vickers microhardness determined using the method expressed as Equation 5.1:

$$HV = 1854.4 \times \frac{P}{d^2} \tag{5.1}$$

Where P is the load [gram-force] and d is the mean length of the indentation diagonal [micron]. The microhardness test is performed using a load of 100 gram-force and hold time of 15 seconds. In Figure 32 it is presented a schematic representation of the Vickers indentation.

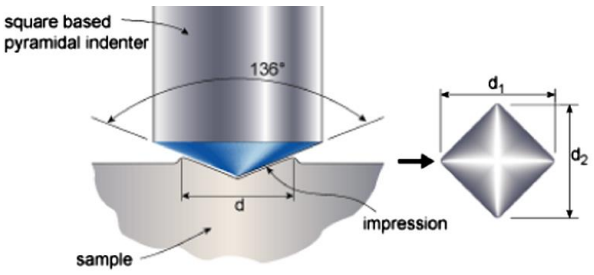

Figure 32 - Schematic of the Vickers indenter and the shape of an indentation.

In the measurement of microhardness, the displacements are controlled by X and Y micrometers on the table.

5.1.2 Dimensional tolerance and internal soundness control

For each produced part, the raw material is identified by the raw material and package number, in order to maintain an accurate database to identify possible raw material defects. Moreover, for this project it is important to identify clearly each raw material used in the production of each part in study, in order to associate the parameters and mechanical properties which characterize the raw material to the final part geometry and possible defects.

In Table 4 is presented the part number the corresponding raw material and package number, material grade and dimensions of the welded tube.

Table 4 - Raw material ID and dimensions.

Part Reference	Raw Material ID	Package ID	Material	Dimensions
E3	E1310012608	AV/5401	AISI 304L-1.4307	18,00 x 1,00 x 285,00
E1	E1140008748	-	AISI 304L-1.4306	16,00 x 0,50 x 175

In order to guarantee the maximum quality of the final part, it is required define the dimensional tolerance class of the raw material, since it has a direct impact on the design and process parameters of the bead geometry. Also, it is necessary to ensure that there are no cracks or other types of internal defects in the raw material. As these types of defects easily propagate during the manufacturing process of the part, as mentioned before, and affect the final quality.

Therefore, the European Standard EN 10217-7 (2005) specifies the technical delivery for welded tubes of circular cross-section made of austenitic and austenitic-ferritic stainless steel. For this study in concrete one of the most important specifications, in ISO 10217-7 (2005), is the point 8.5.2.1 which specifies that the weld area shall be free from cracks, lack of fusion and lack of penetration. For a complete application of EN 10217-7 (2005) and define a correct dimensional tolerance class of the raw material is, also, indispensable the European Standard EN ISO 1127 (1996), which specifies the dimensions, tolerances and masses per unit length of stainless steel tubes. In EN ISO 1127 (1996), the dimensional tolerance class of outside diameter and thickness are present on the point 4.1 and 4.2, respectively. In Table 5 it is presented the referred dimensional classes.

Table 5 - Outside diameter and thickness dimensional tolerance classes according to EN ISO 1127.

Diameter Tolerance Class	Tolerance on Diameter	Thickness Tolerance Class	Tolerance on Thickness
D1	± 1,5 % with ± 0,75mm min.	T1	± 15 % with ± 0,6mm min.
D2	± 1 % with ± 0,5mm min.	T2	± 12,5 % with ± 0,4mm min.
D3	± 0,75 % with ± 0,3mm min.	T3	± 10 % with ± 0,2mm min.
D4	± 0,5 % with ± 0,1mm min.	T4	± 7,5 % with ± 0,15mm min.
		T5	± 5 % with ± 0,1mm min.

In the certificate of the raw material the dimensional tolerance class is identified according to ISO 1127, as referenced above. Which gives the following range of dimensions, for the different raw materials in study, presented in Table 6:

Table 6 - Raw material tolerance classes.

Raw Material ID	Class	Diameter [mm]	Thickness [mm]
E1310012608/AV 5401	D4/T4	18,00 ± 0,1	1,00 ± 0,15
E1140008748	D4/T4	16,00 ± 0,1	0,5 ± 0,15

The length dimensional tolerance is imposed by BorgWarner, as ± 0,5mm.

These tolerances are further analyzed, during the design and manufacturing parameters discussion, in order to understand their influence in design and manufacturing processes.

5.1.3 Raw material properties

Tensile test results

The uniaxial standard tensile testing at room temperature is done by the supplier and the main test parameters and results provided to BorgWarner in the certificate of the raw material. The tensile testing are carried in accordance with ISO 10002-1.

Other tests are performed by the provider in order to ensure the quality of the raw material, however for this study only the results given by the tensile testing are relevant.

The minimum values of the mechanical properties, given by tensile testing, for each grade of stainless steel are also specified in ISO 10217-7.

From the tensile test, carried out by the supplier, performed to stainless steel tubes samples the following mechanical properties are determined:

- Ultimate tensile strength (R_m);
- 0.2% proof strength ($Rp_{0,2}$);
- 1.0% proof strength ($Rp_{1,0}$);
- Elongation (Al).

The mechanical properties of the raw materials in study are presented in Table 7.

Table 7 - Mechanical properties of the raw material.

Raw Material ID	Material	$Rp_{0,2}$ [N/mm^2]	$Rp_{1,0}$ [N/mm^2]	R_m [N/mm^2]	Al [%]
E1310012608	AISI 304L-1.4307	308	339	633	46
E1140008748	AISI 304L-1.4306	254	290	618	62

The relationships between the true stress and the true strain, of the material E1310012608, was approximated by a power law given by Ludwik- Hollomon's equation, presented below

$$\sigma = 1237.3\ \varepsilon^{0.40} \tag{5.2}$$

Where:

- σ is true stress;
- ε is true deformation.

Being achieved a strength coefficient (K) of 1237.3 and a strain hardening exponent (n) of 0.40.

The mechanical properties in the welded zone are evidently different, and to understand and quantify these differences uniaxial tensile tests could have been performed on specimens only of parent metal and containing the weld bead and HAZ. However, manufacturing specimens of a so small dimension is difficult and the tensile testing could be inaccurate as well.

Although studies have been performed on this by several researchers using different materials and the same conclusion has been achieved for most of them. During uniaxial tensile tests on specimens of the parent metal alone and containing the weld bead, it was concluded that the rupture of mixed material specimens differs from that of parent-only specimens. The rupture usually occurred in the middle of the mixed material specimen (in the zone of the weld bead). Also the elongations of the mixed material specimens was a lot less than those of parent only specimens, and the yield stresses, ultimate strength and microhardness much greater than the parent metal, due to the presence of the weld. (Zhan et al. 2010)

Microhardness test results

For this test two specimens was cut from welded tubes (raw material) by a plane perpendicular to the longitudinal axis of the tube and mounted, etched and observed under a microscope in order to identify the weld bead and HAZ area as the microstructure across the weld bead and HAZ differ from that in the parent metal zone. Thus, according to the variation in microstructure, the boundaries of each was defined.

The Vickers microhardness test was carried out across the weld bead, heat affected zone (HAZ) and parent material. The measurement increment used for the three different zones along the X-direction was 0.15mm and the Y-direction was maintained constant. The fact of maintaining the Y-direction constant can lead to measurement errors, because the hardness can vary in the Y-direction. However, the performed measurement errors does not have a significant impact on the final objectives and results.

In Figure 33 it is presented a schematic representation of the measured points across the weld bead, heat affected zone (HAZ) and parent material.

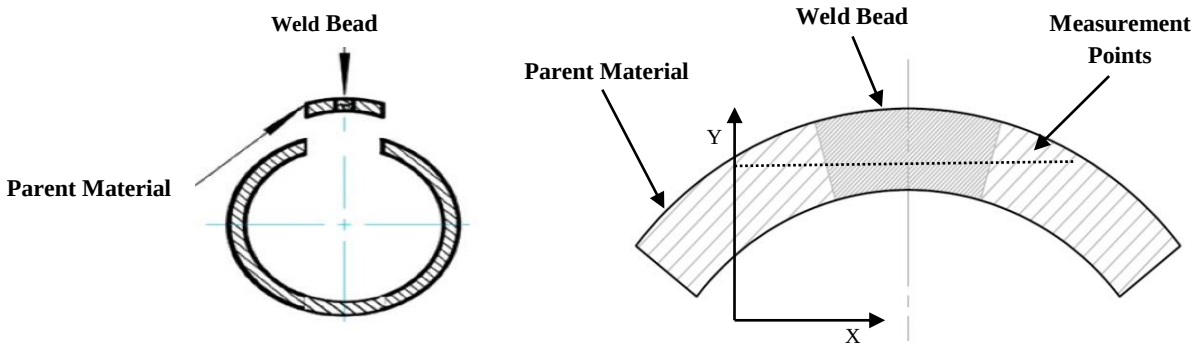

Figure 33 - Representation of the microhardness measurement points distribution.

The microstructure observation also permits to ensure that no defects are present due to the welded process. However this is not a main objective as a raw material quality control plan is realized by the supplier as specified in ISO 10217-7. Although no defects (cracks, inclusions, porosity) are detected in the analyzed specimens. As is observed in Figure 34, the welding has bring a major microstructure modification.

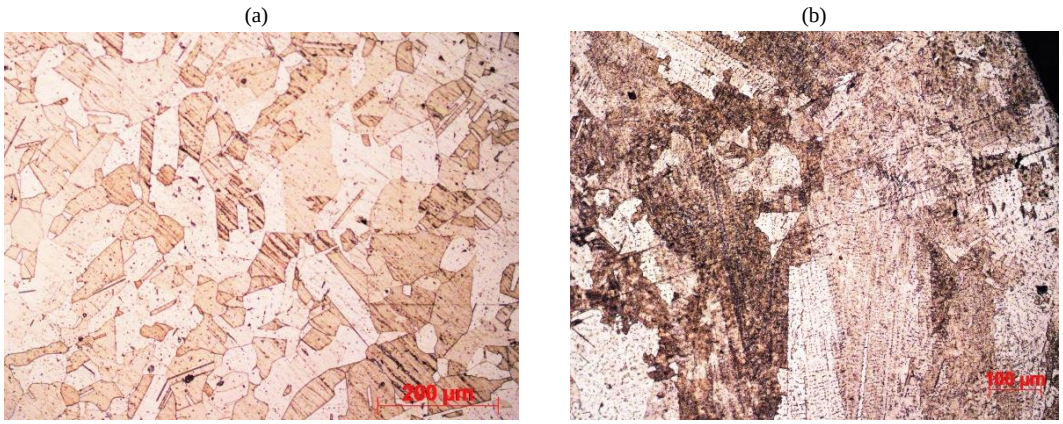

Figure 34 - Etched metallographic section of the weld bead (b) and parent metal (a).

The microhardness distribution across the weld bead, HAZ and parent material typically has the shape of a normal distribution rather than the ideal “top hat” distribution (Zhan et al. 2010) The results of the microhardness tests, presented in Figure 35, clearly verify this prediction.

As a conclusion from the analysis of graphs represented in Figure 35, related to two different specimens of the material E1310012608 and E1140008748 , the microhardness in the weld bead is the greatest, reaching about 270-275 HV. In the parent zone it is the least, around 206-230 HV. Which leads to an increase of approximately 33.5% on the weld area. According to microhardness distribution the width of the weld bead is determined as about 0.45-0.75mm in both welded tubes. The width of HAZ is not as accurate as the weld bead, as from the obtained microhardness profile the width in each side of the weld bead is different. It can be explained by measurement errors and due to the disregard of hardness variation along the y-axis, as explained before. Due to this, is reached an inaccurate and large range for the width of the HAZ of about 0.45-1.00mm, for both tubes in study. However the main objective of the test is not influenced by this inaccuracy. It is clearly concluded that the weld bead and HAZ present a bigger hardness than the parental metal and the farther from the weld center, the less the microhardness value.

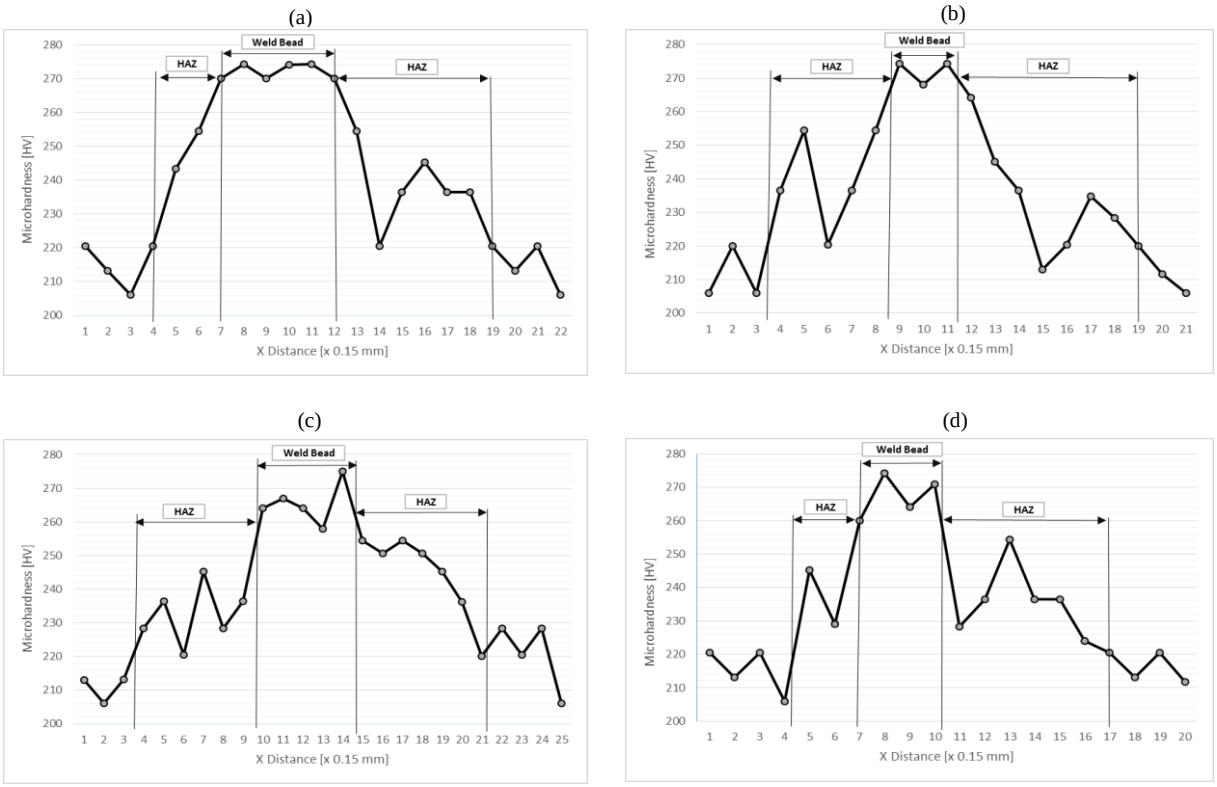

Figure 35 - Microhardness profile of the raw material. E1310012608 - (a) Specimens 1, (b) specimen 2. E1140008748 - (c) Specimen 1, (d) specimen 2.

Several authors have described different relations between the mechanical properties and microhardness values, which are not totally in agreement. Although all these relations show that an increase in the microhardness also reveals a raise in yield and ultimate strength, and a decrease in the material elongation. Therefore, it is possible to conclude that the weld area and HAZ of the tubes presents higher values of strength and lower elongation than the parent material. These can lead to a small asymmetry of the bead geometry, as the HAZ and weld bead area will have a smaller amount of deformation during the compression beading operation. However as the area affected by the welding process it is at most 2.75mm in radial direction, this asymmetry probably does not bring a considerable dimensional defect. Although, during the dimensional control analyses (Chapter 5.2.1) this has been taken into account, in order to realize the real effect of the weld on the final geometry of the bead.

5.2 Part properties and defects analysis

In order to get a deeper understanding in the defects and material behavior during the beading operation, was carried out several tests to the bead geometry related to the part E3 and E1, in order to assess the occurrence of defects in beads applied to different tube reference dimensions.

Thirty parts were manufactured in the same manufacturing conditions, ensuring that the weld line was always positioned in the area subjected to highest stresses during the bending operation (outside radius) which leads to a more severe deformation and guarantee that the practical worst case was performed. It leads to biggest strain hardening, due to bending, that can produce major effects on the mechanical properties of the material subjected to the beading operation.

A dimensional control, metallography test, microhardness mapping, internal surface observation and thickness variation analyses along the bead section was carried out. With the

results of these tests it is expected understand the constraining effects of the weld bead and HAZ, and the possible causes of material cracking.

As well, it is intended to quantify the cracks in the part, to further compare with the results obtained after performing further modifications to the part design or/and manufacturing process.

5.2.1 Dimensional control results

Through the projection of the parts it is possible to characterize the real geometry and get accurate dimensions of the bead.

The main objective of this test apart from characterizing the geometry of the bead and evaluate if the manufacturing process respects the technical drawing requirements, is also to understand if the weld bead has influence on material flow and deformation. According to the test results performed on raw material it is concluded that weld bead and HAZ zone has higher strength and less elongation. Therefore it is predicted that for the same stresses the parent material will develop greater strain which can lead to a non-acceptable bead asymmetry. The dimensional analysis allows a rough understanding whether the material is having a similar flow in the weld bead, HAZ and parent material zone during the beading operation by comparing the dimensions of the bead for two different projected planes.

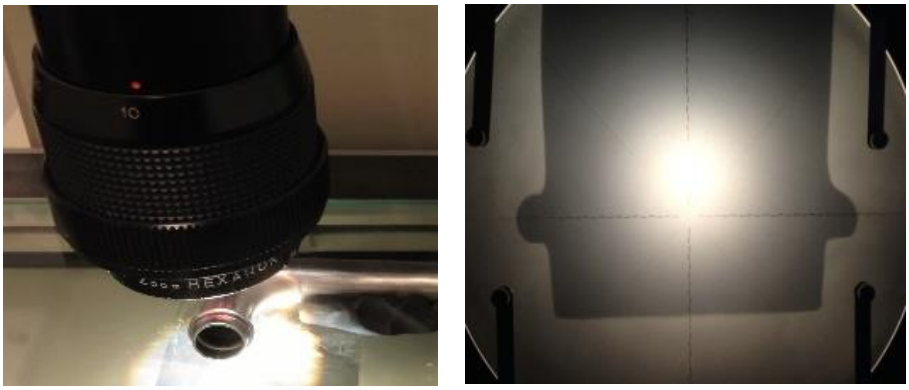

Therefore the projection was performed in a plane which contains the weld bead line and another, perpendicular to this, only containing parent material. In Figure 37 are presented the calculated dimensions that define the bead geometry, and the used nomenclature for each projected plane. The projection was carried out in a Mitutoyo PH-F profile projector.

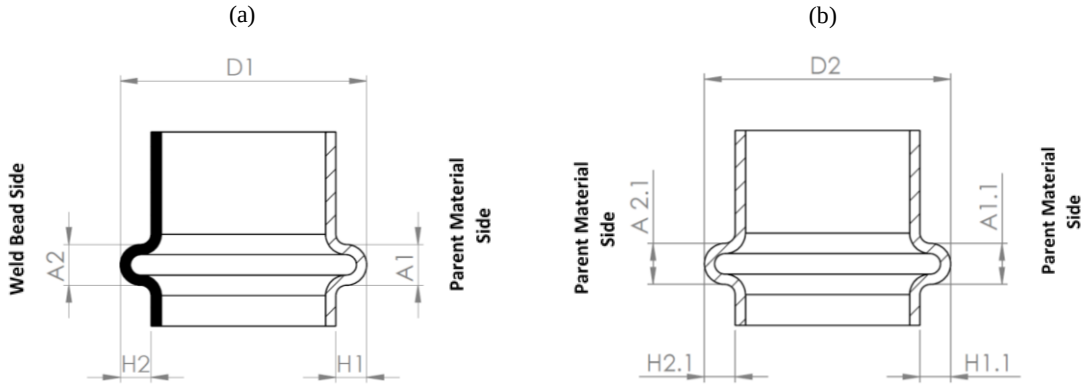

Figure 36 - Measured dimensions and planes related to those dimensions.

Figure 37 - Bead profile (perfil projection) related to the plane which contains the weld bead.

By analyzing the bead profile projections, presented in Figure 36, it is obvious that the contour of the weld bead side is quite different from the side of the parent metal being the tangency between the radiuses not regular in the weld bead side as in the parent material side. It is probably a consequence of the higher resistance to plastic deformation of the weld bead area and HAZ, comparatively to the parent metal. However, this small defect is not considered relevant as it does not present any influence on the function and it is a dimension difficult to control.

The measured bead diameters (D1 and D2), present an almost null variance between the average dimension, however it does not guarantee a centering of the bead. By analyzing the dimensions dispersion charts presented in Figure 38 and 39, related to part reference E3 and E1 (cooler side) respectively, it is concluded that the weld bead has a slight influence in material deformation regarding the fact that the difference between the bead heights are higher in the plane which contains the weld bead. The same can be concluded concerning the bead width. However, it is important to point out that these asymmetries are not only due to the presence of the weld bead. In fact, the manufacturing process variables also induce asymmetries on the bead geometry, which can be caused by a misalignment between the die/punch and the tube or due to a non-uniform material geometry and properties.

Therefore, by quantifying and comparing the asymmetries notice between the two planes, it is concluded that the influence of the weld bead on the material flow in tube compression beading is not significant, not leading to relevant geometrical or dimensional defects.

The agreement between the technical drawing and the part reference E3 is respected but it is necessary to point out that the bead height (A) is near to the upper technical tolerance limit (Figure 38.b and 38.c). Concerning the reference E1 (cooler side), the bead height is not defined in technical drawing therefore it is not controlled during manufacturing. However, the analyzed parts present a bead diameter slightly above the defined limit.

The repetitiveness of the process is acceptable considering that the standard deviation of measurements is quite low. Since the manufacturing process is controllable and according to the technical drawing, it is possible to predict that a possible material cracking in reference part E3 is not being caused by an inaccurate manufacturing process but due to an incorrect design of the bead geometry.

(a)

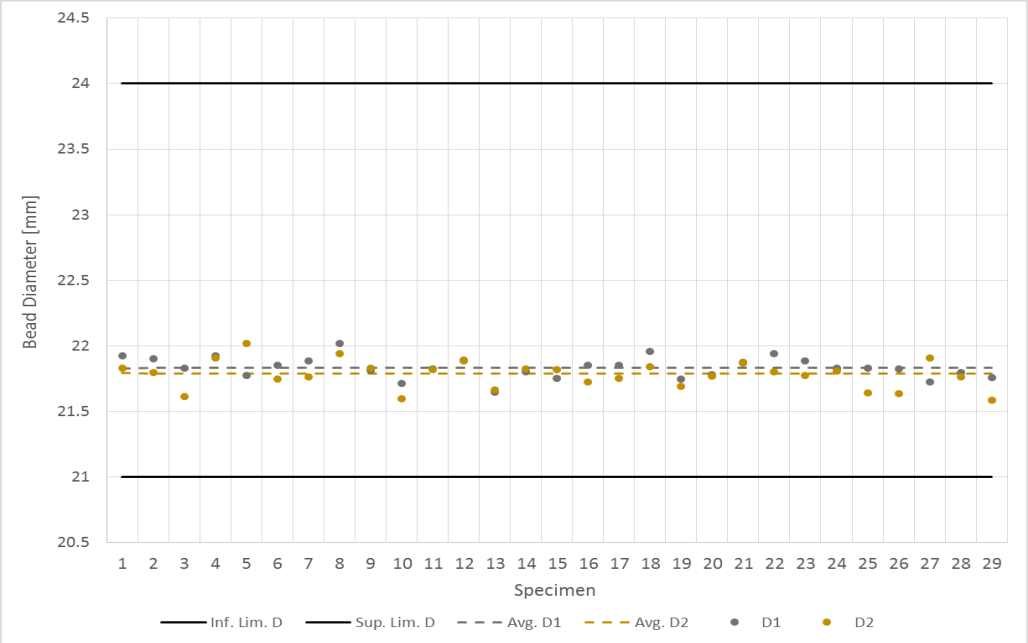

(b)

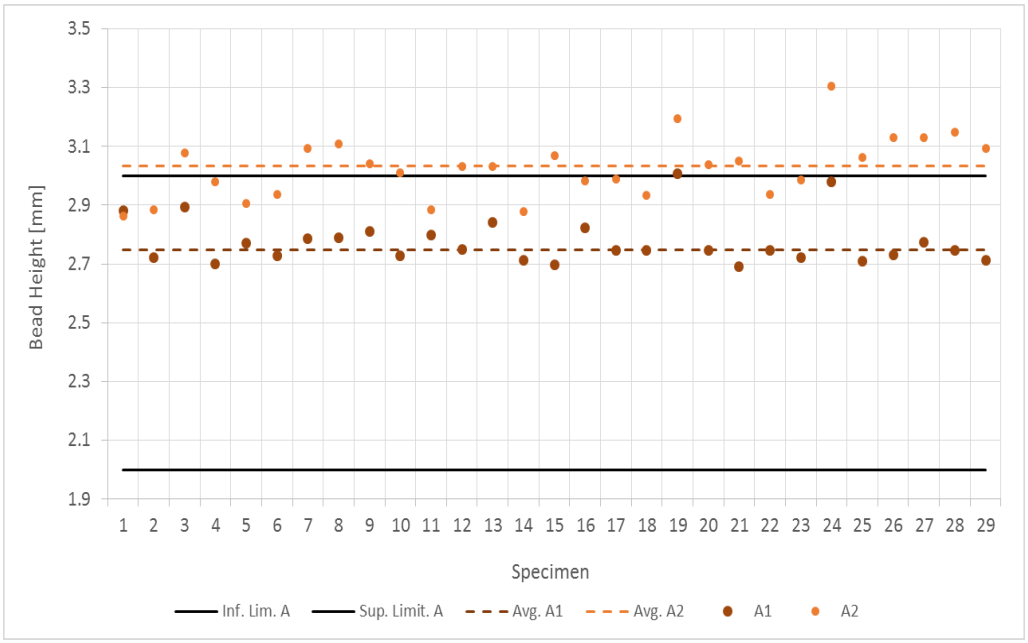
Bead Height [mm]
3.5
3.3
3.1
2.9
2.7
2.5
2.3
2.1
1.9
1 2 3 4 5 6 7 8 9 10 11 12 13 14 15 16 17 18 19 20 21 22 23 24 25 26 27 28 29
Specimen
Inf. Lim. A
Sup. Limit. A
Avg. A1
Avg. A2
A1
A2

(c)

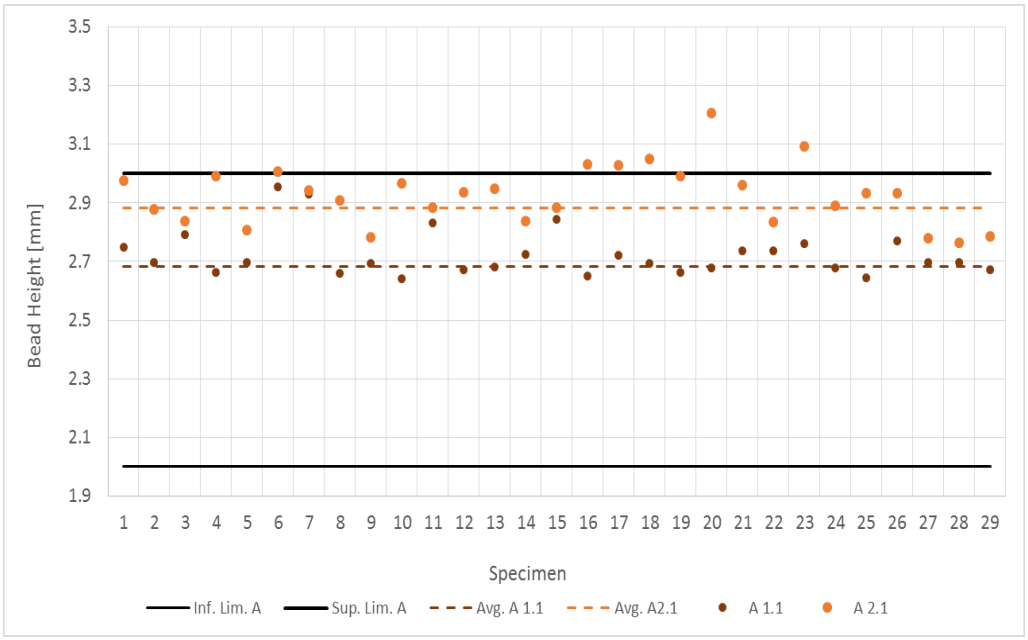
Bead Height [mm]
3.5
3.3
3.1
2.9
2.7
2.5
2.3
2.1
1.9
1 2 3 4 5 6 7 8 9 10 11 12 13 14 15 16 17 18 19 20 21 22 23 24 25 26 27 28 29
Specimen
Inf. Lim. A
Sup. Lim. A
Avg. A 1.1
Avg. A2.1
A 1.1
A 2.1

(d)

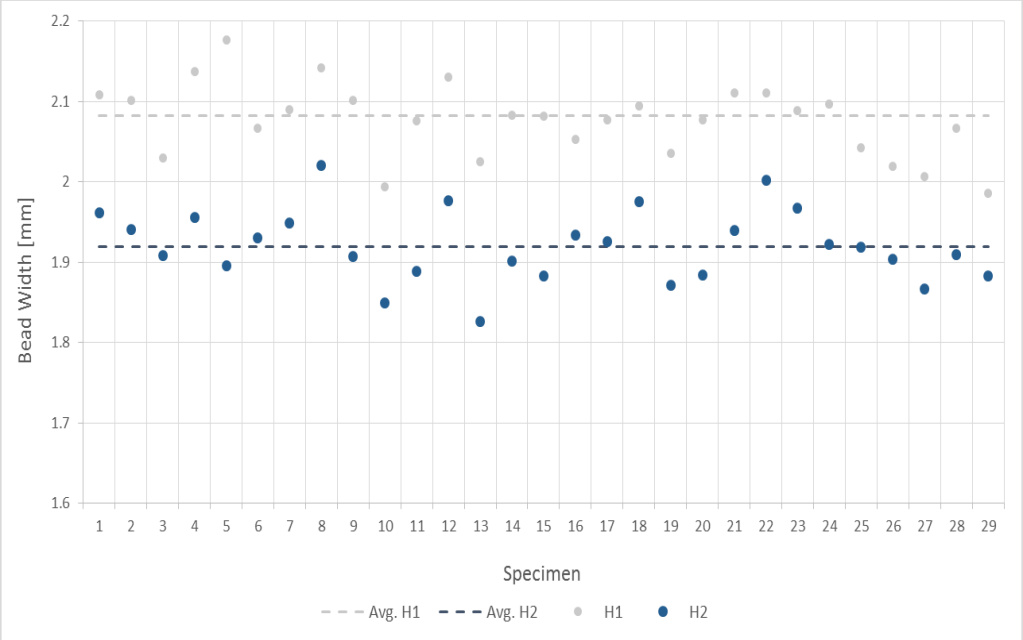

(e)

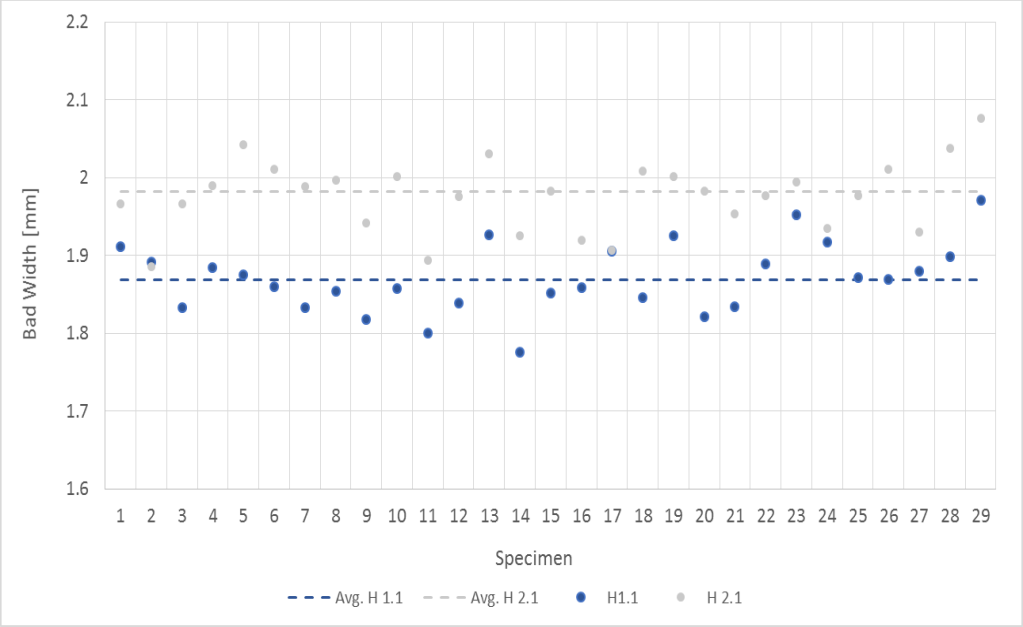

Figure 38 - Dimensional analysis of the reference E3. (a) Bead diameter, (b)/(c) bead height, (d)/(e) bead width.

(a)

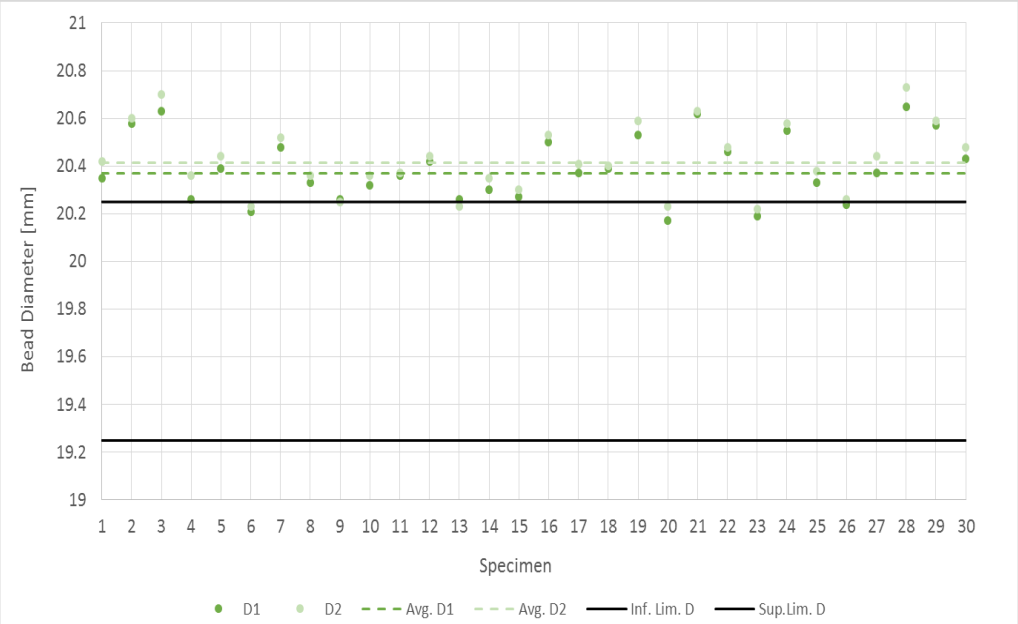
Bead Diameter [mm]
21
20.8
20.6
20.4
20.2
20
19.8
19.6
19.4
19.2
19
1 2 3 4 5 6 7 8 9 10 11 12 13 14 15 16 17 18 19 20 21 22 23 24 25 26 27 28 29 30
Specimen
D1
D2
Avg. D1
Avg. D2
Inf. Lim. D
Sup.Lim. D

(b)

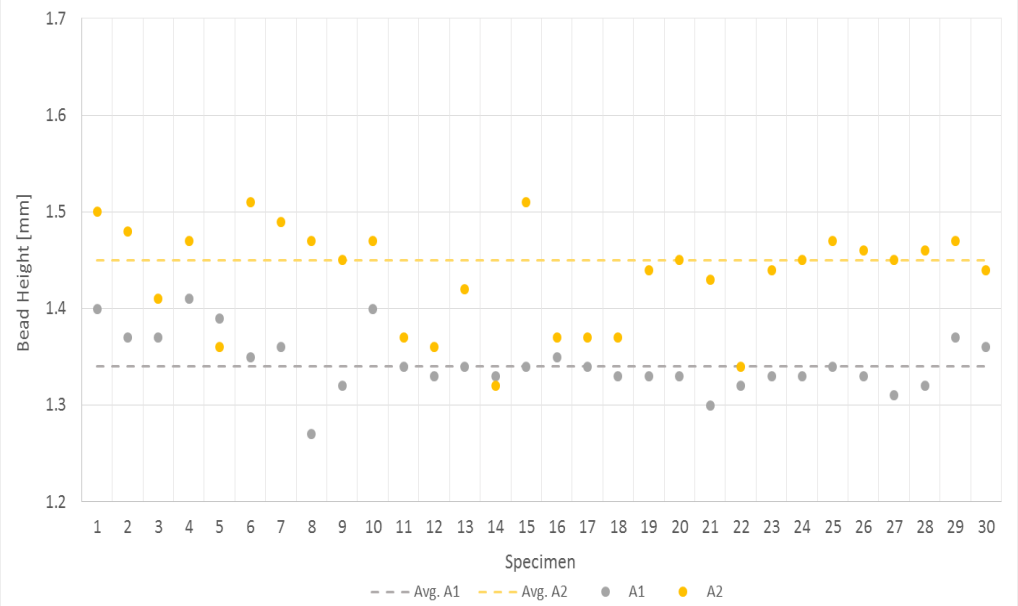
Bead Height [mm]
1.7
1.6
1.5
1.4
1.3
1.2
1 2 3 4 5 6 7 8 9 10 11 12 13 14 15 16 17 18 19 20 21 22 23 24 25 26 27 28 29 30
Specimen
Avg. A1
Avg. A2
A1
A2

(c)

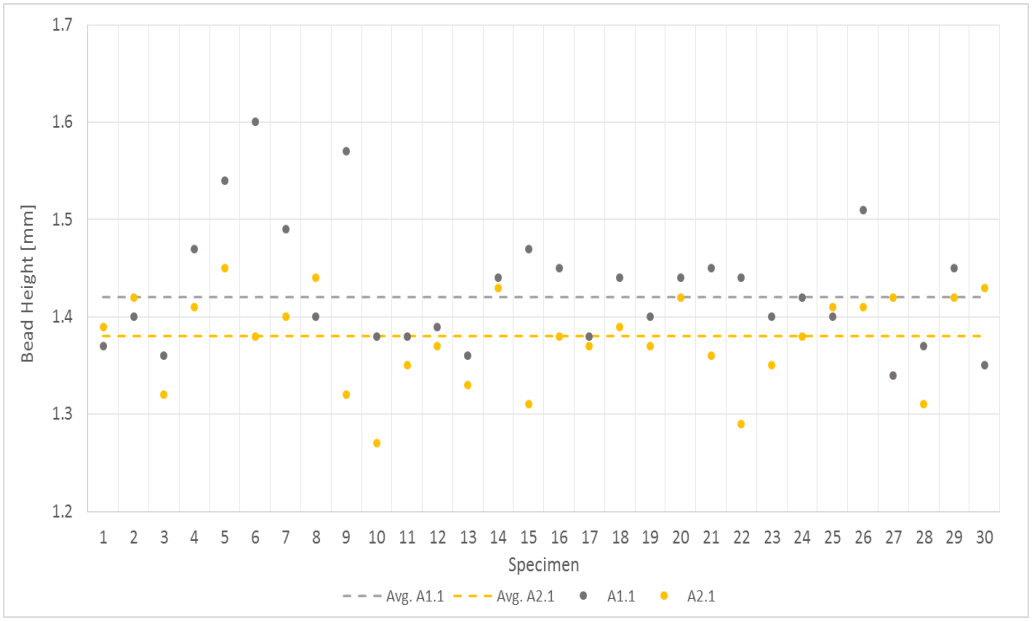
Bead Height [mm]
1.7
1.6
1.5
1.4
1.3
1.2
1 2 3 4 5 6 7 8 9 10 11 12 13 14 15 16 17 18 19 20 21 22 23 24 25 26 27 28 29 30
Specimen
Avg. A1.1
Avg. A2.1
A1.1
A2.1

(d)

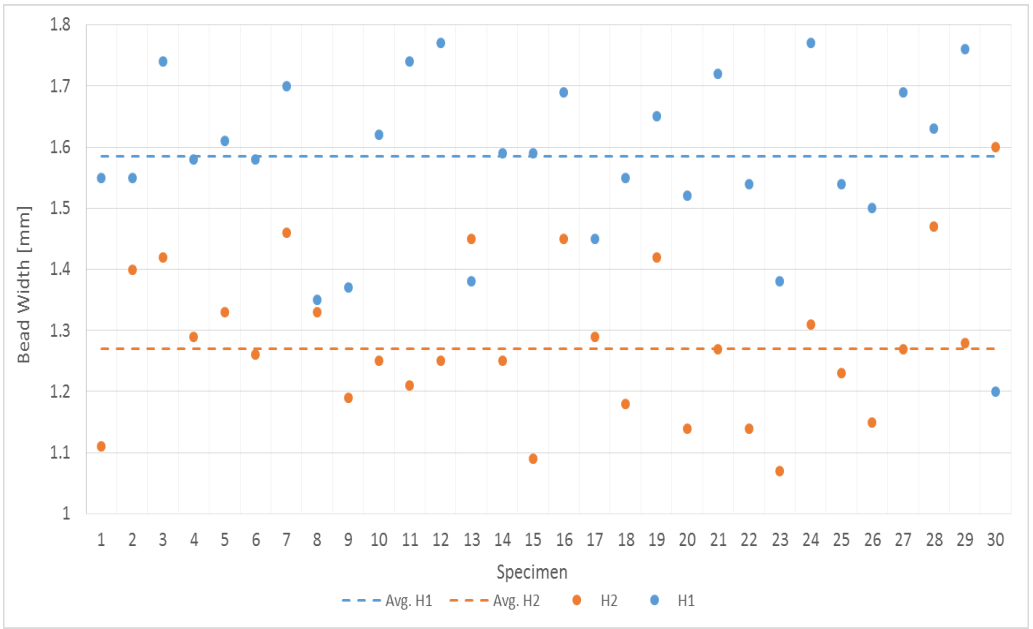
Bead Width [mm]
1.8
1.7
1.6
1.5
1.4
1.3
1.2
1.1
1
1 2 3 4 5 6 7 8 9 10 11 12 13 14 15 16 17 18 19 20 21 22 23 24 25 26 27 28 29 30
Specimen
Avg. H1
Avg. H2
H2
H1

(e)

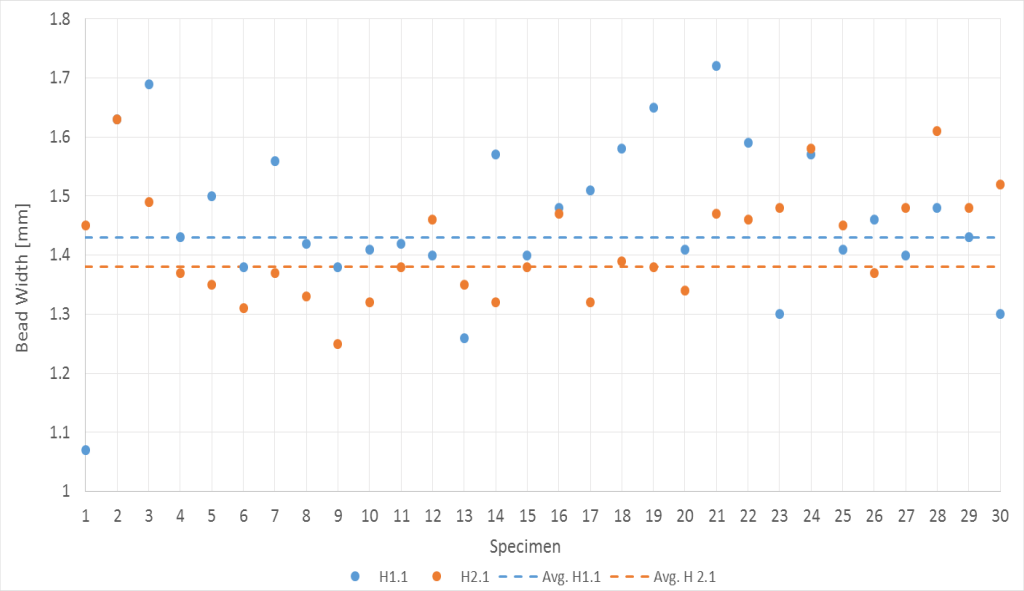

Figure 39 - Dimensional analysis of the reference E1. (a) Bead diameter, (b)/(c) bead height, (d)/(e) bead width.

5.2.2 Metallographic test results

The specimen preparation for metallography test followed the same experimental procedure used in raw material analysis (chapter 5.1.1) and it was performed in four specimens and four different planes, as represented in Figure 40. The plane number 1, is positioned in the weld bead and HAZ zone.

(a) (b)

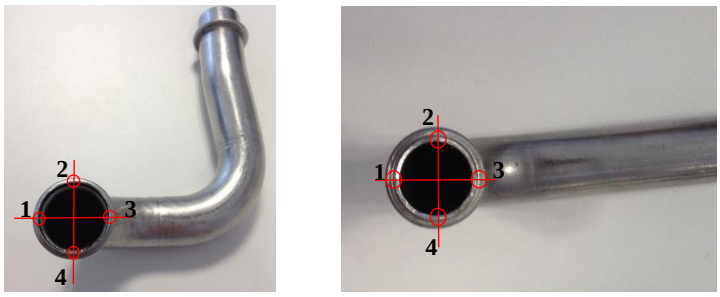

Figure 40 - Metallographic cutting planes representation.

This test permits to quantify the cracking defects, analyze the changes in the microstructure due to plastic deformation and understand how the cracking propagation is developing. The inner surface of the bead was, as well, observed in the stereomicroscope.

Concerning to material cracking, it is not identified any difference in the quantity and length of the cracks between the different cutting planes and specimens. The only identified defects on both part references are cracks, however the length and quantity of the material cracks are higher on the bead geometry related to the reference E1 (cooler side), reaching a length of about 20% and 10% of the thickness, in reference E1 and E3 respectively.

The cracks are mostly presented in the inner area of the bead, and some high roughness and micro-cracks are also observed in the outdoor radius in reference E3, as seen in Figure 42. The metal grains in the inner area of the bead are quite elongated and irregular and presents the original size and geometry the farther the inner area. More metallography's of both references are present in appendix B 1.1 and B 1.2.

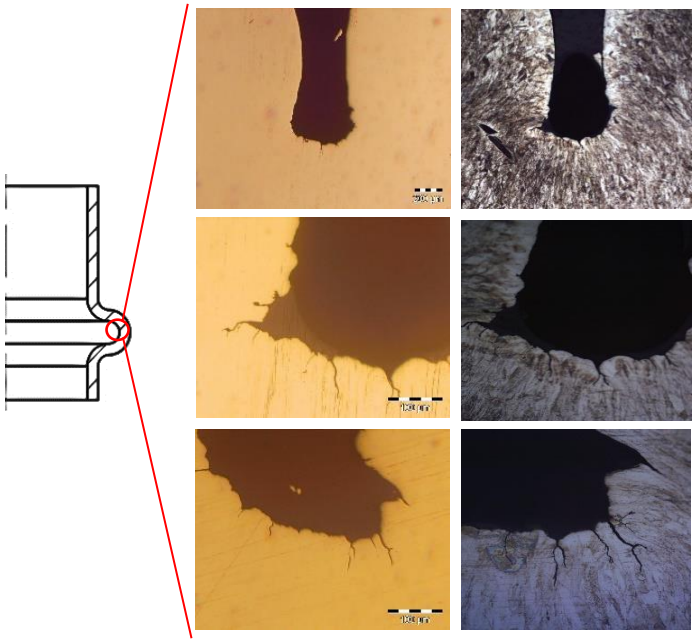

Figure 42 - Metallographic section of the bead of reference E3 (magnification of 75x and 150x).

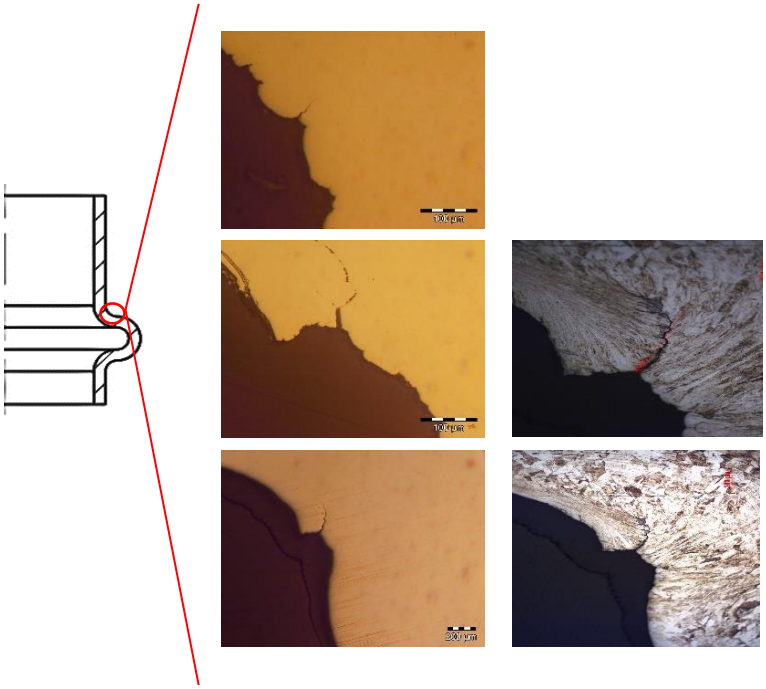

Figure 41 - Metallographic section of the upper radius of the bead of reference E3 (magnification of 75x).

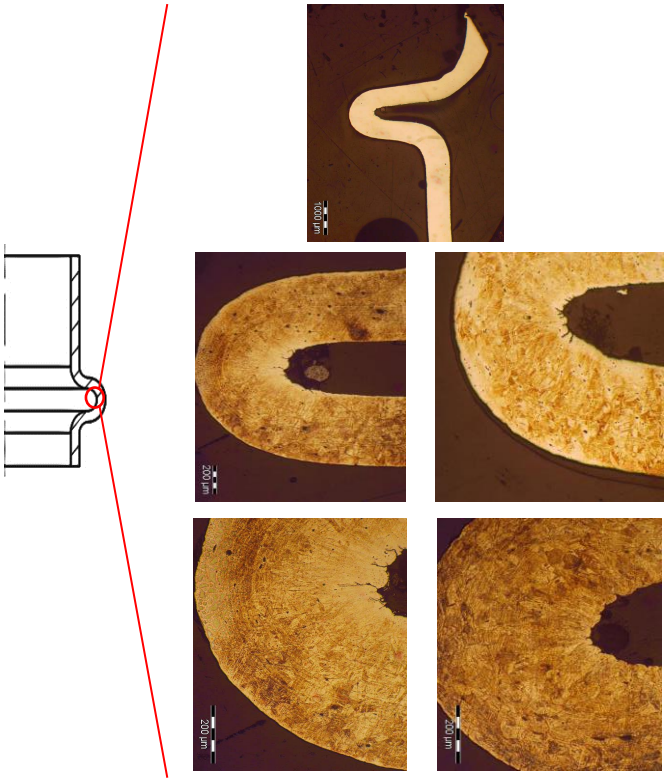

Figure 43 - Metallographic section of the bead of reference E1 (magnification of 23x, 75x and 150x).

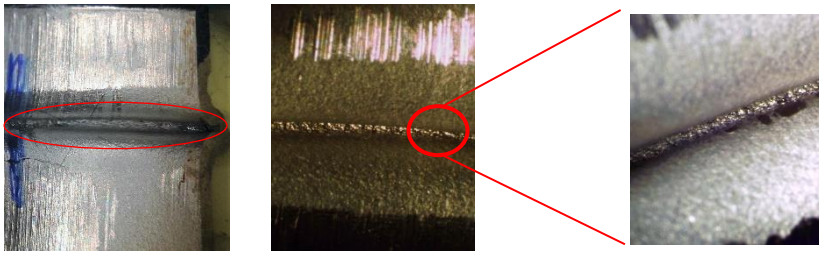

Figure 44 - View of the inner surface of the bead (E3) through a stereomicroscope.

The inner surface of the bead also presents huge roughness (Figure 44) which suggests high strain hardening. This is associated with excessive plastic deformation or due to the absence of enough space to accommodate the deformed material which does not permit that the metal grains achieve an organized structure, leading to an overlapping of the grains and consequently intergranular cracking (Figure 45).

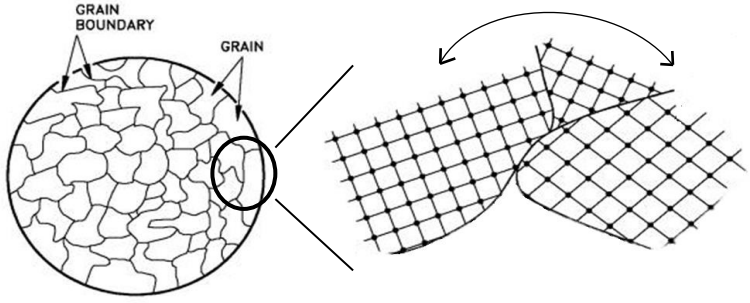

Figure 45 - Grain deformation mechanism due to circumferential or compressive stresses.

Concluding, as huge roughness is observed in the surface and the cracks seem to develop as intergranular cracking it suggests that the cracking is caused by excessive compressive stresses and grain rotation, and due to the lack of space to house all the deformed material.

The parts should only be acceptable when no material discontinuity is identified, as the service induced stresses and loads threshold applied to the part are difficult to be analytically or by numerical simulation predicted it is not possible define the critical crack length. Therefore, as the presence of cracks leads to lower fatigue life cycles and early material failure, it may be avoided.

5.2.3 Microhardness mapping results

The microhardness test followed the same experimental procedure used in the characterization of the raw material (Chapter 5.1.1) and it is performed in 3 specimens, each one related to a different cutting plane. The main objective of this test is mapping the Vickers microhardness along the bead zone in order to understand which areas are more affected by plastic deformation and estimate the deformation level of the material. It also allows to conclude if the material is strain hardened due to the bending operation as it leads to a major effect in the mechanical properties of the material. The obtained results are represented in Figure 46.

(a)

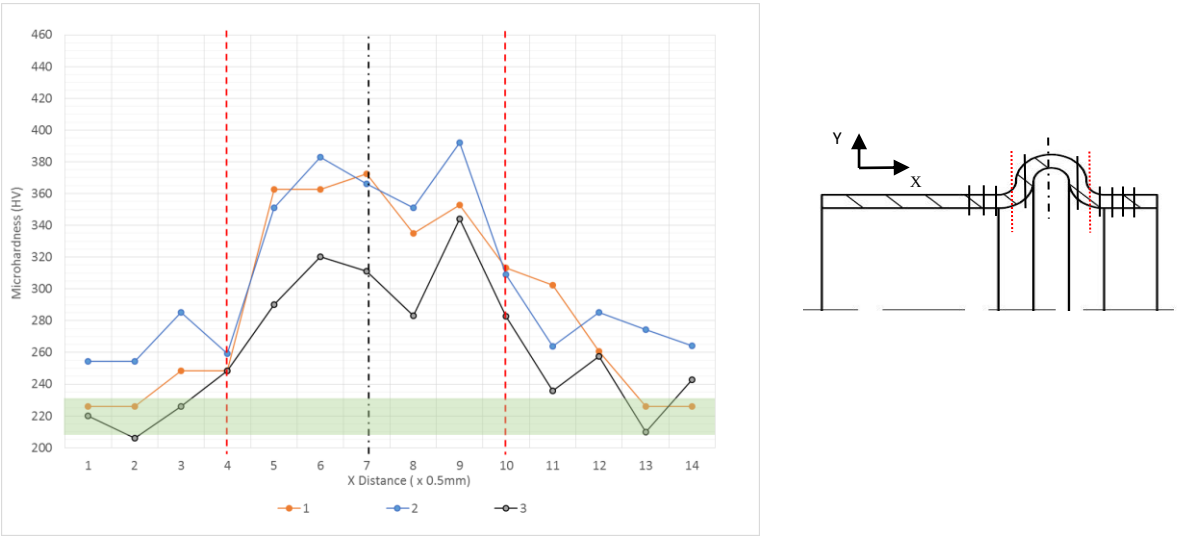

(b)

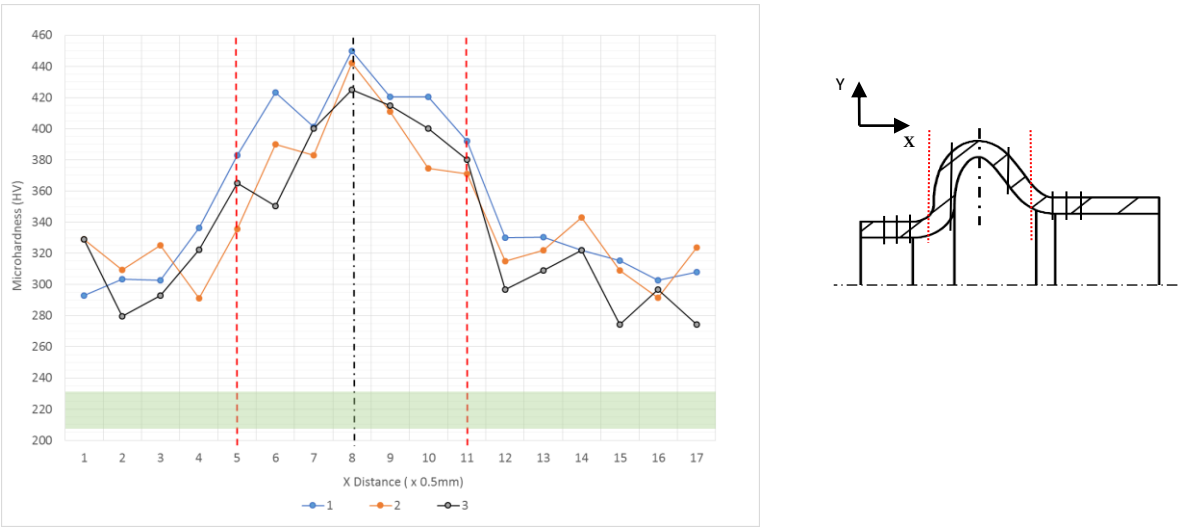

Figure 46 - Microhardness profile along the bead section and respective measurement points. (a) Reference E3, (b) reference E1.

The microhardness relatively to the bead of the part E3 show that the higher values of microhardness are in the upper and lower radius of the bead. In this area the microhardness is about 1.7 times higher than the microhardness measured in the raw material (206-220 HV), which represents a significant increase (Figure 46.a).

The microhardness profile also shows that there is a slight reduction in the middle area of the bead comparatively with the lower and upper radius area, which was not expected as the middle area of the bead supposedly has a higher deformation. This unexpected outcome can result from an inaccurate measurement as the difference between microhardness values are small. The higher microhardness values obtained in specimen 2 can be explained by the fact that this plane is the one which supposedly contains the weld bead. However, this is not taken into account since according to the metallography analysis the microstructure does not showed a major alteration.

Relative to reference E1, the higher values of microhardness are in the middle area of the bead, as expected, reaching a value 1.8-2 times higher than the microhardness of the raw material (Figure 46.b). In this reference is important to point out that the microhardness in the straight length of the specimen present a microhardness value of around 280-330 HV, that are also higher than the microhardness reference of the raw material (206-220 HV). It means that in this area the material has been affected by the bending operation performed before the tube end forming operations. Therefore the material area, where the bead is performed, has higher tensile and yield strength and lower ductility, which decreases the forming limit of the material. Consequently, this have to be taken into account during the design process as the mechanical properties of the raw material cannot be used to dimensioning the bead geometry.

The microhardness profile relative to the reference E3 does not reveal any constraining effect due to the bending operation, based on that is possible to estimate a distance between the bend and the bead, for a bending radius of 21 mm and bending angle of 110º, which guarantees that the material mechanical properties are not affected by plastic deformation. Therefore, based on reference E3 is achieved a distance of 9 mm. However, a deeper study may be carry out as the constraining effects due to the bending operation are affected by several parameters as bending angle and radius, and tube diameter and thickness.

Based on the study of M.Milad et al. (2007), it is possible to estimate the percentage of deformation imposed to Stainless Steel-AISI 304 due to forming operations. Based on the developed relation between hardness (HV) and cold reduction (%), presented in Figure 47, is achieved a material strain hardening of around 45% and 55% for the reference E3 and E1, respectively. Values that are near to the elongation of both materials.

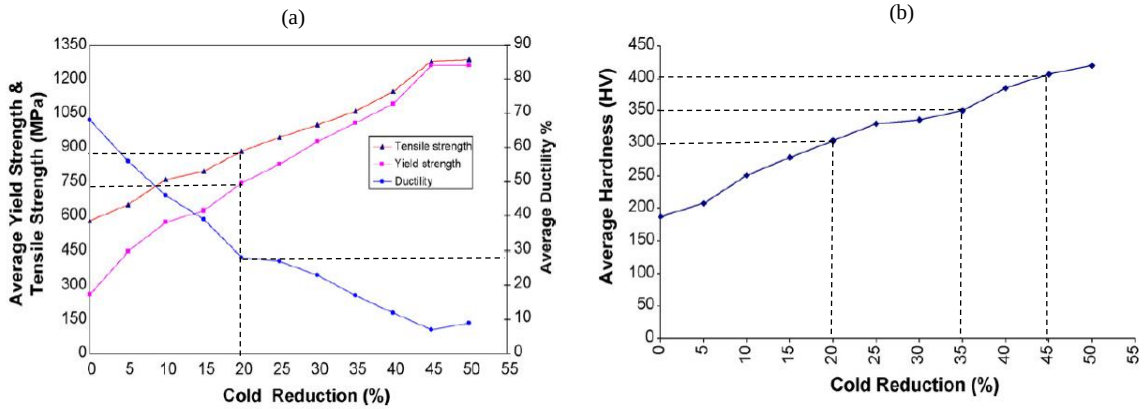

Figure 47 - Effect of cold rolling on the tensile properties (a) and on the Vickers hardness of AISI 304 (b).

Also based on this relation is possible to predict the elongation, tensile and yield strength of the material affected by bending operation (strain hardened). A microhardness of 300 HV corresponds to a strain hardening of 20%, a material elongation of 30% and a tensile and yield strength around 800MPa and 900MPa, respectively. These values are a rough estimation, however, as it was not possible by experimental tests perform a relation for the material in study, this approximation is a good indicator to base the design parameters.

In order to estimate the influence of bending on the flat section of the tube where is applied the bead geometry, it was performed a microhardness mapping around the bending section. This permits achieve a rough estimation of the length affected by the cold forming operation (bending) and predict the mechanical properties along the flat section by applying the same method presented above. This test have been only performed for the tube reference ⌀16x0.5mm and bending radius of 22mm and a bending angle of 45º, 60º and 90º. More experiments for more bending radius and tube dimensions should be carried out to achieve more reliable results. However, an experimental methodology is defined to assess the influence of the bending in the material properties and consequently in the bead design.

In Figure 48 is schematic represented the Vickers microhardness measurement points distribution. The measurement increment used for the X-direction was 0.5mm.

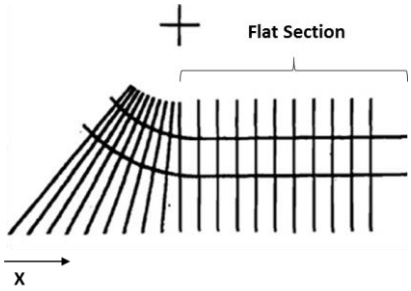

Figure 49 - Representation of the microhardness measurement points along the bend section.

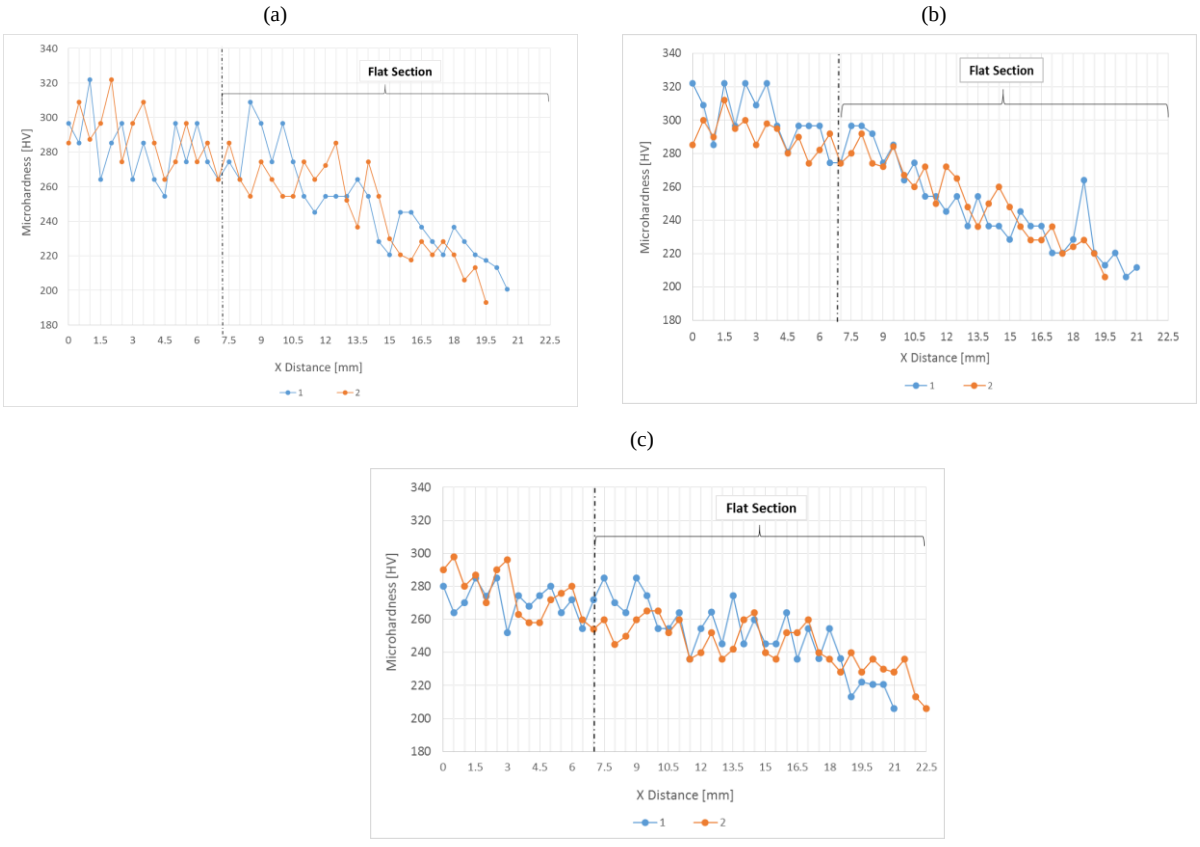

Figure 48 - Microhardness profile along the bend section. (a) 45º bend, (b) 60º bend, (c) 90º bend.

Comparison of the results, presented in Figure 49, for the 45°, 60º and 90° specimens, as expected, showed that the flat section is more affected by plastic deformation for specimens that have a bending angle of 90°. Based on the microhardness profile is possible to estimate a distance between the bend and the bead which guarantees that the material mechanical properties are not affected by plastic deformation. Being reached distances of 12.5-13.5mm, 12.5-14mm and 14-15mm for bending angles of 45º, 60º and 90º, respectively.
The results showed quite clearly the effect of the amount of cold-working on the increase in the microhardness values and consequently increase in yield strength and decrease in elongation of the material. The influence of the thickness on the amount of strain hardening was not possible to evaluate.

5.2.4 Thickness variation along the bead section

The thickness variation along the bead section was also studied in order to estimate the amount of plastic deformation along the thickness direction. The geometry of the bead does not allowed to accurately define measurement points for each specimen, however was possible to achieve a rough understanding. In Figure 50 it is presented the thickness variation profile, along the bead section.

A uniform thickness increase along the tube length subject to axial compression stresses is expected, before the beginning of formation of the compression bead, as reviewed in Chapter 2.1.3. Due to the bead formation, the results showed a 10-25 % thickness increase along the bead section, in both studied references. These results shows high material deformation in the thickness direction.

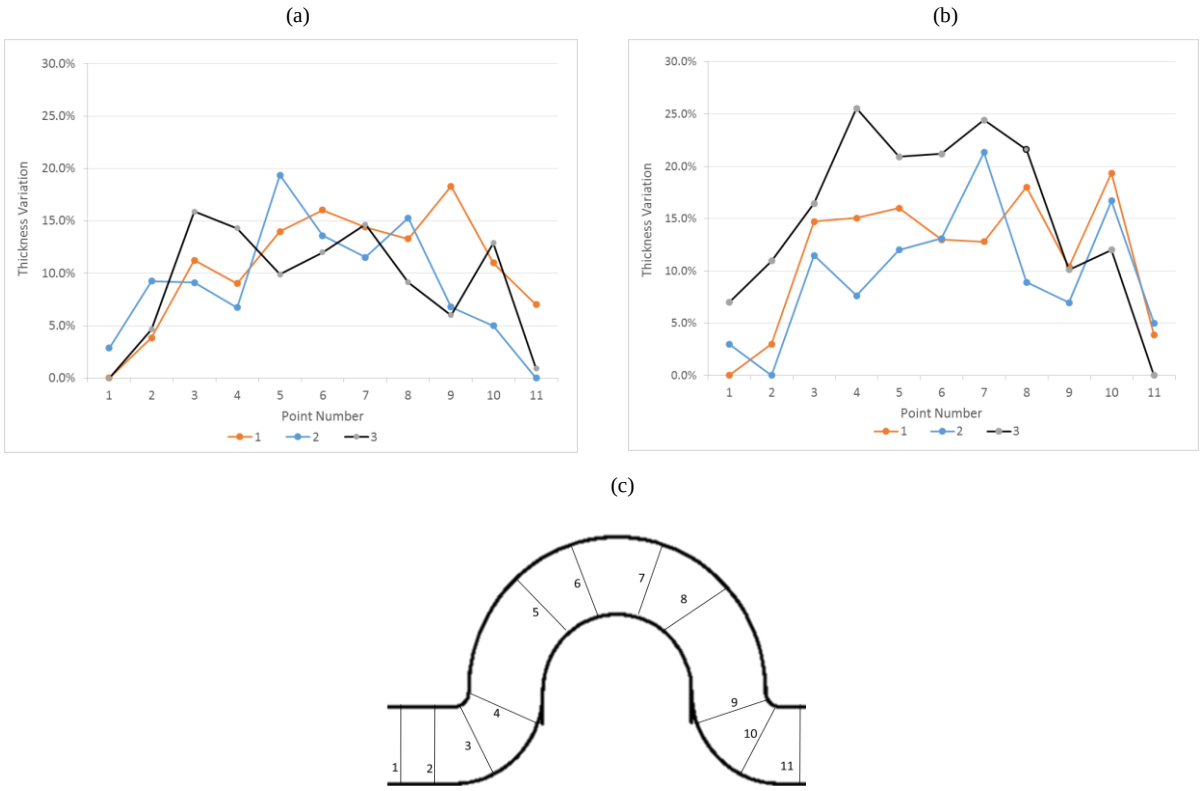

Figure 50 - Thickness variation. (a) Reference E3, (b) reference E1, (c) schematic representation of the measurement points.

5.3 Discussion and proposed solution

Through the development of an overall analysis regarding the results obtained, it was concluded that the material cracking defects are due to an incorrect design, since the manufacturing process respects the specified dimensions by the technical drawing. So, the efforts to improve the final quality of the parts should focus on the designing parameters of the bead geometry taking into account the current manufacturing process.

However it is important to point out that the dimensional control tools of the reference E1 should be improved, as it does not perform an accurate control of all of the specified dimensions and geometries. Between the bending and tube end forming operations, is performed a first control of the geometry of the tube bends, however the tool mechanism in use does not perform an accurate control of the all geometry, guaranteeing only the position of the tube ends. That can leads to problems during the tube end forming operations, as if an incorrect geometry is achieved during the bending operation it will lead to a misalignment between the forming tools and the tube end, which can cause an asymmetry in the tube bead geometry. These types of defects are regularly reported, thus some possible improvements in the manufacturing processes that could minimise its occurrence will be subsequently presented, in Chapter 7.

The dimensional/geometry control tools also do not control the bead height, which is an important dimension to guarantee a correct bead geometry, therefore a bead height control tool should be developed in order to guarantee that the final geometry is in fully agreement with the technical drawing.

The dimensional analyses also reveals that the material flow is not influenced by the weld bead of the tube, as is not notice any major influence of it in bead geometry or dimensions, even if it is positioned on the outside radius of the bend. Regarding the effect of the weld in the material properties and consequently lower material formability limit and higher probability of occurrence of material cracking in this area, it is not identified any difference in the quantity and length of the cracks between the different analyzed sections therefore the effect of the weld can be also despised in the occurrence of material cracking. However, during experimental analyzes, carried out in Chapter 6, it will once again taken into account.

By the metallography, stereomicroscope and microhardness results it is possible to point out the reasons for the occurrence of material cracking due to the tube compression beading operation. By analysing the collected data, in both references the material is almost reaching the formability limit (elongation) as revealed by the microhardness values and an evidence of high strain hardening by stereomicroscope observation. Also, wrinkles can be observed due to high compressive and circumferential stresses, which lead to grain overlapping and consequently cracking initiation.

As the manufacturing process cannot be modified, the solution has to be based on the modification of the bead geometry but ensuring that the practical function of it is not committed and that ensure minimal impact on the coolant spigot final dimensions and assembly process of the spigot to the cooler outlet shell.

The proposed solution objective is to decrease the induced forming stresses, mainly the compressive stresses, and material deformation. As no basic design rule has been developed until now it is proposed to base a first dimensioning approach of the bead geometry in the minimum sheet bending radius theory, expressed in Equation 5.3.

$$R_{min} = \frac{50t_0}{Al} \cdot \frac{t_0}{2} \tag{5.3}$$

Based on that radius can be defined the minimum bead height (Equation 5.4),

$$A_{min} = 2(R_{min} + t_0) \tag{5.4}$$

Where:

- *Al* is the elongation of the raw material;
- t_0 is the thickness of the reference tube;
- R_{min} is the minimum sheet bending radius;
- A_{min} is the minimum height of the bead.

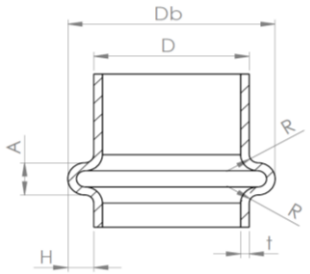

Figure 51 - Characteristic dimensions of the bead geometry.

The R_{min} is obtained by considering the minimum raw material elongation for reference E3 and E1 (Engine side), and the expected elongation of the material in the bead area, as explained in chapter 5.2.3, for reference E1 as the material area where the bead is applied is strain hardened due to the bending operation. The thickness of the tube has a great influence, therefore the maximum admissible thickness is considered to calculate the $R_{min,}$ in order to guarantee that it is admissible for all the thickness tolerance range (for a thickness tolerance class T4) according to EN ISO 1127. These influence is analysed in Table 8.

Table 8 - Influence of tube thickness in the minimum bending radius.

Part Reference	**t_0 [mm]**	**D_0 [mm]**	**Material Elongation [%]**	**R_{min} Upper Tolerance [mm]**	**R_{min} Lower Tolerance [mm]**
E1 (Cooler Side)	0.5±0.15	16±0.1	30	0.35	0.1
E1 (Engine Side)			40	0.26	0.08
E3	1±0.15	18±0.1	40	0.73	0.4

As shown in Table 9, the technical drawing and true dimension for both references do not respect the minimum bending radius theory, being expected that the forming limits have been exceeded.

Table 9 - Minimum required bead height for each reference.

Part Reference	**R_{min} [mm]**	**A_{min} [mm]**	**A [mm] (Technical Drawing)**	**A [mm] (True Dimension)**
E1 (Cooler Side)	0.35	1.70	NA	1.34-1.44
E1 (Engine Side)	0.26	1.53	NA	NA
E3	0.73	3.47	2.00-3.00	2.75-3.00

The maximum bead diameter could be defined analytically as the minimum bead height however according to tube compression beading deformation mechanism the relation between the bead diameter or bead width and the bead height can only be defined by experimental work or numerical simulation. However, the bead diameter also plays an important role, as it can compromise the minimum internal radius of the bead. That influence is studied in Chapter 6, being analysed by numerical simulation and experimental work.

An overall analyses of the bead design applied to the coolant spigot parts that are currently in production at BWES show that almost of them (≈70%), presents a bead height that compromise the minimum bending radius theory. Some bead designs have a bead height smaller than twice of the thickness of the tube, which lead to a *crush* of the material.

6 Proposed solution validation - Experimental and numerical analysis

6.1 Experimental procedure and testing plan

The tests were performed in the production line, on the references E3 (⌀18x1 mm) and E1 (⌀16x0.5 mm) on the bead engine side, by only applying design changes to the forming die. The bead referent to the cooler side of the part E1, that has been in study in Chapter 5.2, was also tested, however to achieve this bead geometry a tube expansion operation is also needed, being necessary improve the designed tool in order to succeed.

The testing procedure was designed in order to validate the proposed solution, presented in Chapter 5.3, and to verify the influence of the initial gap height (L_{gap}), the height of the forming die (H_b) and the ratio between the reference radius (r_0) and thickness (t_0), of the tube, on the achieved bead geometry and consequently on the occurrence of material cracking and other minor defects. The technical drawing of the developed manufacturing tools, for the tube reference ⌀18x1 mm, are presented in Figure 52 and Annex C1.1.
As described previously, the experimental work plan presented in Table 10 was carried out.

Table 10 - The plan of experiments.

Case	D_0 [mm]	t_0 [mm]	H_b [mm]	L_0	L_{gap}
1	18	1	2	13	8.1
2				13.9	9
3				14.5	9.6
4			3	13	8.1
5				13.9	9
6				14.5	9.6
7			4	13	8.1
8				13.9	9
9				14.5	9.6
10	16	0.5	1.7	14.2	5.2
11				15.2	6.2
12				16.2	7.2
13			3	14.2	5.2
14				15.2	6.2
15				16.2	7.2
16			3.5	14.2	5.2
17				15.2	6.2
18				16.2	7.2

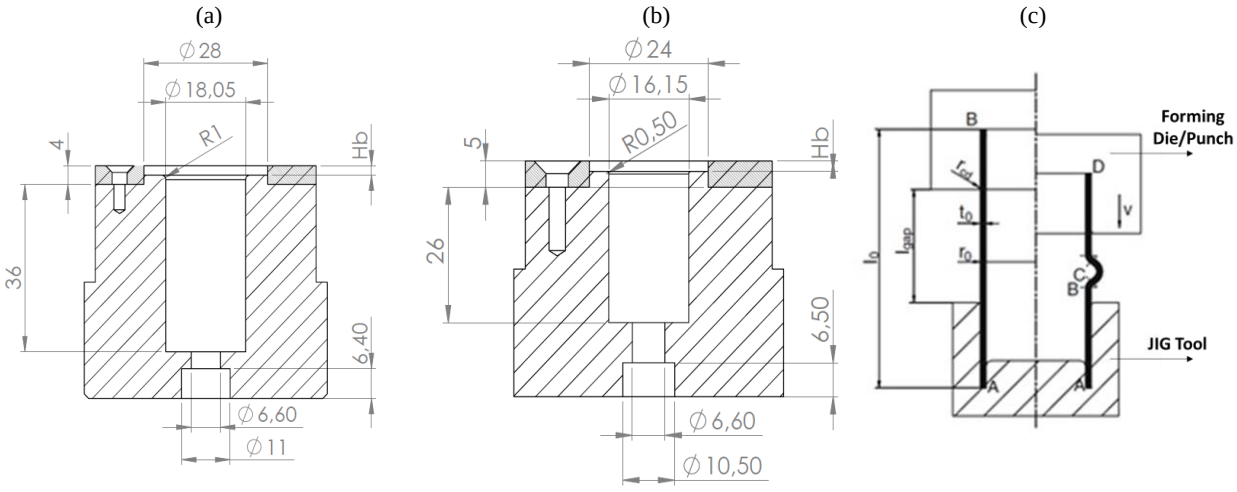

Figure 52 - Technical drawing of the forming dies. (a) Reference E3, (b) E1 (cooler side), (c) schematic representation of the tool assembly and major process parameters.

For each case were performed 5 parts to ensure that the process were repeatable. The metallography analysis, to verify the occurrence of metal cracking, was only performed in 4 specimens for each reference (Case 2, 5, 7, 8 and 11, 13, 16, 17), as these cases are the most representative of the influence of the bead dimensions in material cracking.

The process parameters (H_b, L_o, L_{gap}) differs for each reference, as the use of the same parameters led to bead defects, material failure or material non-deformation and therefore would not meet the purpose of the experimental design of validate the purposed solution (Chapter 5.3).

For case 7, 8, 9 and 10, 11, 12 it is imposed a minimum bead height (A_{min}) according to the purposed solution plus a security coefficient of 15% regarding noise manufacturing variables, as die height tolerance (prototype tools), L_{gap} and L_0 tolerance, and lubrication regime. Regarding the performed experiments for the tube ∅16x0.5 mm was not possible conduct tests for a die height (H_b) lower than the purposed minimum die height, due to forming tool limitations, which will be important to validate the purposed solution as this would permit verify if material cracking will occur for a bead geometry that not respect the minimum bending radius theory.

6.2 Numerical simulation

The numerical modelling of the compression beading operation of the part reference E3 (∅18x1mm) was accomplished by means of FEA Software Abaqus 6.1 and planned in accordance to the experimental procedure in order to reproduce all the experimentally observed modes of deformation and resultant bead geometries.

The forming tools are modelled as discrete rigid shell surfaces by using four-node rigid element type (R3D4). The boundary conditions are defined in order that no deflections or rotations are allowed for nodes constituting the surface, and velocity boundary condition along the y-axis.

A four-node shell element (S4R) is used to model the tube, as the ratio between the reference radius and thickness is high and, the stresses and strains along the thickness of the tube are negligible. That way, time and computational memory saving and an easier post processing analysis can be achieved. A y-lock boundary condition was used for the tube ends plane nodes, which fixes the displacement in the y direction, not being defined any other boundary condition for the other nodes. A constant element size of 1mm was used, being the results convergent for that mesh size.

The contact between tools and the tube are modelled as penalty contact and a coefficient of friction of 0.15 is used. The coefficient of friction was not measured experimentally, however it is a standard value for a combination of lubricated steel surfaces.

The incremental displacement, along the Y-axis, of the punch/die is 1.2mm which represents around 10% of the length of the tube (L_0).

The modelled material properties were the same one used to produce the reference part E3, AISI 304 L related to material number E1310012608 (Table 8 and Equation 5.2). The data provided to Abaqus was:

- Young's Modulus E – 195 GPa;
- Poisson's Coefficient ν – 0.3;
- Density – 7.9 Kg/m^3;
- Points which defines the relation True Stress vs. True Strain (Equation 5.2).

The material was considered isotropic and the mechanical properties in the weld bead and HAZ not considered.

In all the simulations run, the standard coordinate system was:

- X and Z perpendicular to the tube axis;
- Y for the vertical direction, parallel to the tube axis and die travel.

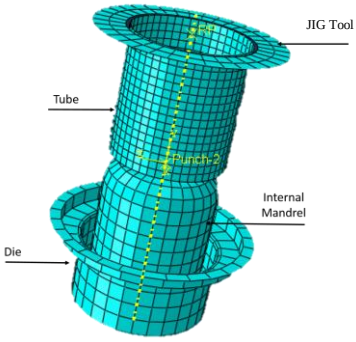

Figure 53 - Finite element model of the tube compression beading operation.

6.3 Results and discussion

By analyzing the numerical and experimental results it is noticed that the width of the beads depends on the L_{gap} and die height (H_b). The H_b (Annex C1.1 - Figure 1), also defines the bead height (A) while the L_c dimension of the die (Annex C1.1 - Figure 3) sets the positioning of the bead (distance between the tube end and the bead).

Figure 54 shows the relation between the mentioned manufacturing parameters and the bead width, and also a comparison between the experimental and numerical results, for cases 1 to 9, revealing a good agreement between them.

(a) (b)

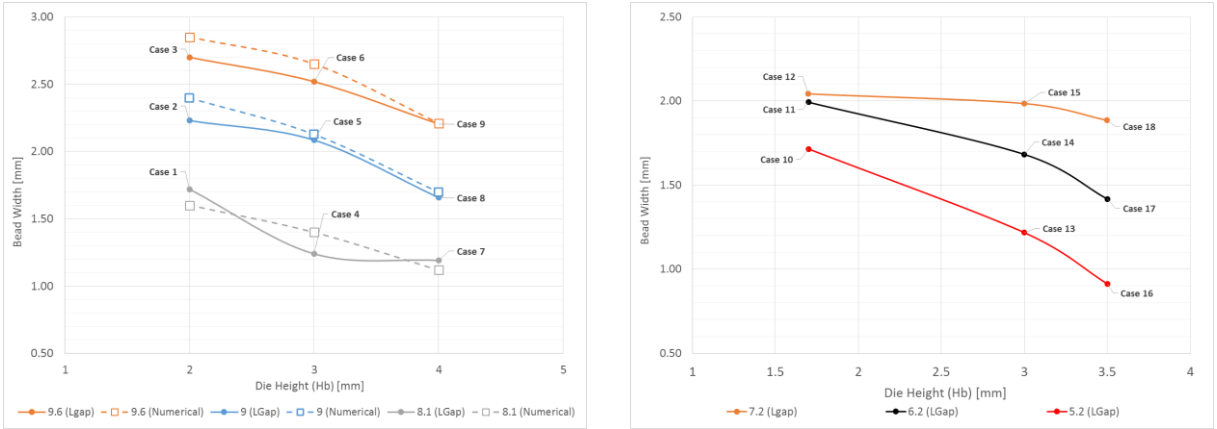

Figure 54 - Relation between manufacturing parameters and bead width. (a) ⌀18x1mm, (b) ⌀16x0.5mm.

As expected, the width of the beads increases with the gap opening and decreases with the die height. For the reference diameter of ⌀16x0.5 mm, it is noticed a bead width threshold of 2 mm (case 12) as a decrease of the gap opening does not lead to an increase of the bead width. Moreover, in case 11 and 12, it can be visually observed the beginning of a surface geometrical depression and an almost null radius of concordance (≈ 90º).

Although the designed experimental and testing plan did not permit to successful conclude about the influence of the diameter and thickness of the reference tube, is noticed that a lower ratio between the reference radius and thickness, r_0/t_0, allows to obtain a wider bead.

Considering the practical function of the beads, although a small bead width is obtained in case 7 and 16, it is considered acceptable as design and manufacturing requirements are not compromised.

During production and measurements of the specimens was also detected some asymmetries and a non-uniform height of the bead, mainly in the specimens that present higher diameters. These asymmetries are mainly caused by a misalignment between the die and the tube ends, and due to geometry imperfections of the raw material. Those geometric imperfections will become more influential as the L_{gap} increases. The misalignment was mainly registered during the production of reference E1 (Engine side), due to a non-effective control of the tube geometry after the bending operation and a clearance between the tube and the JIG tool.

More than the relation between the process parameters and the bead width it is essential to evaluate the overall geometry of the bead and its influence on the occurrence of material cracking. Figure 55 shows the predicted geometry of the bead, related to reference E3, by numerical simulation. According to the achieved numerical results, the increase of the bead width leads to a decrease of the inner radius of the bead. As a matter of fact, due to the plastic deformation mechanism, the increase of the bead width leads to an elliptical geometry, a smaller inner radius and consequently an increase of the compressive stresses and metal grains rotation at the tip of the bead in order to absorb the plastic deformation. In Figure 56 is presented metallographic sections of beads that have the same height. Being easily noticed what was described above regarding the deformation mechanism. It has not been relevant to develop a numerical analysis regarding other tube dimensions (r_0/t_0 ratio) since there aren't any differences revealed between them, as far as material flow is concerned.

Therefore as explained in the purposed solution (Chapter 5.3), it is not sufficient to guarantee a bead height dimension since the bead width or bead diameter also plays an important role. Then, the design guidelines should define the minimum bead height and the maximum bead diameter/width, in order to guarantee that the formability, regarding material cracking, are not exceed. However, a greater bead height allows to achieve larger bead diameters without compromising the inner radius and is indispensable to guarantee that a minimum radius is accomplished.

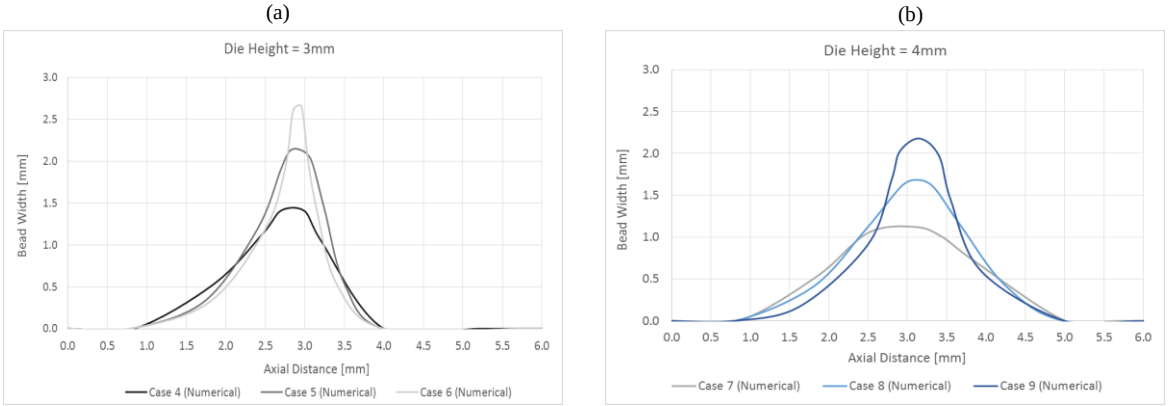

Figure 55 - Geometry of the achieved bead for different manufacturing parameters (numerical simulation).

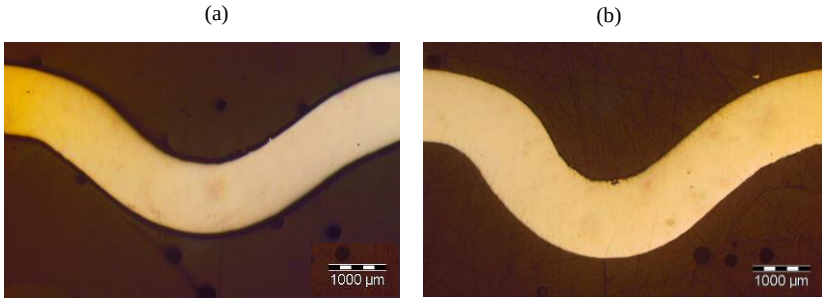

Figure 56 - Metallographic sections referent to case 16 (a) and 17 (b). (Both specimens have the same bead height)

The first analyses of the inner surface of specimen correspondent to case 2, 5, 8 and 11, 14, 16 reveals lower roughness for the beads which present a higher height and smaller diameter, as noticed in Figure 57 and 58. Concerning case 2, referent to a bead height and die height of 2mm the area which reveals roughness is small due to the fact that the inner surfaces of the bead are adjacent.

Comparatively to the analyses done in Chapter 5.2.2 referent to the bead geometry applied to reference E3 (⌀18x1 mm), currently in production, the results for cases 5 and 8 show evidently lower roughness. The lowering ratio cannot be quantified however, it is easily verified by visual observation. Concerning the first analyses done in Chapter 5, related to bead geometry applied to E1 a comparison cannot be presented, as it was not possible to perform experiments to this reference, as mentioned before.

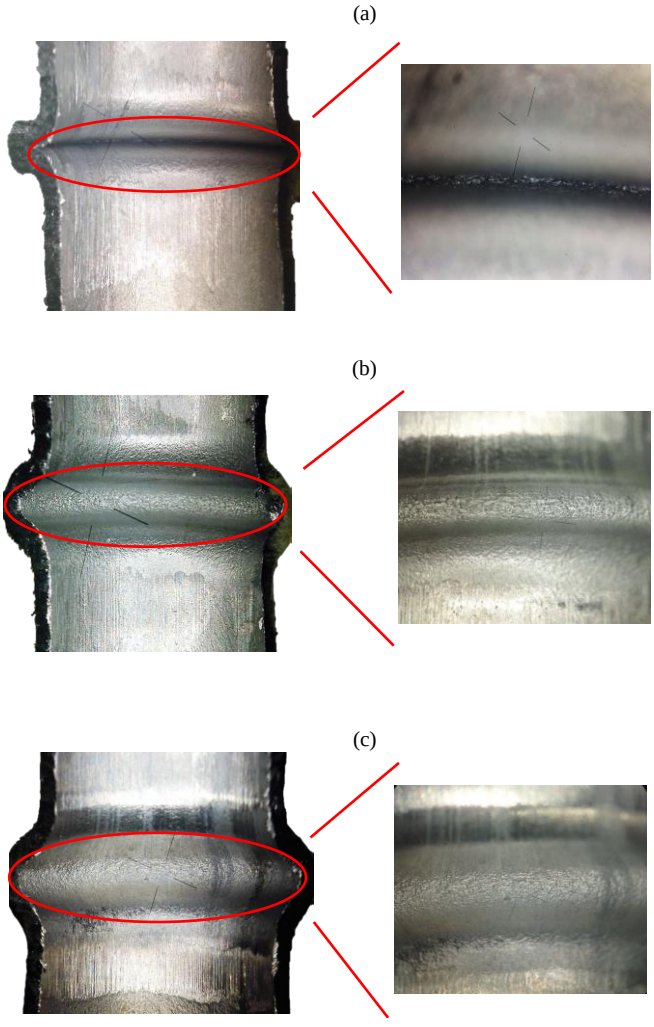

Figure 57 - View of the inner surface of the bead through a stereomicroscope. (a) Case 2, (b) case 5, (c) case 8.

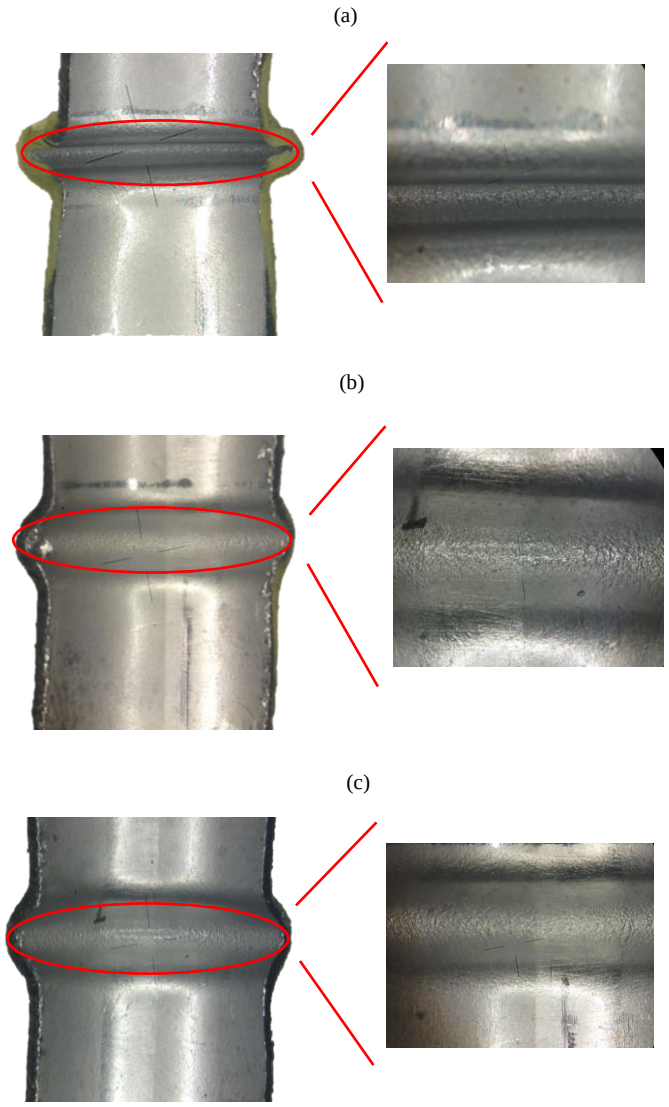

Figure 58 - View of the inner surface of the bead through a stereomicroscope. (a) Case 11, (b) case 14, (c) case 16.

The metallographic tests regarding cases 2, 5 that are related to the bead applied to the reference part E3 (⌀18x1 mm) reveal material cracking on the inner surface at the tip of the bead, as detected before (Chapter 5.2.2). The crack length, related to case 5, is really short however it cannot be acceptable as the effects of it in part lifetime are not known and because it is possible to achieve suitable bead geometries, which are crack free, and guarantee higher quality.

The results related to cases 7 and 8, do not reveal any material cracking being only detected some roughness due to compressive stresses, grain rotation and thickness increase. As no material discontinuity is revealed and the bead geometry is within the design and manufacturing requirements, the achieved bead dimensions in cases 7 and 8 are considered acceptable. The achieved range of dimensions (bead height, bead diameter) that guarantee no material cracking, presented in Table 11, are narrow however they are suitable for the bead application. In Figure 48 are presented the metallographic results for case 7, being the other results shown in Annex D1.1, 1.2, 1.3 and 1.4.

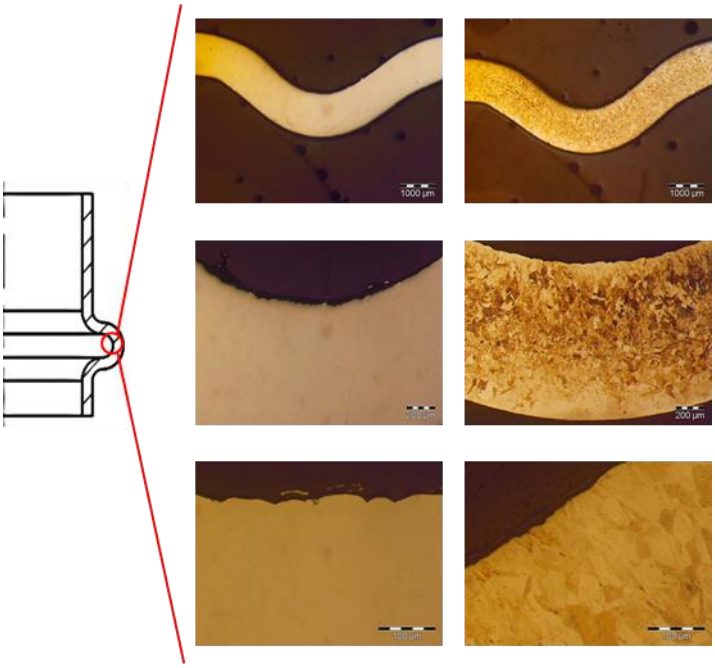

Figure 59 - Metallographic section of the bead referent to case 7 (magnification of 23x, 75x and 150x).

Concerning the bead related to the ⌀16x0.5 mm tube (cases 11, 14, 16 and 17), applied to the reference part E1 (Engine side) the metallographic results do not show any material cracking for all the experiments performed (cases 10 to 18). A different outcome will be unexpected, as the die height (H_b) used in these cases is higher than the purposed minimum bead height in Chapter 5.3. However some of these specimens presented some geometrical defects, as mentioned above, therefore not all of them can be acceptable, as apart from eliminating the material cracking it is also supposed to avoid geometrical and dimensional defects and ensure that the bead is easy to manufacture. Since one of the causes for these dimensional and geometrical defects related to a design parameter (bead width/ diameter), it has to be limited. Therefore, based on the metallographic and dimensional results, are only considered acceptable the specimens which reproduce cases 10, 13, 14, 16, 17. The bead dimensions related to these cases are presented in Table 11.

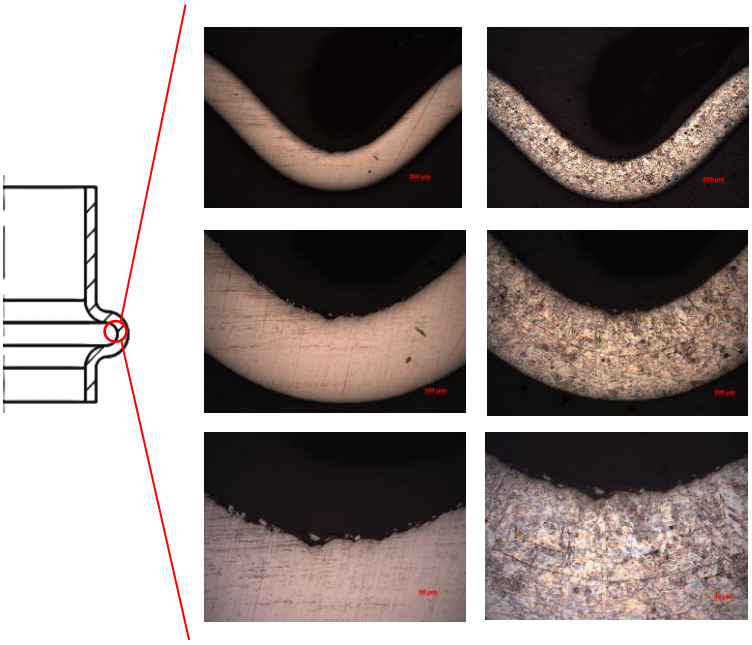

Figure 60 - Metallographic section of the bead referent to case 14 (magnification of 23x, 75x and 150x).

The minimum bead width is defined, as 1.2 mm, in order to guarantee that the practical application of it is not compromised. These minimum bead width has been defined in partnership with the manufacturing department in order to guarantee that the manufacturing requirements are met. To guarantee no material cracking is enough impose a minimum bead height and maximum bead width.

Regarding the purposed solution, presented in Chapter 5.2, which defines a minimum bead height based on the minimum bending radius rule for sheet bending. The experimental tests that impose these calculated bead heights are cases 7, 8, 9 and 10, 11, 12, as mentioned above.

According to the metallographic results, related to tube dimensions of ⌀18x1 mm, the only specimens which do not show material cracking are those that reproduce cases 7 and 8 and respect the minimum bead height, analytically defined. The same is related to the bead geometry applied to tube dimensions of ⌀16x0.5 mm, not being detected material cracking for beads that have a bead height equal or above 1.7mm. However it was not possible verify the occurrence of material cracking for bead heights lower than the defined minimum bead height, due to forming tools limitations.

Based on the experimental results were defined the bead dimensions and tolerances for two tube references, which guarantee no material cracking and lower dimensional and geometry defects. For tube references that have not been studied during this project, may have its height defined by applying Equation 5.2 (plus a security coefficient of ≈15%) and a bead width equal to the minimum bead width (1.2 mm) defined according to design and manufacturing requirements. For design requirements that impose a bead width wider than 1.2 mm, a metallographic test should be performed in four different planes (Figure 40) to assess the occurrence of material cracking. The part may only be acceptable if no material discontinuity is identified in order to guarantee that it is according to the quality requirements.

Regarding the influence of the bends in the material mechanical properties, analyzed in Chapter 5.2.3, it is also essential taking it into account in the bead design as the developed design rules can only be applied for virgin material (not affected by plastic deformation). Therefore is necessary define a minimum distance between the bead and the bend (L) which guarantee that the bead is applied in a flat section that is not affected by plastic deformation. The experimental tests performed in Chapter 5.2.3 shows the influence of plastic deformation in the Vickers microhardness. Based on that are achieved the minimum L distance for a tube reference dimension of ⌀16x0.5 mm, a bend radius of 22mm and a bending angle of 45º,65º and 90º.

In Table 11 and 12 are presented the dimensions that must be applied to the bead geometry, and in Figure 61 the technical drawing of a generic bead and bend geometry.

It is important to point out, that an analyses to the bead design applied to the coolant spigot parts that are currently in production at BWES show that 70% of them does not respect the defined design guidelines, therefore there is a risk of material cracking, at the bead zone, in these part references.

Table 11 - Reference dimensions for the bead geometry (in mm).

Raw Material	Reference Outside Diameter (D_0)	18 (± 0.1)	16 (± 0.1)	NA
	Reference Thickness (t_0)	1 (± 0.15)	0.5 (± 0.15)	NA
Bead Geometry	Minimum Bead Height (A)	4	3	Eq. 5.2 + 15%
	Bead Width (H)	1.2	1.2	1.2
		1.7	1.6	
	Minimum Concordance Radius (R)	1	1	1

Table 12 - Minimum distance reference between the bead and the bend (in mm).

Raw Material	Reference Outside Diameter (D_0)	18 (± 0.1)			16 (± 0.1)		
	Reference Thickness (t_0)	1 (± 0.15)			0.5 (± 0.15)		
Bending Geometry	Bend Radius (R_b)	21			22		
	Bend Angle (α)	45º	60º	90º	45º	60º	90º
	L	9[(a)]			13.5	14	15

[(a)] Based on the results obtained for the part reference E3 (Chapter 5.2.3).

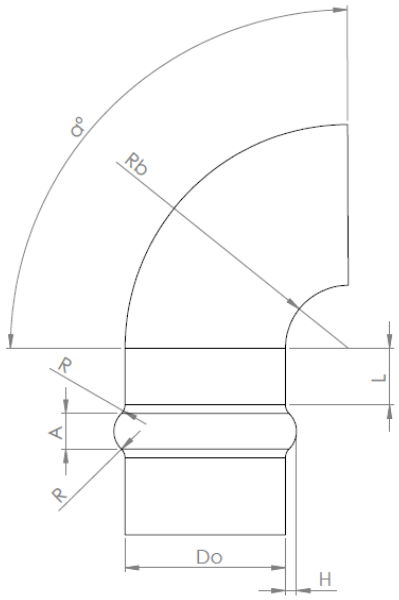

Figure 61 - Technical drawing of a coolant spigot sample.

7 Conclusions and future developments

This chapter summarizes the main conclusions of the project and sets out the main developments and results achieved. Moreover, further work aimed at increasing the knowledge in the field of tube compression beading and accomplishing possible improvements to the current process in BorgWarner Emissions Systems will also be proposed.

7.1 Conclusions

This project presents an overall analysis of quality defects in the bead geometry applied to coolant spigot parts, with focus on material cracking that occurs during the tube compression beading operation regarding an incorrect design of the bead geometry, as concluded from a first analysis of the manufacturing process and bead properties.

From a first analysis, regarding the effect of the weld in material mechanical properties it is concluded, for stainless steel (AISI 304) welded tubes, that it does not have a major effect on the final quality of the bead geometry as material cracking and major dimensional or geometry asymmetries are not identified, on the weld plane. Consequently, during the design and manufacturing process it is not relevant to take it into account.

Regarding the material cracking detected in both studied part references, through the analysis of the microhardness results, metallographic tests, and stereoscopic observation it has been observed that it occurs because the formability limit of the material is almost exceeded. In accordance with these result analyses, basing the bead dimensioning on the minimum sheet bending radius theory in order to minimize the material deformation, and compressive and circumferential stress is proposed.

In order to validate the proposed design, an experimental procedure and forming tools according to the required bead geometries were developed. The experimental results show no material cracking for specimens which respect the defined minimum bead height dimension based on the minimum sheet bending radius theory. It is necessary to point out that the bead diameter also plays an important role on material cracking as verified from numerical results. However, it has also been seen that the analytically defined, minimum bead height enables us to achieve larger bead diameters without compromising the inner radius of the bead.

Regarding the influence of the raw material in the bead design, as far as material cracking is concerned, the parameters that have a direct influence on the design are the reference thickness of the tube and material elongation.

Based on the experimental results, design guidelines for two tube references, which guarantee no material cracking and lower dimensional and geometry defects were designed. For tube references that have not been studied during this project, the design should be supported on the defined minimum bead height and width, as it guarantees that the occurrence of material cracking is limited as proved by experimental tests. Regarding raw material requirements, the

welded tube dimensional class tolerance should be defined as T4/D4 or T5/D5 in order to guarantee that the thickness impact on the bead dimensions is as minimal as possible.

With respect to the influence of bending on the mechanical properties of the material on the flat section of the tube, where the bead geometry is applied, a minimum distance between the bend and the bead was defined which ensures that the material is not strain hardened and the minimum bead height design rule can be correctly applied, for a tube reference of ⌀16x0.5mm. For other tube reference dimensions, the same experimental methodology should be carried out.

Considering the influence of major process parameters, experimental results show that the bead width increases with the gap opening (Lgap) and decreases with the die height (Hb). The bead height is set by the die height and the position of the bead is defined by the Lb dimension of the forming tool. With regard to the influence of the tube reference dimensions, the experimental plan was not suitable to come to watertight conclusions. However, it is noticed that a lower ratio between the reference radius and the thickness of the tube (r0/t0) enables us to achieve wider beads.

The developed design guidelines and the study of the influence of the major manufacturing parameters will certainly have a positive impact on the occurrence of defects and on the efficiency of the design and manufacturing development process.

7.2 Future developments

Implementation of the design guidelines in BWES

The experimental results are restricted to only two tube references; therefore in order to fully define a design guideline for bead geometries based on experimental results, the methodology followed in this report should be carried out regarding more tube references.

In the short term, there is the need to apply the developed design guidelines at BWES. It is necessary for the quality and manufacturing department together to define the necessary adjustments to the manufacturing process and to quality and dimensional control tests performed on the different production lines for new coolant spigot references.

Regarding other coolant spigot parts that are currently in production, about 70% of them do not respect the defined design guidelines, therefore it is necessary to study the possibility of adjusting the bead design applied to these coolant spigot references and perform metallographic tests to those parts that are considered critical. One example of these parts is part reference E4, being presented in Annex E1.1 the metallographic test results, which shows material cracking.

Studying proposals for improvements to the manufacturing process

During manufacturing, noise manufacturing parameters that lead to dimensional and geometry defects were identified. As mentioned during that report, the misalignment between the die and the tube end and the clearance between the tube and the JIG tool have a huge influence on geometry/dimensional asymmetries. The suggestion to overcome this problem is to improve the dimensional/geometry control tools regarding the bending operation, related to reference E1 and E2, as it does not perform an effective control of the overall geometry. The geometry control tool referent to the reference E3 can be used as an example of an effective tool.

However, the best solution might be to perform the beading operations before the bending operation. That way the constraining effects due to bending (material hardening, misalignment between tube and die, non-calibrated tube) will not be experienced in the beading operation and the calibration operation will not be necessary which will also enable the achievement of a short cycle time. Regarding the clearance between the tube and the JIG

tool a dimensional inspection of the JIG tool should be performed at the beginning of the production of each new batch.

References

Ahmetoglu, M. and T. Altan. 2000. "Tube hydroforming: state-of-the-art and future trends". *Journal of Materials Processing Technology* no. 98 (1):25-33.

Alaswad, A., K. Y. Benyounis and A. G. Olabi. 2012. "Tube hydroforming process: A reference guide". *Materials & Design* no. 33:328-339.

Almeida, B. P. P., M. L. Alves, P. A. R. Rosa, A. G. Brito and P. A. F. Martins. 2006. "Expansion and reduction of thin-walled tubes using a die: Experimental and theoretical investigation". *International Journal of Machine Tools and Manufacture* no. 46 (12–13):1643-1652.

Alves, L. M. and P. A. F. Martins. 2012. "Tube branching by asymmetric compression beading". *Journal of Materials Processing Technology* no. 212 (5):1200-1208.

Alves, L. M., C. M. A. Silva and P. A. F. Martins. 2014. "End-to-end joining of tubes by plastic instability". *Journal of Materials Processing Technology* no. 214 (9):1954-1961.

Alves, L. M., C. M. A. Silva and P. A. F. Martins. 2015. "Innovative Cold Joining Technologies Based on Tube Forming". (Manufacturing Review).

Alves, L.M., J.G. Medeiros and P.A.F. Martins. 2011. "Cold End Forming of Welded Steel Tubes". *International Journal of Manufacturing, Materials, and Mechanical Engineering* no. 1:18-30.

Alves, L.M.M. and P. A. F. Martins. 2013. "Innovative Tube Forming and Joining ". Paper presented at 46th Plenary Meeting Proceedings in Paris.

Alves, Luis M., Eduardo J. Dias and Paulo A. F. Martins. 2011. "Joining sheet panels to thin-walled tubular profiles by tube end forming". *Journal of Cleaner Production* no. 19 (6–7):712-719.

Alves, M. L., B. P. P. Almeida, P. A. R. Rosa and P. A. F. Martins. 2006. "End forming of thin-walled tubes". *Journal of Materials Processing Technology* no. 177 (1–3):183-187.

Baddoo, N. R. 2008. "Stainless steel in construction: A review of research, applications, challenges and opportunities". *Journal of Constructional Steel Research* no. 64 (11):1199-1206.

Badoo, N. R. and B. A. Burgan. 2012. *Structural Design of Stainless Steel*. The Steel Construction Institute

Barralis, J. and G. Maeder. 2005. *Prontuário de Metalurgia* Fundação Calouste Gulbekian.

BorgWarner. Accessed March 28, 2016. http://www.borgwarner.com.

Gonçalves, A. 2013. "Numerical and Experimental Analysis of Asymmetric Instabilities by Tube Forming", Instituto Superior Técino

Gouveia, B. P. P, L. M. Alves, P. A. R. Rosa and P. A. F. Martins. 2006a. "End-Forming Operations of Thin-Walled Tubes using a Die: Expansion, Reduction and Inversion". Paper presented at 5th International Conference on Mechanics and Materials in Design.

Gouveia, B.P.P, L. M. Alves, P. A. R. Rosa and P.A.F. Martins. 2006b. "Compression beading and nosing of thin-walled tubes using a die: experimental and theoretical investigation". *International Journal of Materials and Design* no. 3:7-16.

Handbook of Stainless Steel. 2013. Outokumpu.

Hussain, Jaffar, K. Palaniradja, N. Alagumurthi and R. Manimaran. 2012. "Effect of Exhaust Gas Recirculation (EGR) on Performance and Emission characteristics of a Three Cylinder Direct Injection Compression Ignition Engine". *Alexandria Engineering Journal* no. 51 (4):241-247.

"Introduction to Stainless Steels". In. 1994. *Stainless Steels* ASM International.

Joseph, A.D. 1988. "Forming of Stainless Steel". In *Forming and Forging - ASM Handbook*. ASM International.

Leitão, P. 2013. "Novo Processo Tecnológico para o Fabrico de Flanges em Tubos", Instituto Superior Técnico.

Mori, Ken-ichiro, Niels Bay, Livan Fratini, Fabrizio Micari and A. Erman Tekkaya. 2013. "Joining by plastic deformation". *CIRP Annals - Manufacturing Technology* no. 62 (2):673-694.

Ren, N., M. Zhan, H. Yang, Z. Y. Zhang, Y. T. Qin, H. M. Jiang, K. S. Diao and X. P. Chen. 2012. "Constraining effects of weld and heat-affected zone on deformation behaviors of welded tubes in numerical control bending process". *Journal of Materials Processing Technology* no. 212 (5):1106-1115.

Rosa, Pedro A., Jorge M. C. Rodrigues and Paulo A. F. Martins. 2004. "Internal inversion of thin-walled tubes using a die: experimental and theoretical investigation". *International Journal of Machine Tools and Manufacture* no. 44 (7–8):775-784.

S.D., Washko and Aggen G. 1990. "Wrought Stainless Steels". In *Properties and Selection: Irons Steels and High Performance Alloys - ASM Handbook*. ASM International.

Schaeffer, L. and A. M. Brito. 2007. "FEM Numerical Simulation and Experimental Investigation on End-Forming of Thin-Walled Tubes Using a Die". *Steel Research International* no. 78:798-803.

Tekkaya, A. Erman, Horst Baier, Dirk Biermann, Jürgen Fleischer, Gisela Lanza, Volker Schulze, Michael F. Zäh, Alessandro Selvaggio, L. M. Alves and P. A. F. Martins. 2014. "Rubber Assisted Compression Beading of Tubes". *Procedia CIRP* no. 18:45-50.

Zhan, Mei, Hongfei Du, Jing Liu, Ning Ren, He Yang, Haomin Jiang, Keshan Diao and Xinpin Chen. 2010. "A method for establishing the plastic constitutive relationship of the weld bead and heat-affected zone of welded tubes based on the rule of mixtures and a microhardness test". *Materials Science and Engineering: A* no. 527 (12):2864-2874.

Zhan, Mei, Kun Guo and He Yang. 2016. "Advances and trends in plastic forming technologies for welded tubes". *Chinese Journal of Aeronautics* no. 29 (2):305-315.

ANEXO A 1.1: Technical Drawing – Coolant Spigot Reference E1

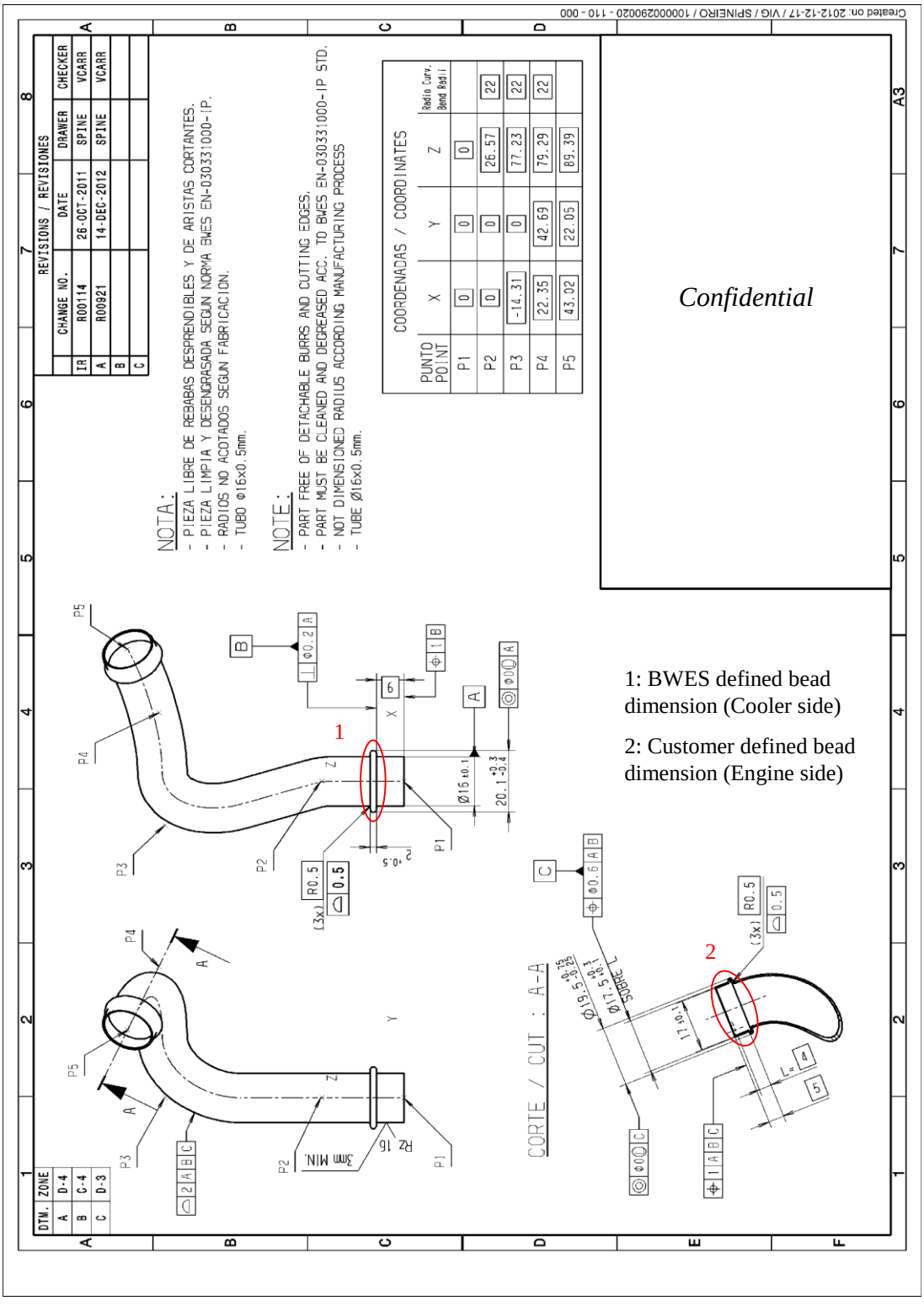

ANEXO A 1.2: Technical Drawing – Coolant Spigot Reference E2

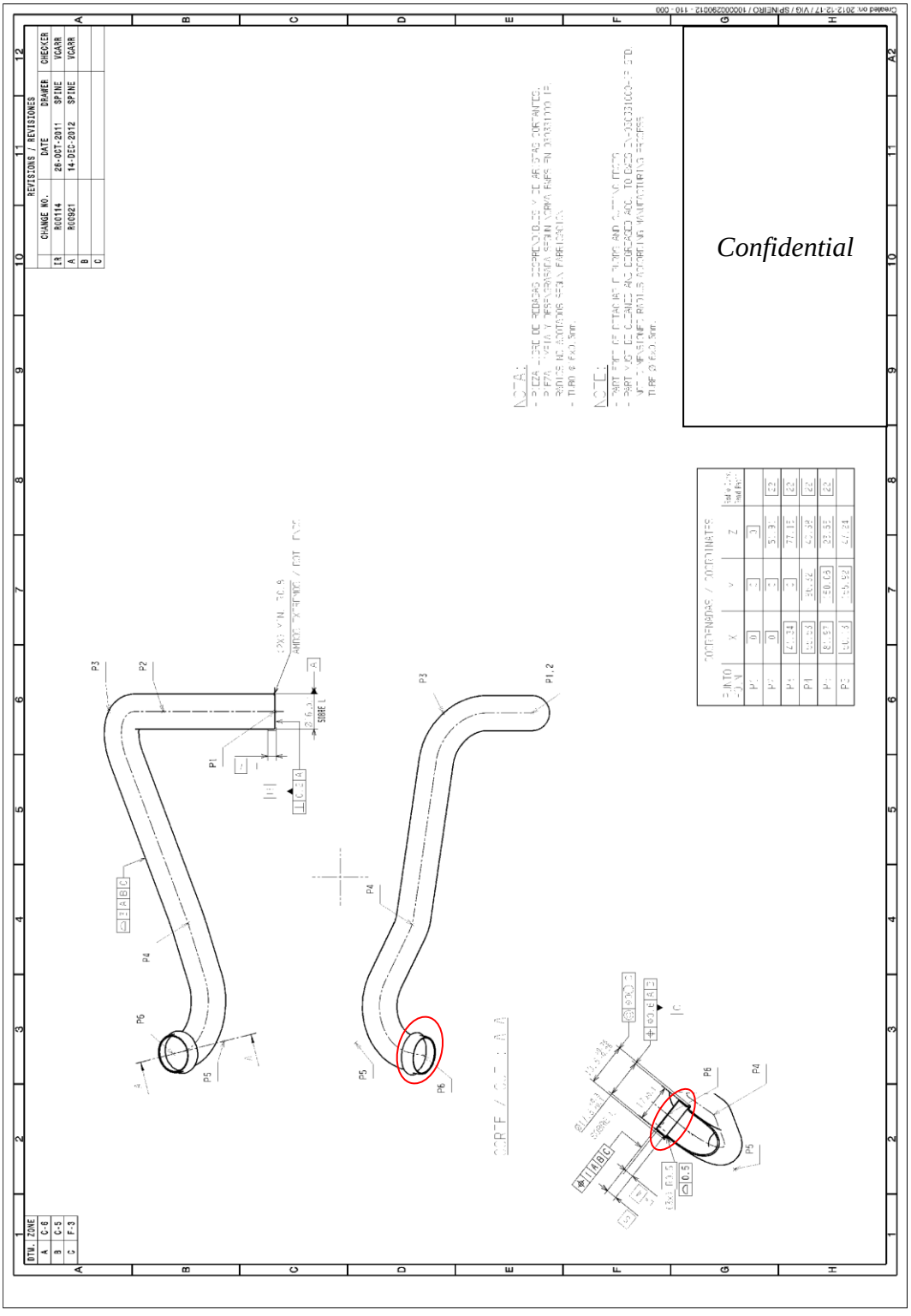

ANEXO A 1.3: Technical Drawing – Coolant Spigot Reference E3

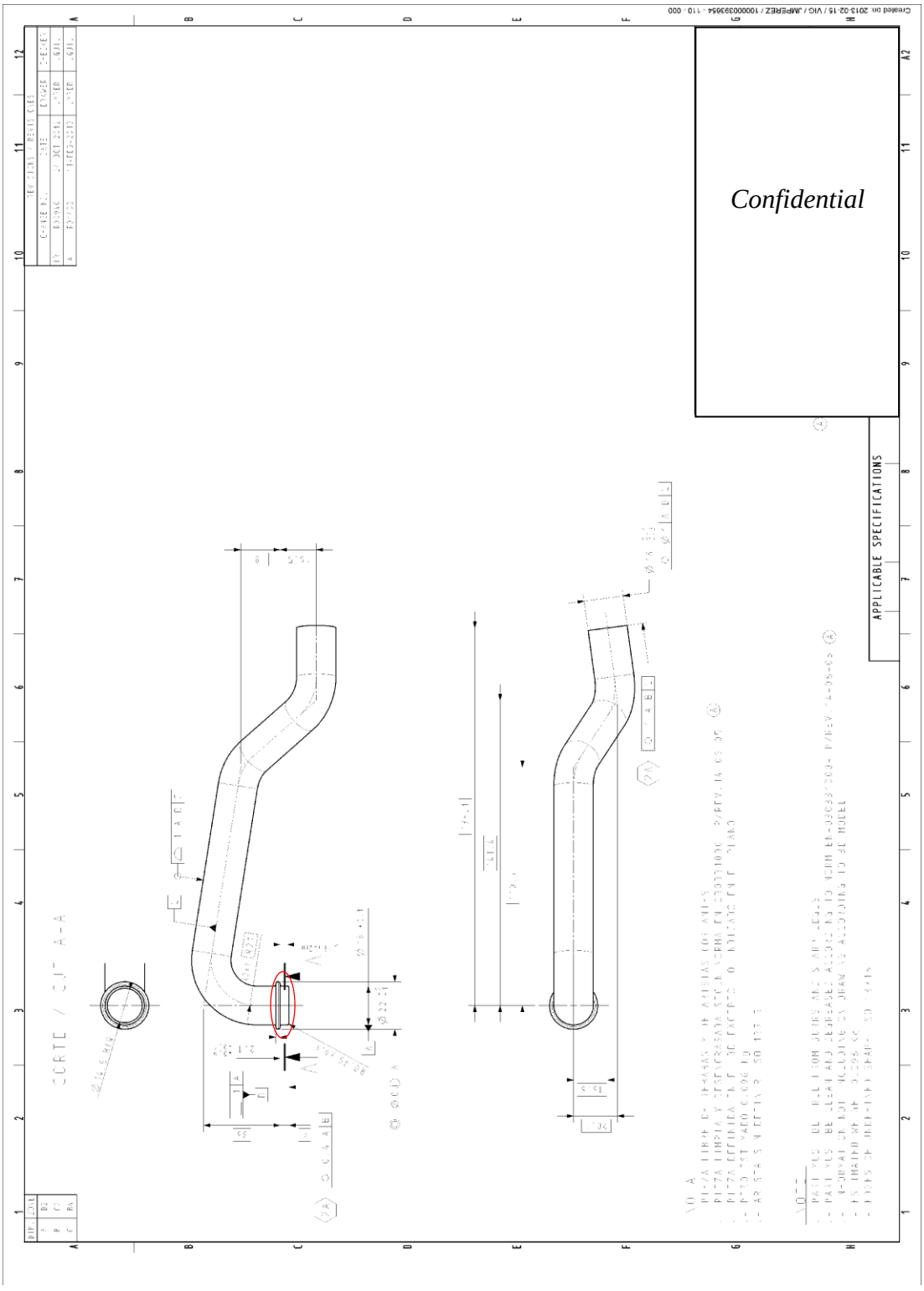

ANEXO A 2.1: Control Instructions – Coolant Spigot Reference E1

BorgWarner

INSTRUÇÃO DE CONTROLO

Página 1 de 2

GAMA Nº : GC-02144

DATA : 24/03/2015

Confidential

1

Peças sem golpes, nem deformações.

Verificar ausência de rugas nas curvas. Ver peças amostra no posto.

2

2.2.- Verificar a posição neste extremo atendendo à cala P/NP.

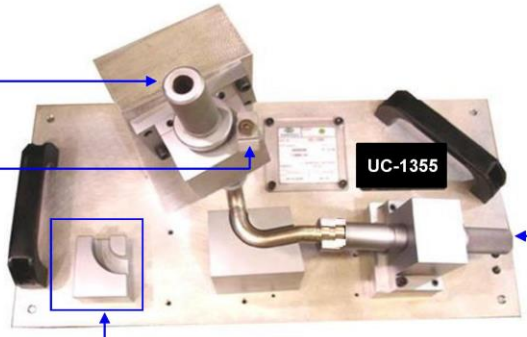

2.1.- Montar o tubo e verificar a posição neste extremo com a brocha a tope, jogo zero. O tubo deve tocar no fundo da brocha.

2.3.- Verificar o percurso da curva com a contraforma.

Nº	Controlo a realizar	Medida e tolerância	Meio controlo	A realizar por	Frequência	Registos
1	Aspecto	Ver indicações no croquis	Visual	Montador	5P Iní/Série	DT.9.1.5.1
				Autocontrolo	100%	
2	Geometria	Montabilidade no útil de controlo	UC-1355 *9095	Montador	5P Iní/Série	
				Autocontrolo	3Pças/15min	

VISTOS	M.Q.E./P.L.	A.E.	OBSERVAÇÕES:	Controlo revisões	Data	Causa
					14/03/13	Alteração das fotos dos UC´s. Evolução da refª cliente.
					02/08/13	Alterado calibre P/NP de controlo Ø bordeado lado saída.
					24/03/15	Transferência do processo fabricação para Viana Castelo.

BorgWarner	**INSTRUÇÃO DE CONTROLO** *Página 2 de 2*	GAMA Nº : GC-02144 DATA : 24/03/2015

Confidential

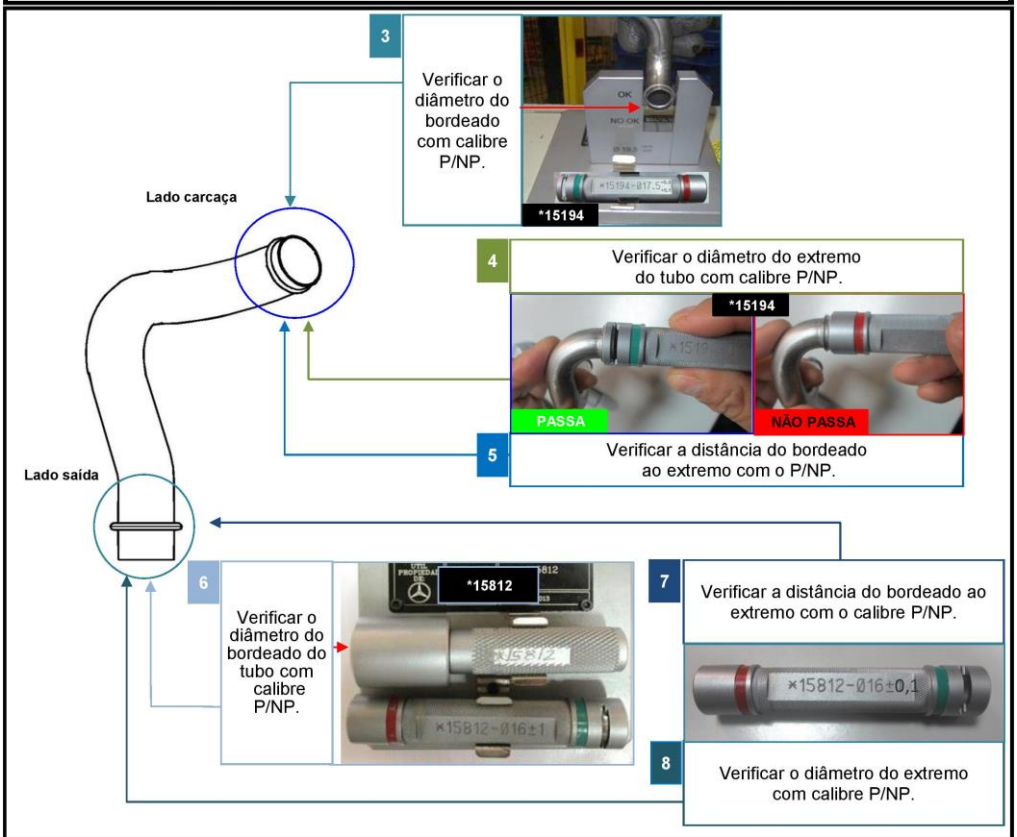

Nº	Controlo a realizar	Medida e tolerância	Meio controlo	A realizar por	Frequência	Registos
3	Ø bordeado lado carcaça ($19{,}5^{+0{,}75}_{-0{,}25}$)	Segundo Calibre de controlo P/NP ou paquimetro	UC-2219 *15194	Montador	5P Iní/Série	DT.9.1.5.1
				Autocontrolo	5Pças/Hora	
4	Ø extremo tubo lado carcaça ($17{,}5^{+0{,}3}_{+0{,}1}$)			Montador	5P Iní/Série	
				Autocontrolo	5Pças/Hora	
5	Distância bordeado lado carcaça (5±0,5)			Montador	5P Iní/Série	
				Autocontrolo	5Pças/Hora	
6	Ø bordeado lado saída ($20{,}1^{+0{,}3}_{-0{,}4}$) CS	Segundo Calibre de controlo P/NP ou paquimetro	UC-2242 *15812	Montador	5P Iní/Série	
				Autocontrolo	100%	
7	Distância bordeado lado saída (9±0,5)			Montador	5P Iní/Série	
				Autocontrolo	5Pças/Hora	
8	Ø extremo tubo lado saída (16±0,1)			Montador	5P Iní/Série	
				Autocontrolo	5Pças/Hora	

VISTOS	M.Q.E./P.L.	A.E.	OBSERVAÇÕES: Caracteristica significativa CS	Controlo revisões	Data	Causa
					14/03/13	Alteração das fotos dos UC´s. Evolução da refª cliente.
					02/08/13	Alterado calibre P/NP de controlo Ø bordeado lado saída.
					24/03/15	Transferência do processo fabricação para Viana Castelo.

ANEXO A 2.2: Control Instructions – Coolant Spigot Reference E2

BorgWarner | **INSTRUÇÃO DE CONTROLO** *Página 1 de 2* | GAMA Nº : GC-02148 | DATA : 24/03/2015

Confidential

1.- ASPECTO

Peças sem golpes, nem deformações.

Verificar a ausência deste defeito (bordeado amassado).

Verificar ausência de rugas nas curvas. Ver peças amostra no posto.

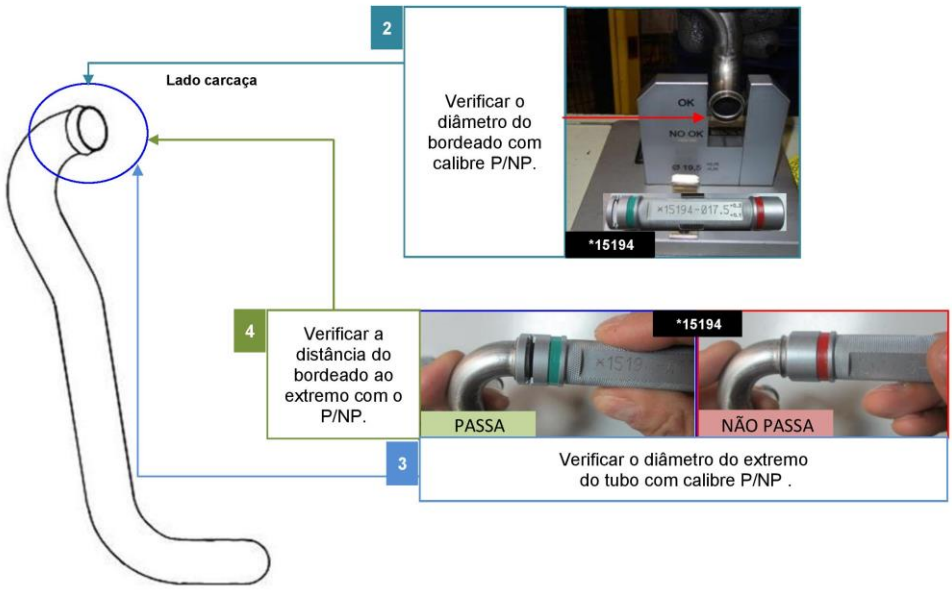

Nº	Controlo a realizar	Medida e tolerância	Meio controlo	A realizar por	Frequência	Registos
1	Aspecto	Ver indicações no croquis	Visual	Montador	5P Iní/Série	DT.9.1.5.1
				Autocontrolo	100%	
2	Diâmetro bordeado ($19,5^{+0,75}_{-0,25}$)	Segundo calibres de controlo ou paquimetro	UC-2219 *15194	Montador	5P Iní/Série	
				Autocontrolo	5Pças/Hora	
3	Diâmetro extremo tubo ($17,5^{+0,3}_{+0,1}$)			Montador	5P Iní/Série	
				Autocontrolo	5Pças/Hora	
4	Posição bordeado (5±0,5)			Montador	5P Iní/Série	
				Autocontrolo	5Pças/Hora	

VISTOS: M.Q.E./P.L. | A.E.

OBSERVAÇÕES:

Controlo revisões

Data	Causa
16/08/12	Migração da referência.
14/03/13	Alteração do UC. Evolução da refª cliente.
24/03/15	Transferência do processo fabricação para Viana Castelo.

BorgWarner

INSTRUÇÃO DE CONTROLO

Página 2 de 2

GAMA Nº : GC-02148

DATA : 24/03/2015

Confidential

5.- GEOMETRIA

5.6.- Subir o cilindro para controlar a rota da curva ao nominal.

5.1.- Montar o tubo no útil de controlo e fixá-lo com o apertador.

Utilizar esta cala para a início da curvadora.

5.4.- Controlar a posição neste extremo atendendo à cala P/NP.

5.2.- Verificar a posição neste extremo com a brocha a tope, jogo zero.

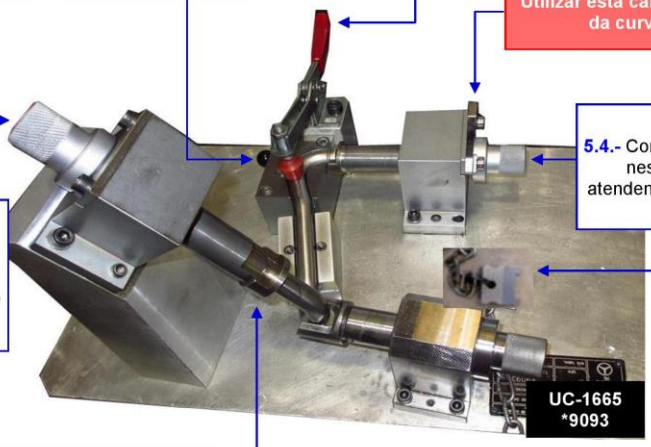

5.3.- Verificar que o tubo faz tope contra o fundo da brocha.

5.5.- Controlar a rota do tubo com a cala PASSA.

Nº	Controlo a realizar	Medida e tolerância	Meio controlo	A realizar por	Frequência	Registos
5	Geometria	Montabilidade no útil de controlo	UC-1665 *9093	Montador	5P Iní/Série	DT.9.1.5.1
				Autocontrolo	5Pças/Hora	

VISTOS	M.Q.E./P.L.	A.E.	OBSERVAÇÕES:	Controlo revisões	Data	Causa
					16/08/12	Migração da referência.
					14/03/13	Alteração do UC. Evolução da refª cliente.
					24/03/15	Transferência do processo fabricação para Viana Castelo.

ANEXO A 2.3: Control Instructions – Coolant Spigot Reference E3

BorgWarner

INSTRUÇÃO DE CONTROLO

Página 1 de 1

GAMA Nº : GC-03701

DATA : 30/11/2015

Confidential

1.- ASPECTO

Peças sem golpes, rebarbas nem deformações.

2.- GEOMETRIA CURVADO E RECORTADO

2.1.- Montar a peça na maquete de controlo, verificando que o tubo acopla na contraforma.

2.2.- Verificar com a brocha a orientação do extremo. A brocha deve entrar até ao fim (ver pela ranhura) e o comprimento com o P/NP.

2.3.- Verificar o comprimento do tubo atendendo à cala P/NP.

2.4.- Verificar com as 3 torretas a altura do tubo.

2.5.- Verificar com o P/NP o diâmetro do bordeado.

2.6.- Verificar com o P/NP o diâmetro do extremo Ø18±0,1.

2.7.- Verificar com o P/NP o diâmetro do extremo $Ø18^{-0,1}_{-0,3}$.

2.8.- Verificar o diâmetro e a espessura do bordeado atendendo à cala P/NP.

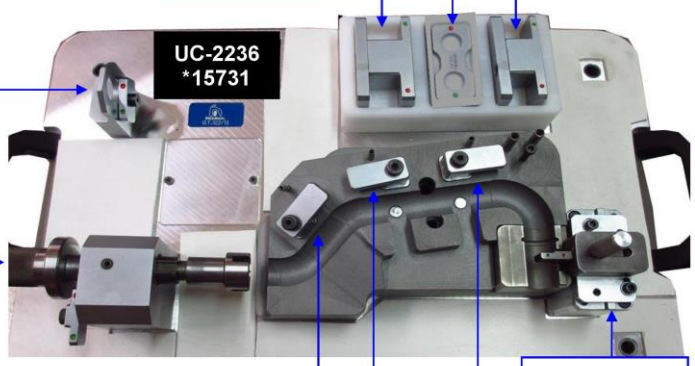

Nº	Controlo a realizar	Medida e tolerância	Meio controlo	A realizar por	Frequência	Registos
1	Aspecto.	Ver indicações no croquis	Visual	Operário	100%	DT.9.1.5.1
2	Geometria	Segundo maquete de controlo	UC-2236 *15731	Operário	100%	
	Diâmetro bordeado ao extremo	P/NP		Operário	5P Iní/Turno e cada hora	
	Ruptura bala	Bala inteira	Visual	Operário	1Pça/Hora e final lote	

VISTOS: M.Q.E./P.L. | A.E.

OBSERVAÇÕES:

Controlo revisões

Data	Causa
30/11/15	Evolução da refª: alteração componentes.
06/06/14	Evolução da refª.
23/09/14	Evolução da refª.

ANEXO B 1.1: Metallographic Sections - Reference E3

Figure 1 – Metallographic section: reference E3 (23x)

Figure 2 - Metallographic section: reference E3 (23x)

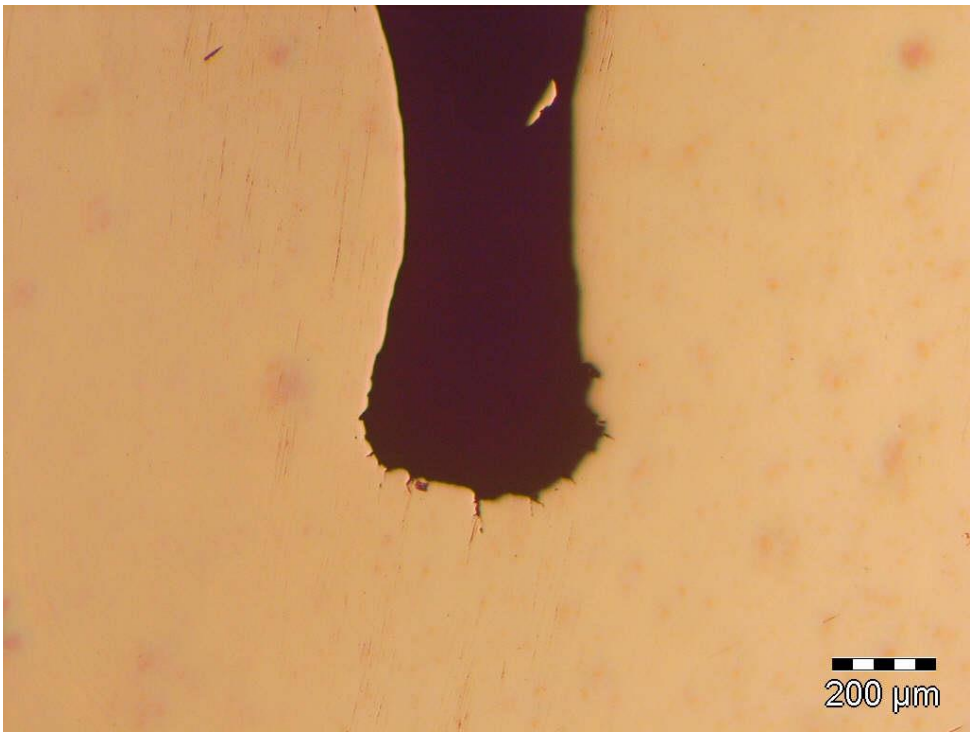

Figure 3 - Metallographic section: reference E3 (75x)

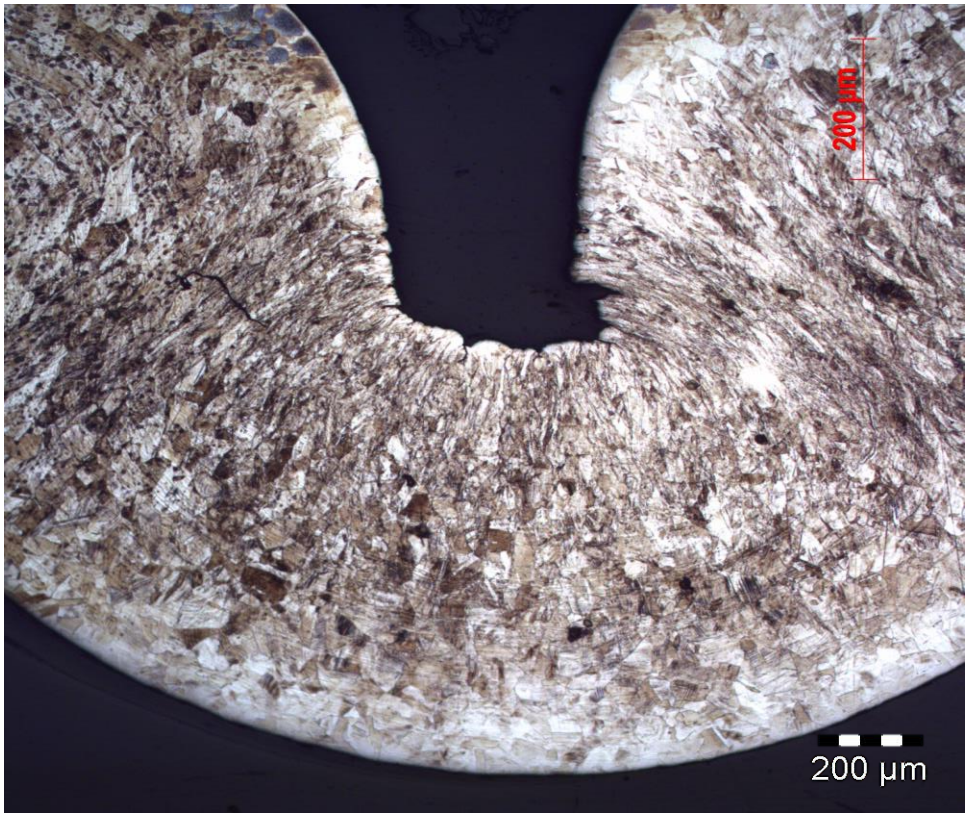

Figure 4 - Metallographic section: reference E3 (75x)

Figure 5 - Metallographic section: reference E3 (150x)

Figure 6 - Metallographic section: reference E3 (150x)

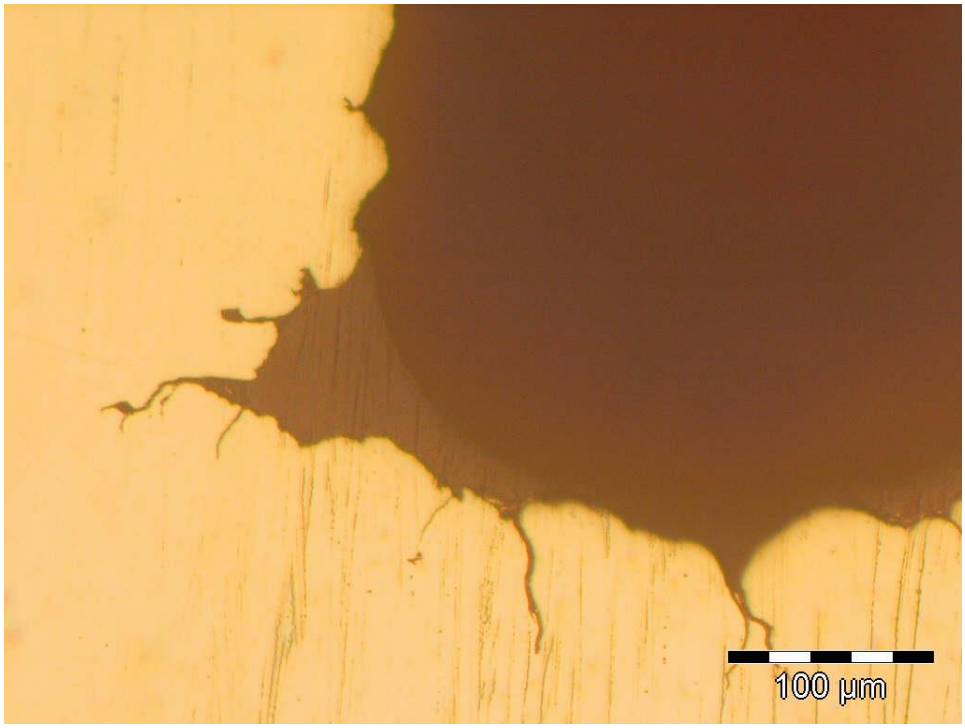

Figure 7 - Metallographic section: reference E3 (300x)

ANEXO B 1.2: Metallographic Sections - Reference E1 (Cooler side)

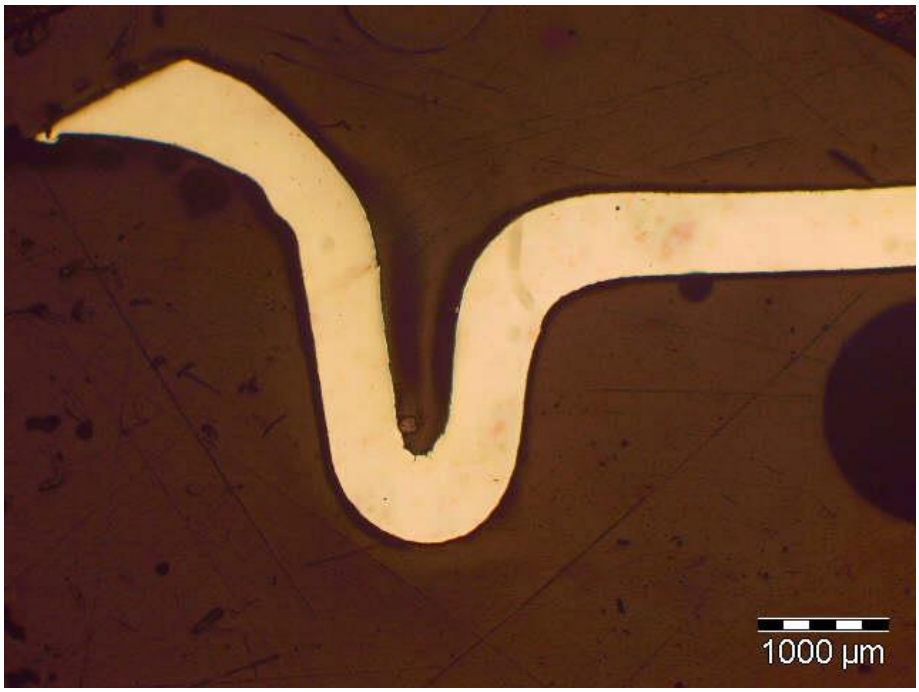

Figure 1 - Metallographic section: reference E1 (23x)

Figure 2 - Metallographic section: reference E1 (23x)

Figure 3 - Metallographic section: reference E1 (75x)

Figure 4 - Metallographic section: reference E1 (75x)

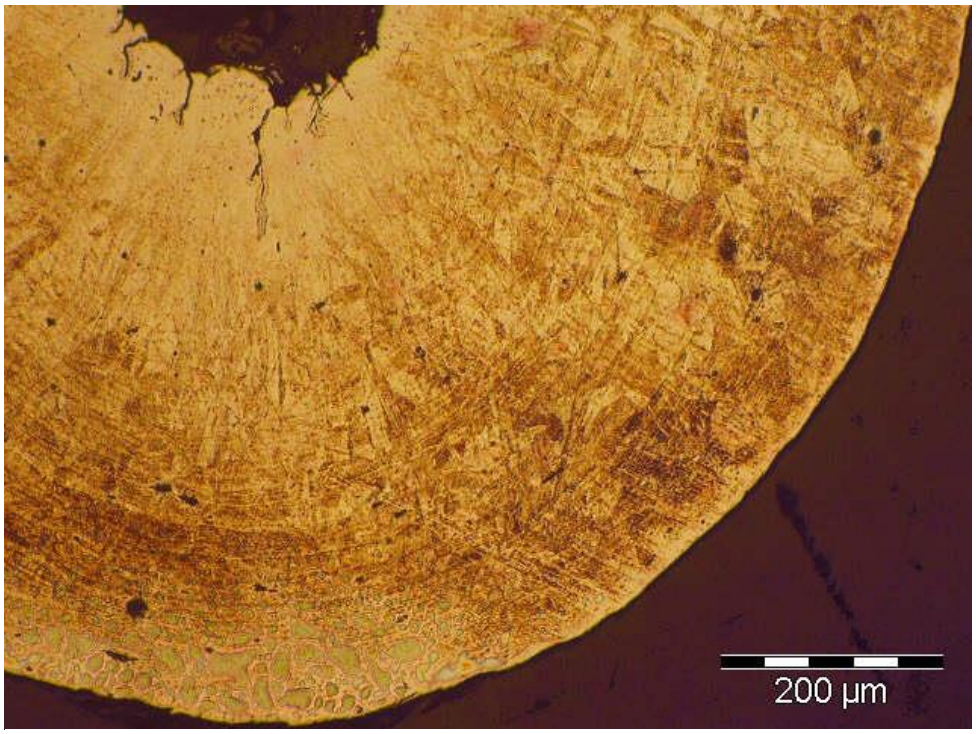

Figure 5 - Metallographic section: reference E1 (150x)

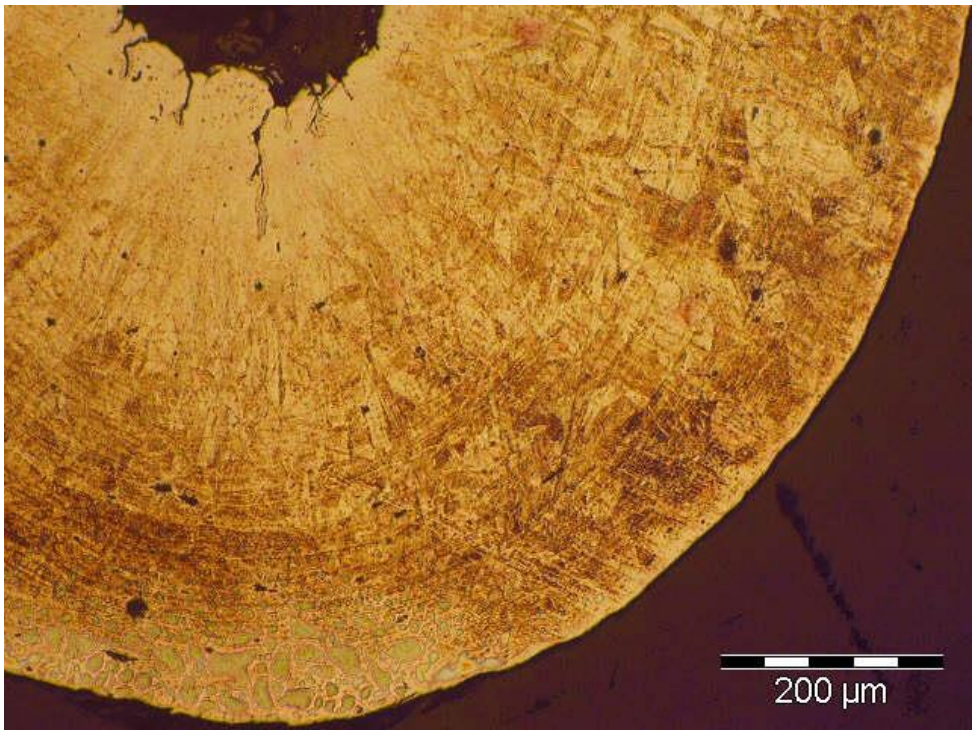

Figure 6 - Metallographic section: reference E1 (150x)

ANEXO C 1.1: Technical Drawing of the Forming Tools – Reference E3

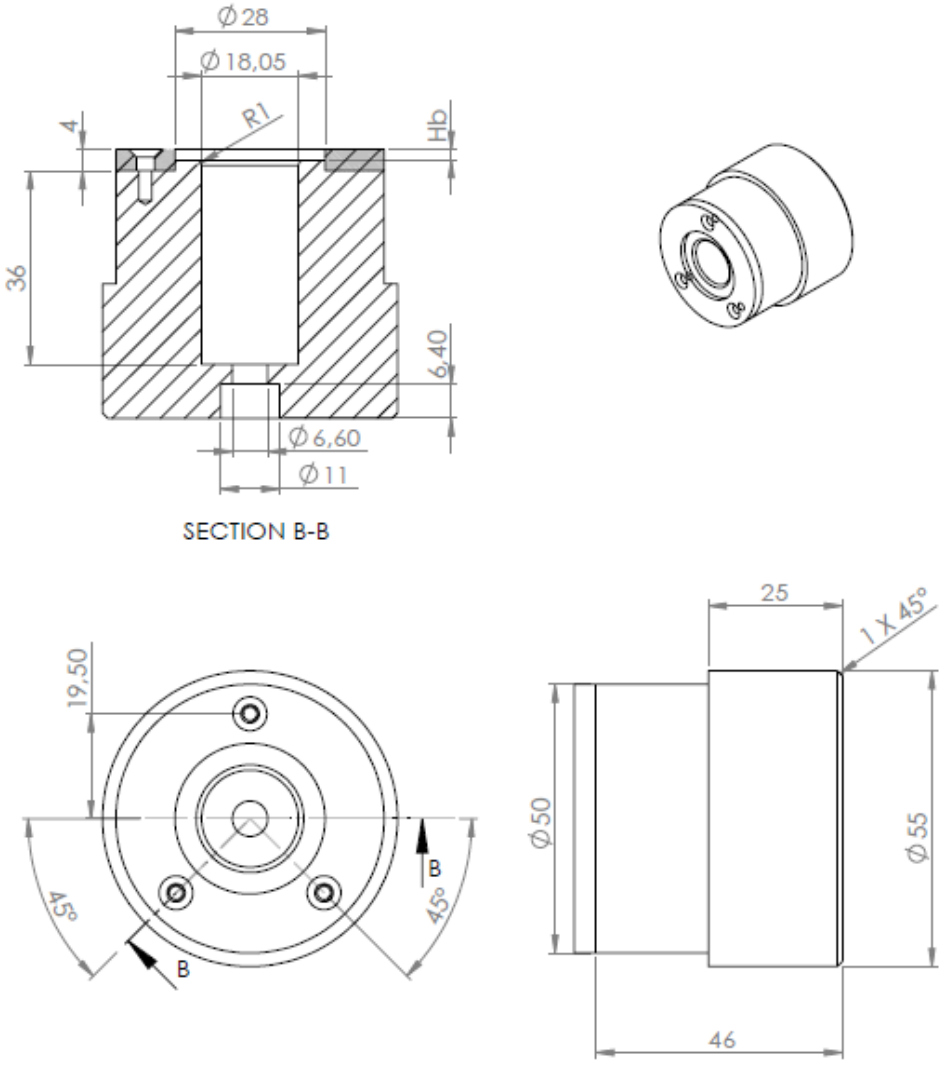

Figure 1 – Technical drawing of the forming die

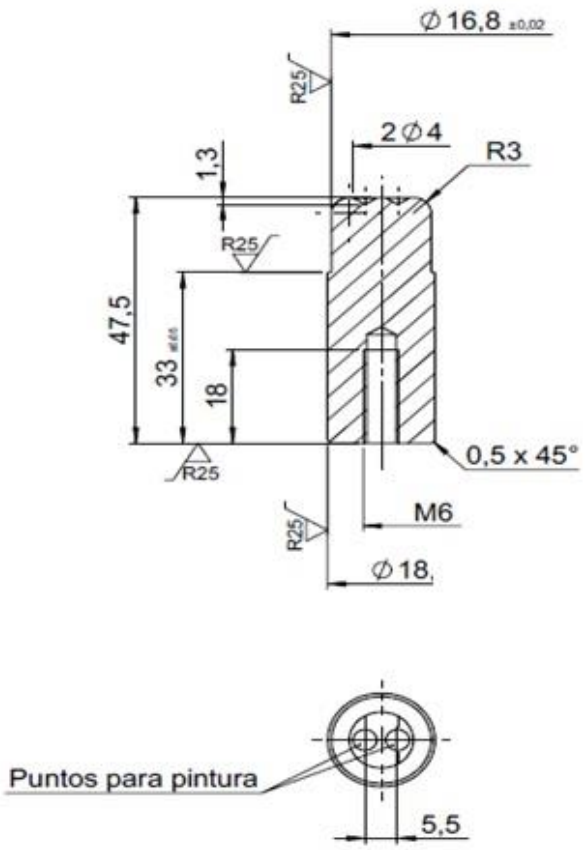

Figure 2 – Technical drawing of the internal mandrel

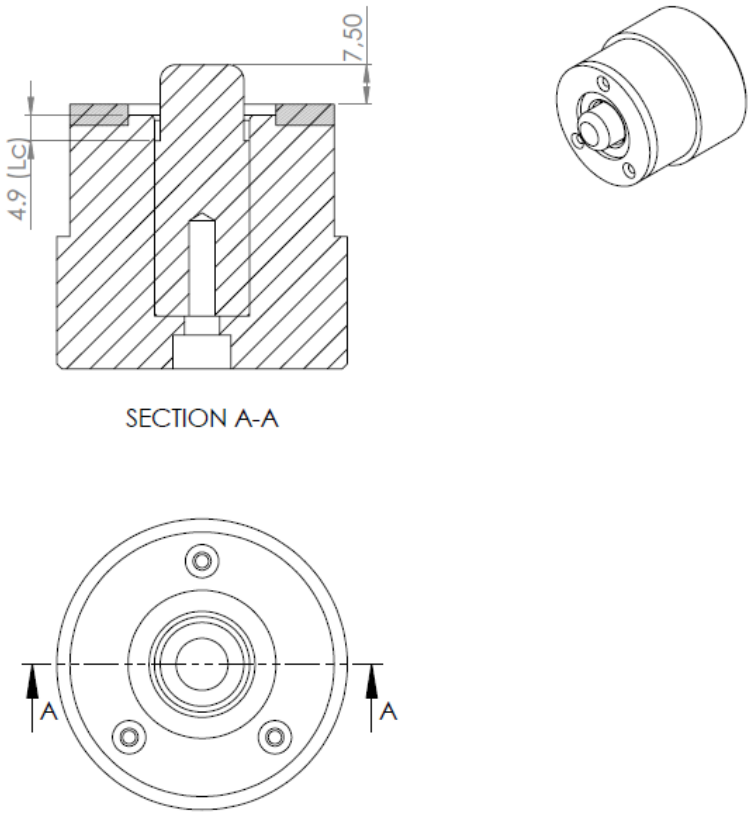

Figure 3 -Tool assembly

ANEXO D 1.1: Metallographic Sections – Case 2

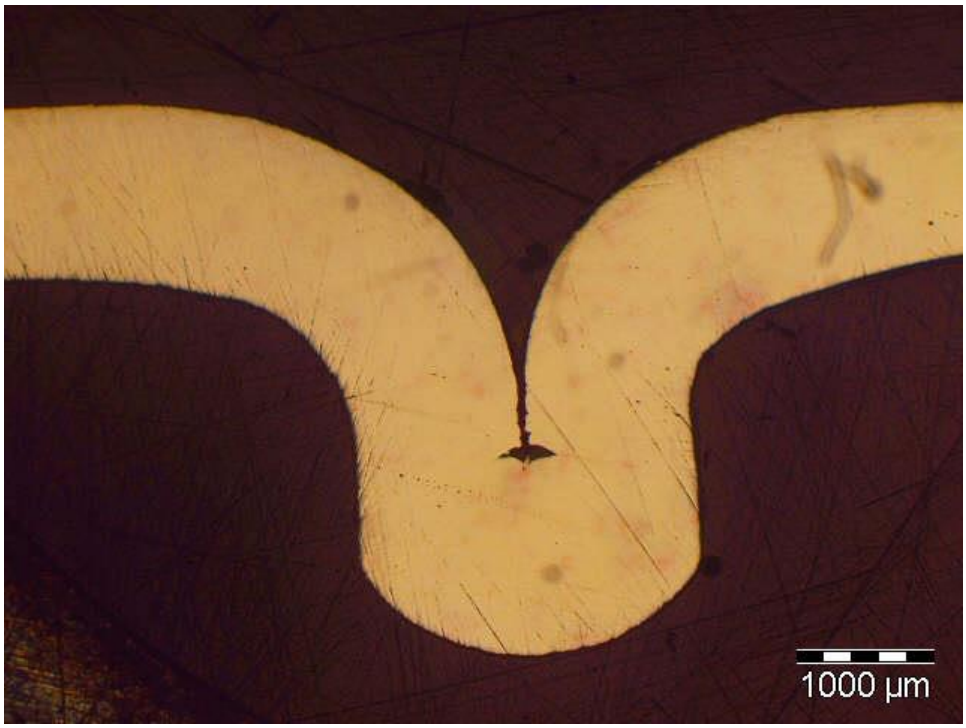

Figure 1 - Metallographic section: Case 2 (23x)

Figure 2 - Metallographic section: Case 2 (23x)

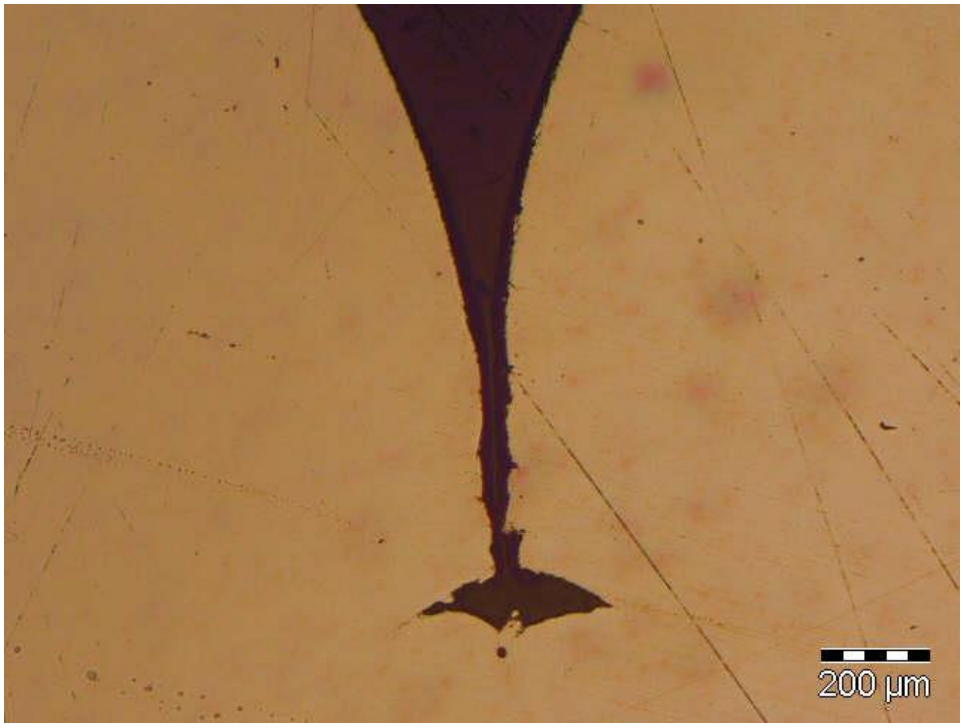

Figure 3 - Metallographic section: Case 2 (150x)

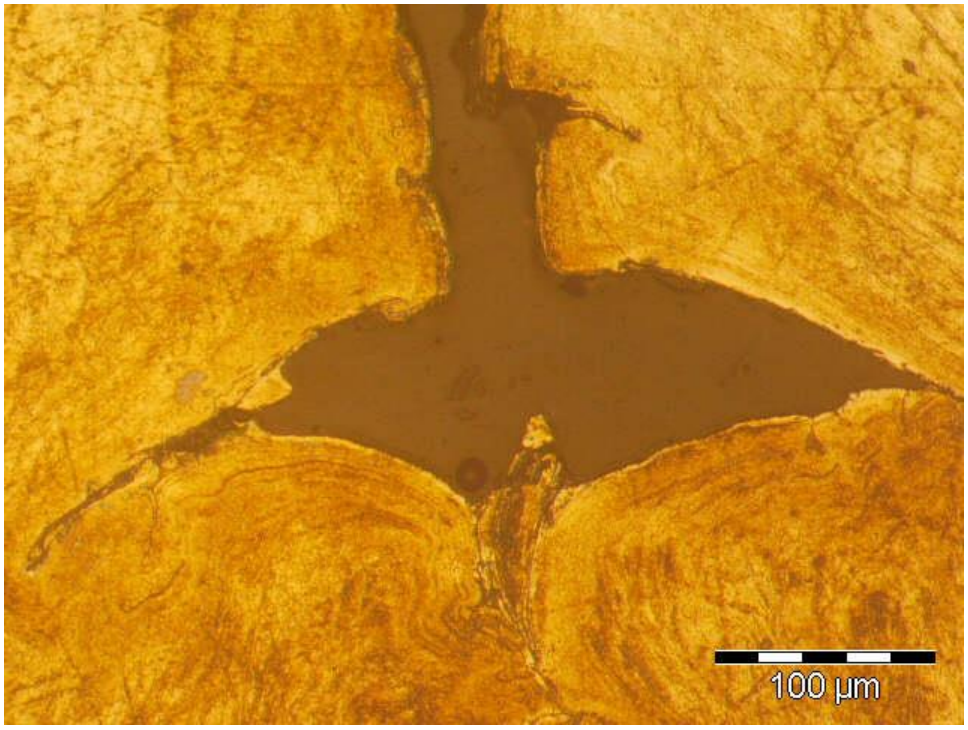

Figure 4 - Metallographic section: Case 2 (150x)

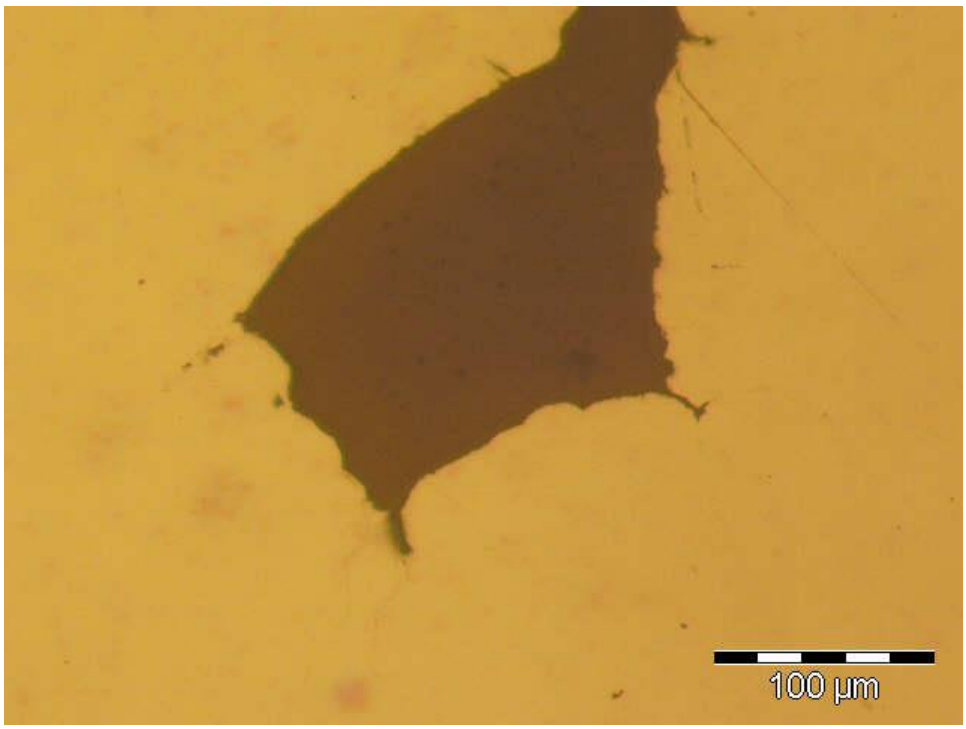

Figure 5 - Metallographic section: Case 2 (150x)

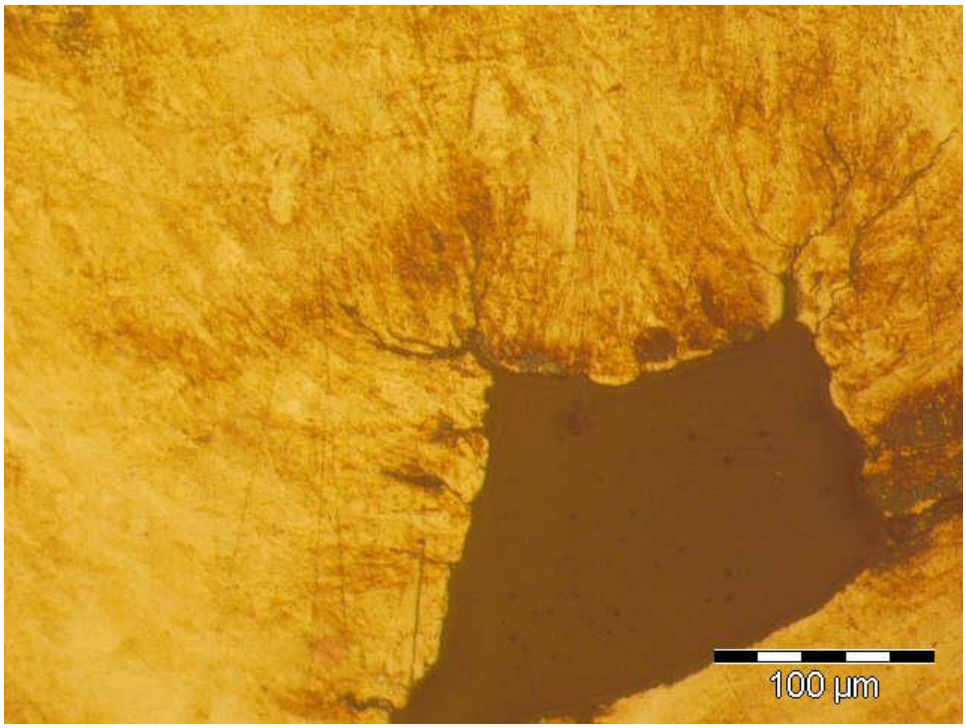

Figure 6 - Metallographic section: Case 2 (150x)

ANEXO D 1.2: Metallographic Sections – Case 5

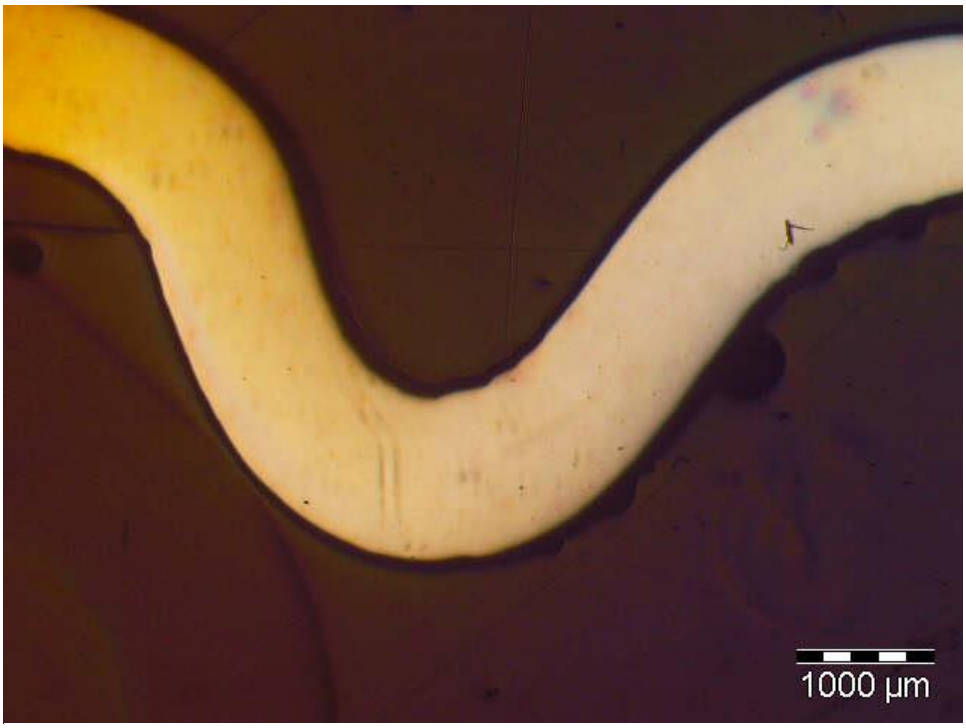

Figure 1 - Metallographic section: Case 5 (23x)

Figure 2 - Metallographic section: Case 5 (23x)

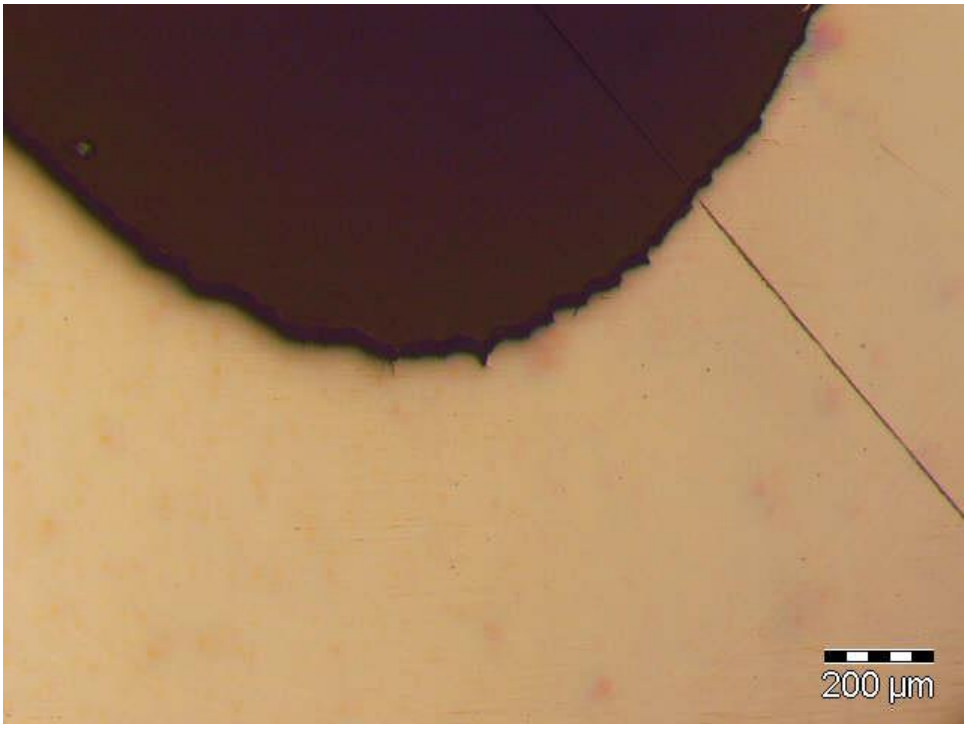

Figure 3 - Metallographic section: Case 5 (75x)

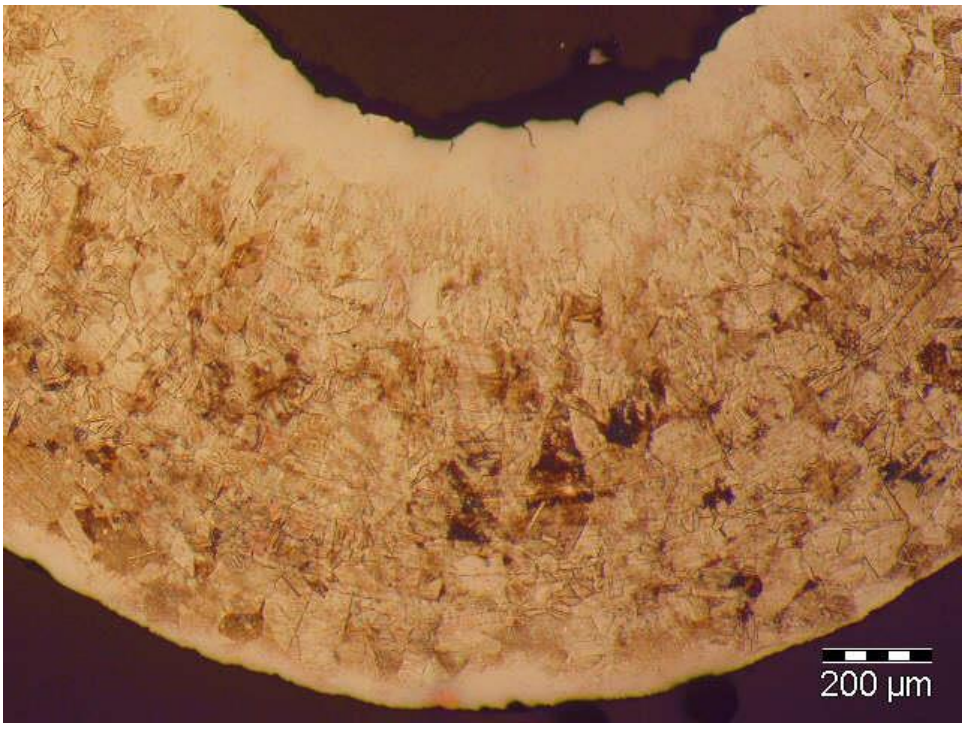

Figure 4 - Metallographic section: Case 5 (75x)

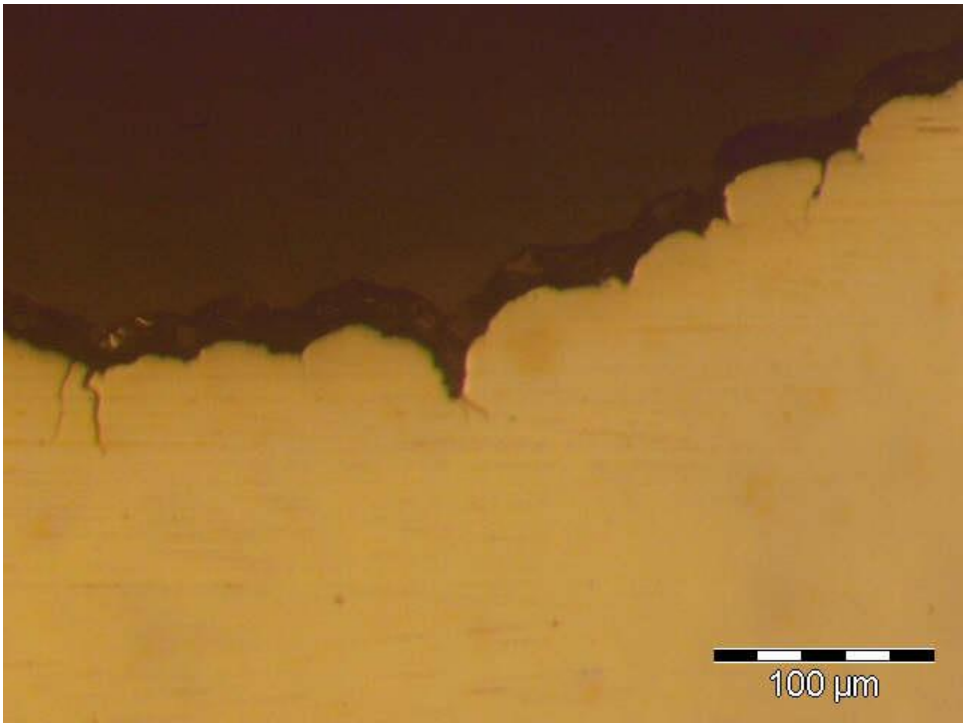

Figure 5 - Metallographic section: Case 5 (300x)

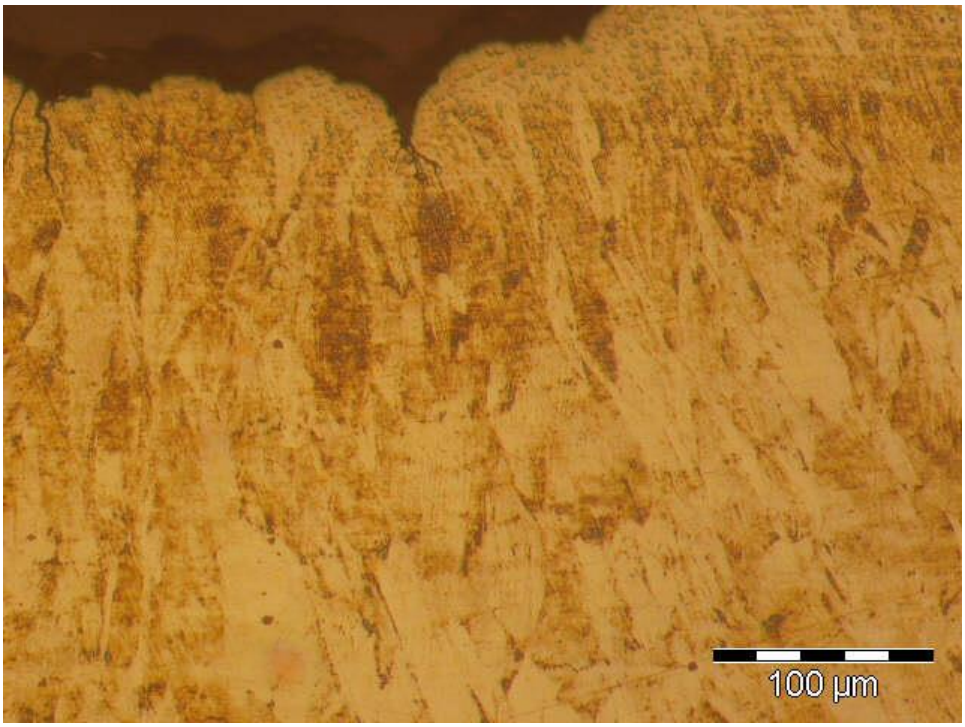

Figure 6 - Metallographic section: Case 5 (300x)

ANEXO D 1.3: Metallographic Sections – Case 7

Figure 1 - Metallographic section: Case 7 (23x).

Figure 2 - Metallographic section: Case 7 (23x9.

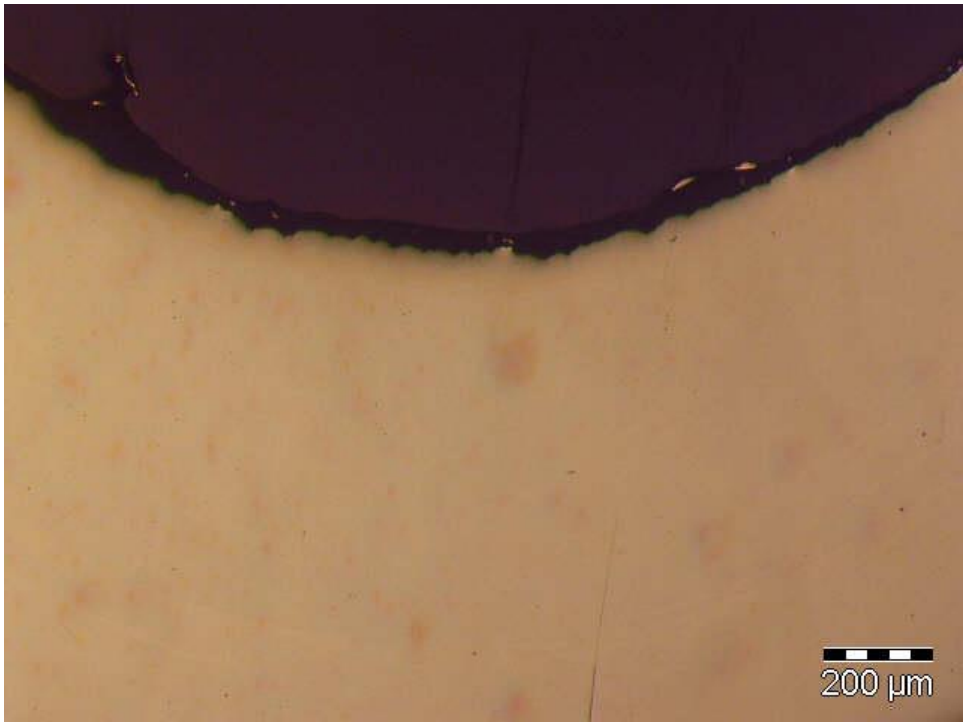

Figure 3 - Metallographic section: Case 7 (75x).

Figure 4 - Metallographic section: Case 7 (75x).

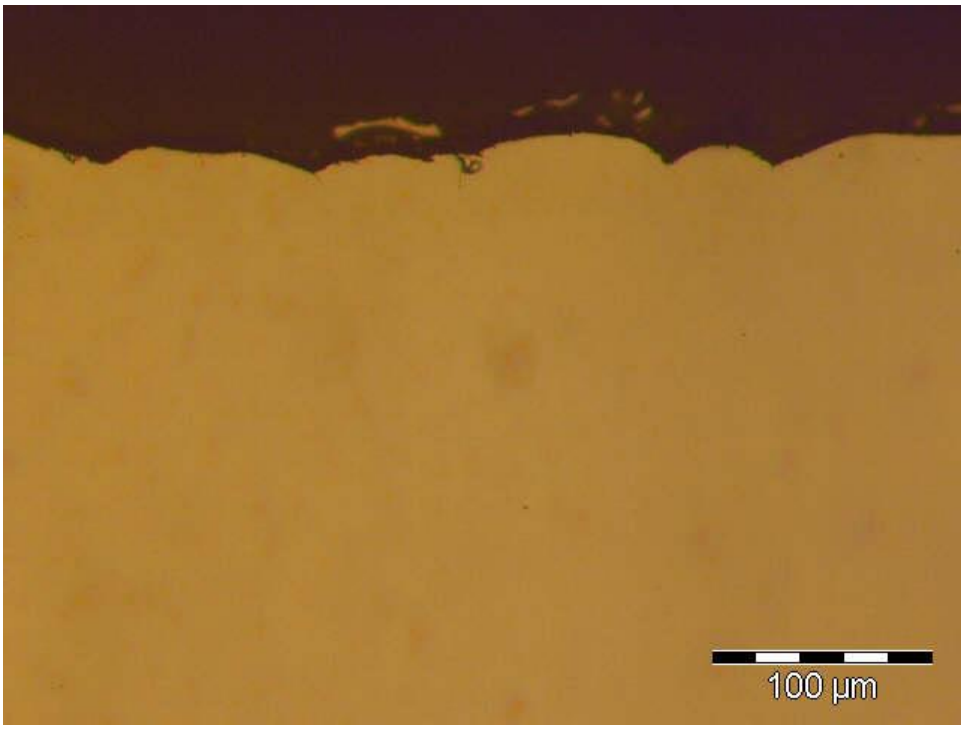

Figure 5 - Metallographic section: Case 7 (300x).

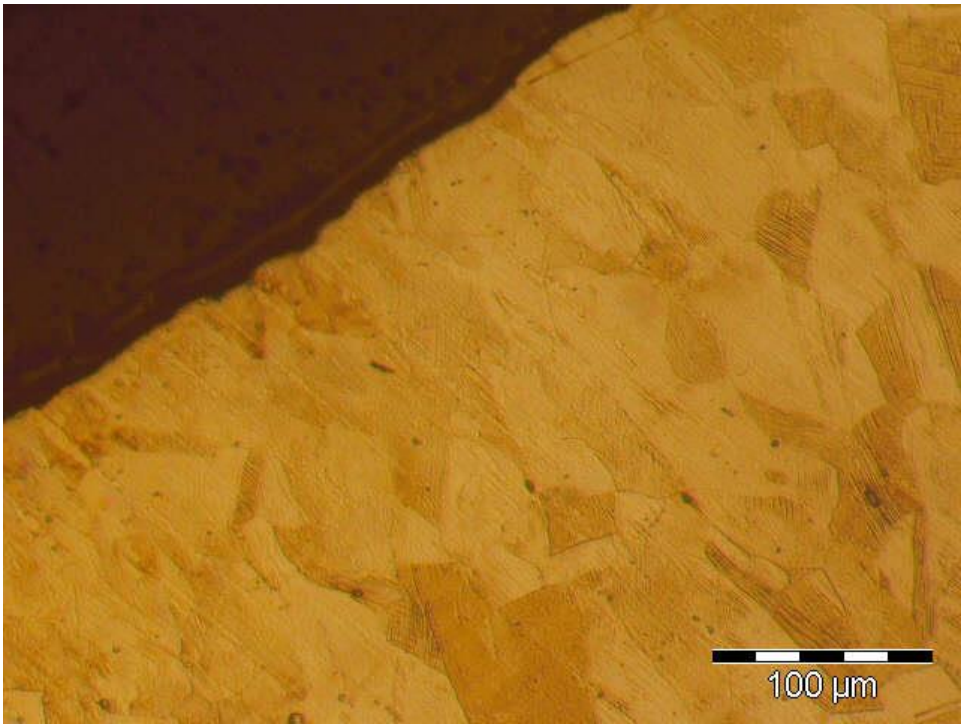

Figure 6 - Metallographic section: Case 7 (300x).

ANEXO D 1.4: Metallographic Sections – Case 8

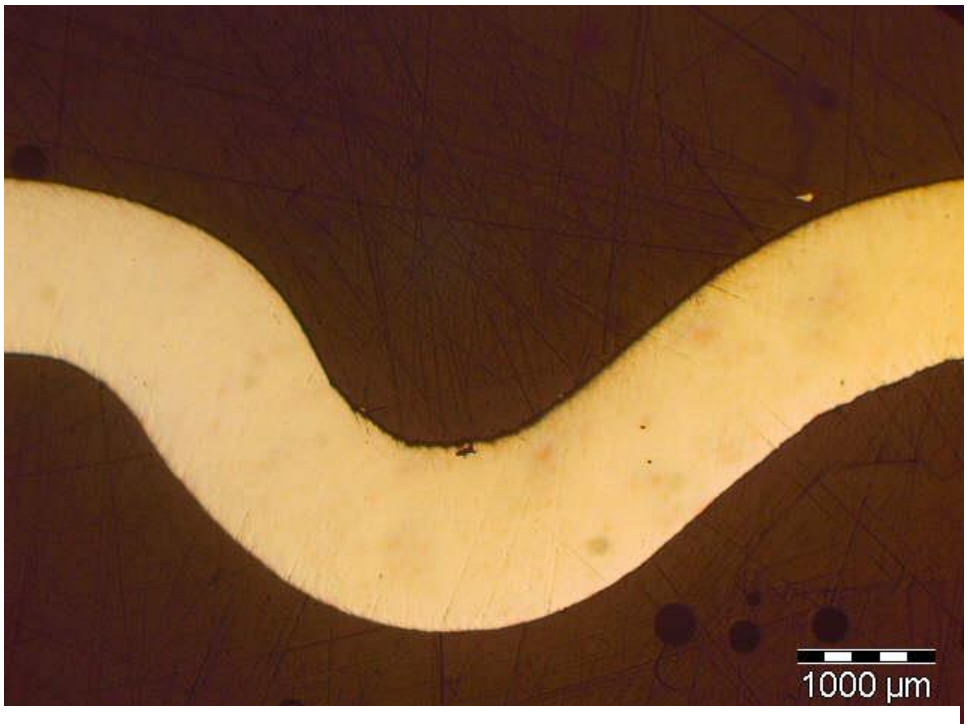

Figure 1 - Metallographic section: Case 8 (23x).

Figure 2 - Metallographic section: Case 8 (23x).

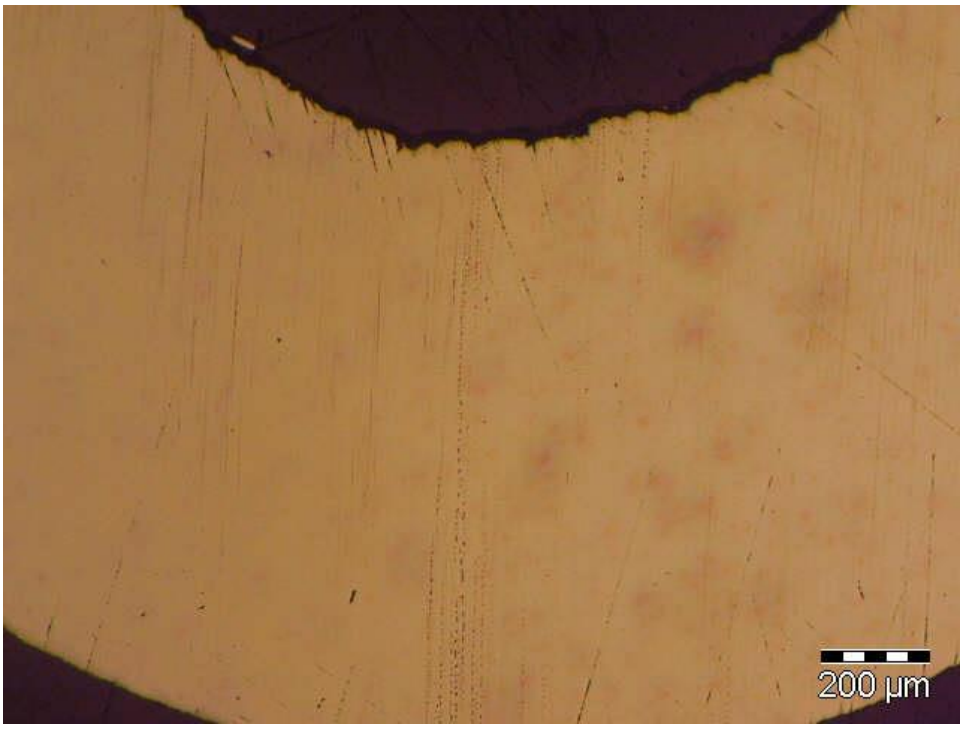

Figure 3 - Metallographic section: Case 8 (75x).

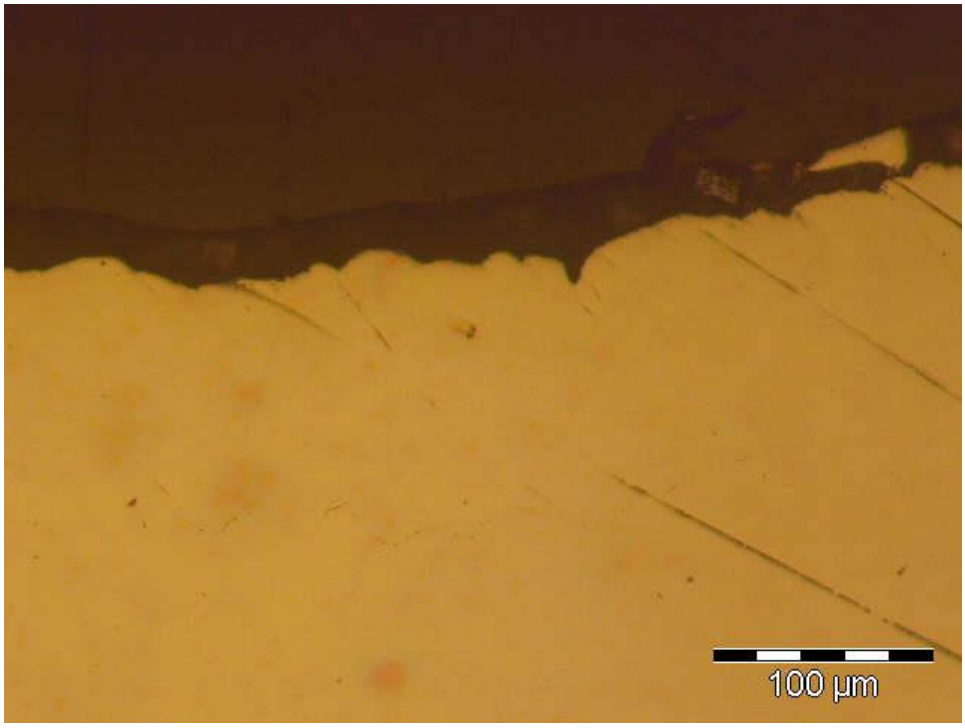

Figure 4 - Metallographic section: Case 8 (300x).

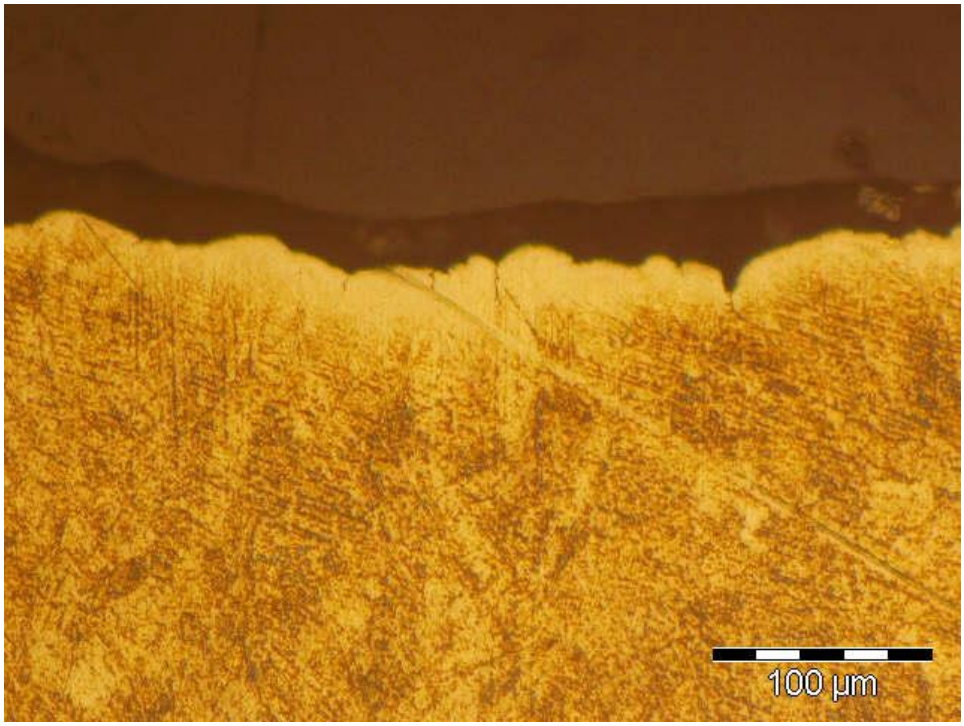

Figure 5 - Metallographic section: Case 8 (300x).

ANEXO D 2.1: Metallographic Sections – Case 11

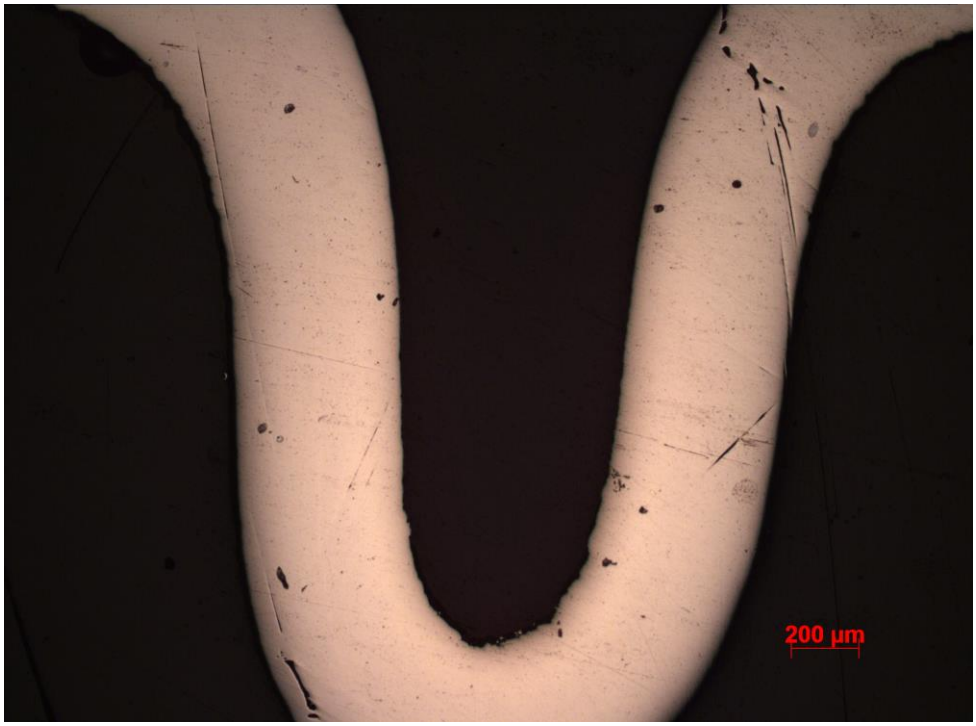

Figure 1 - Metallographic section: Case 11 (23x)

Figure 2 - Metallographic section: Case 11 (23x)

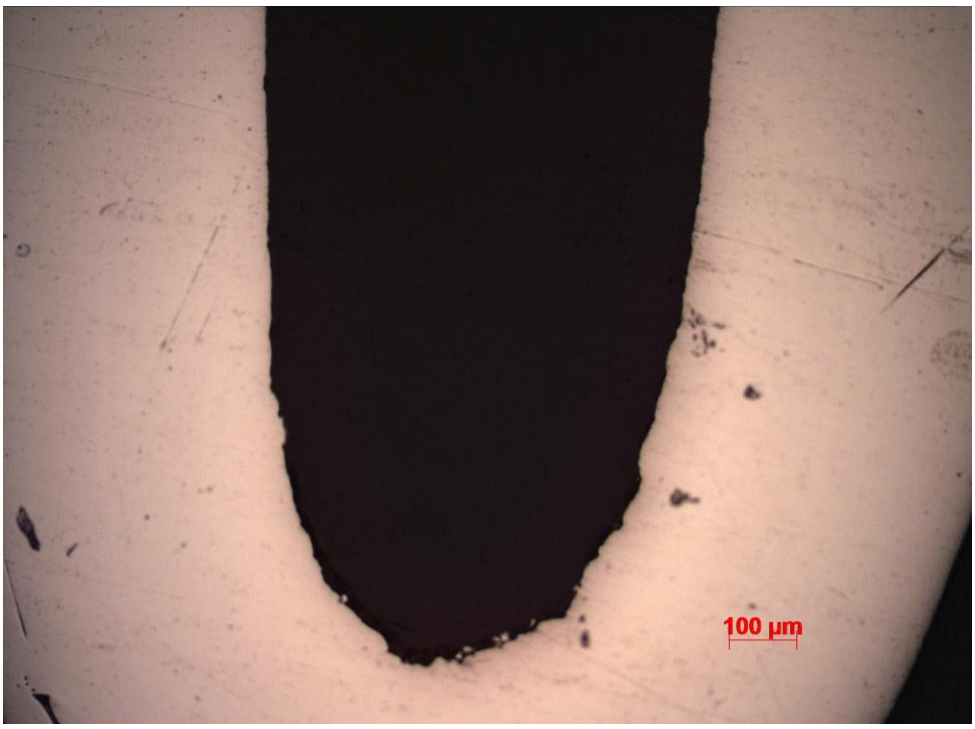

Figure 3 - Metallographic section: Case 11 (75x)

Figure 4 - Metallographic section: Case 11 (75x)

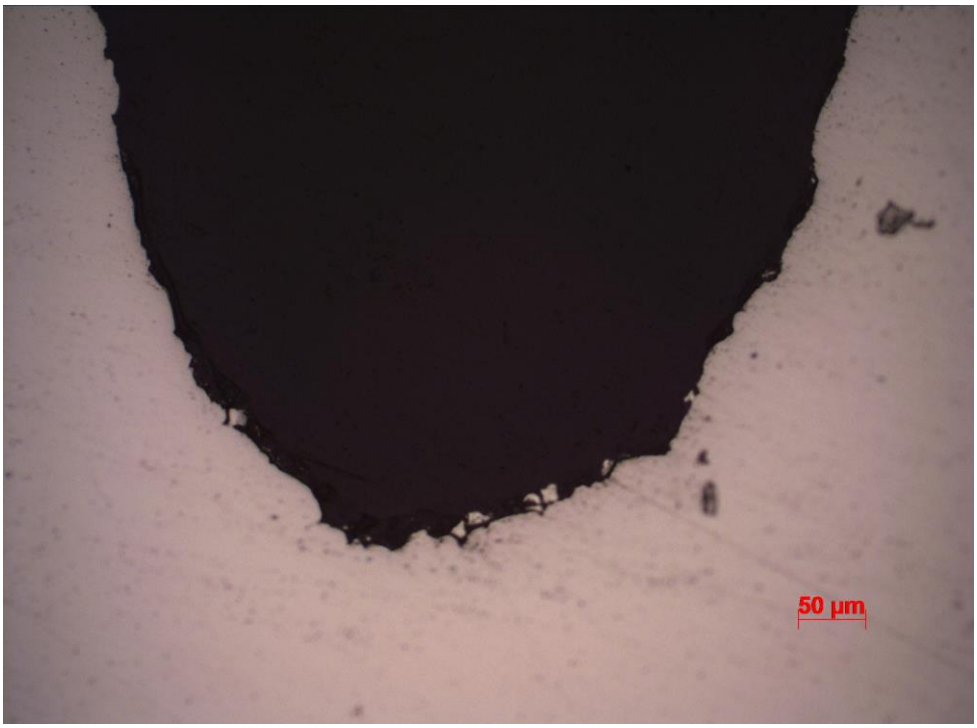

Figure 5 - Metallographic section: Case 11 (150x).

Figure 6 - Metallographic section: Case 11 (150x)

ANEXO D 2.2: Metallographic Sections – Case 13

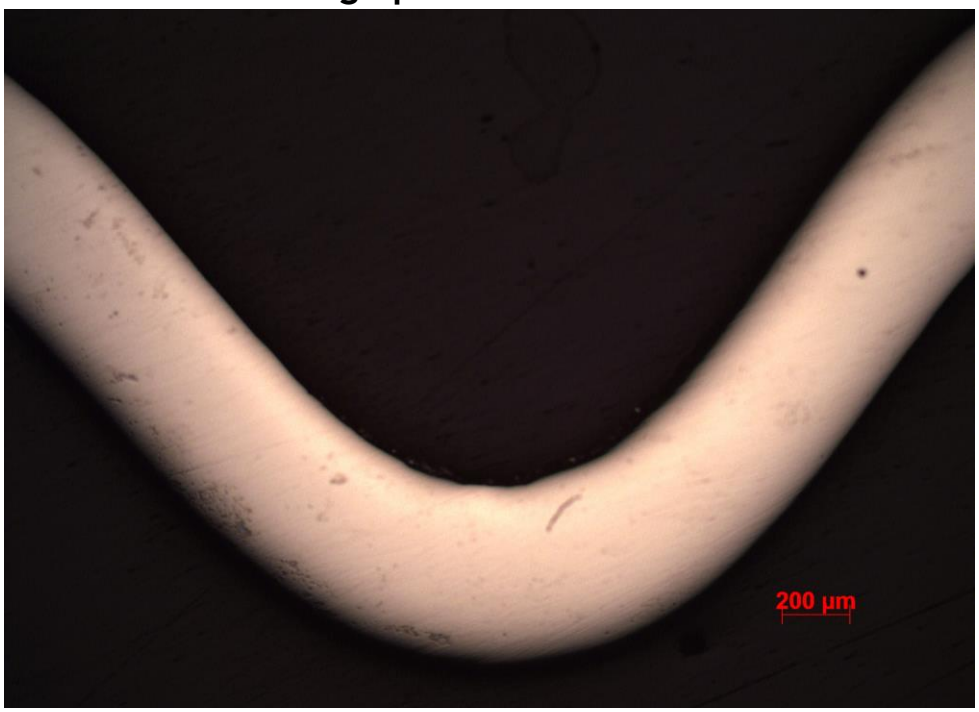

Figure 1 - Metallographic section: Case 13 (23x)

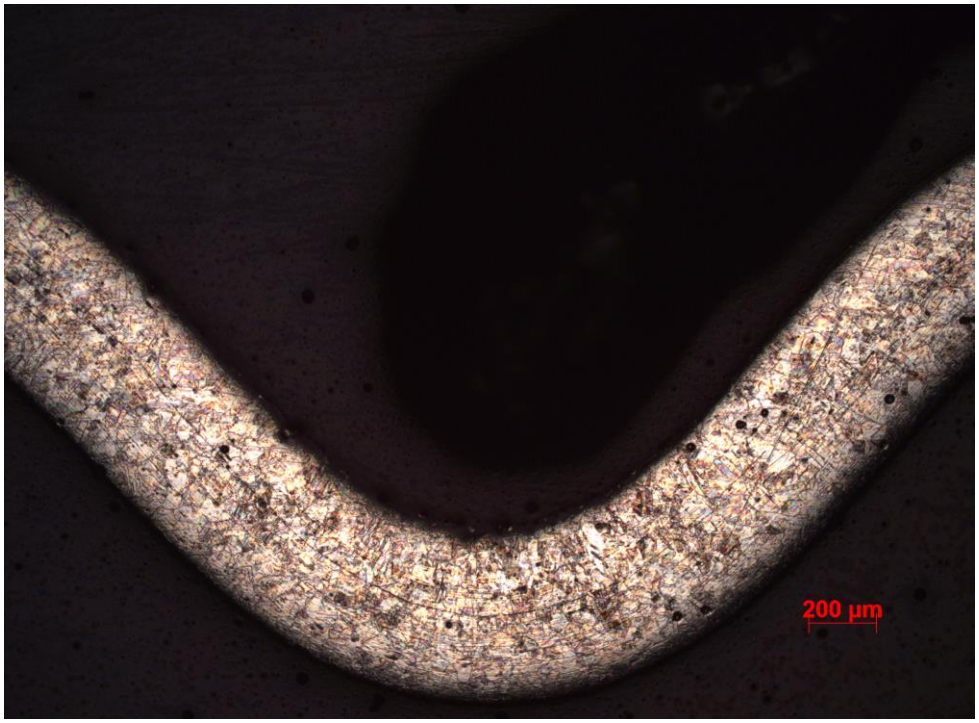

Figure 2 - Metallographic section: Case 13 (23x)

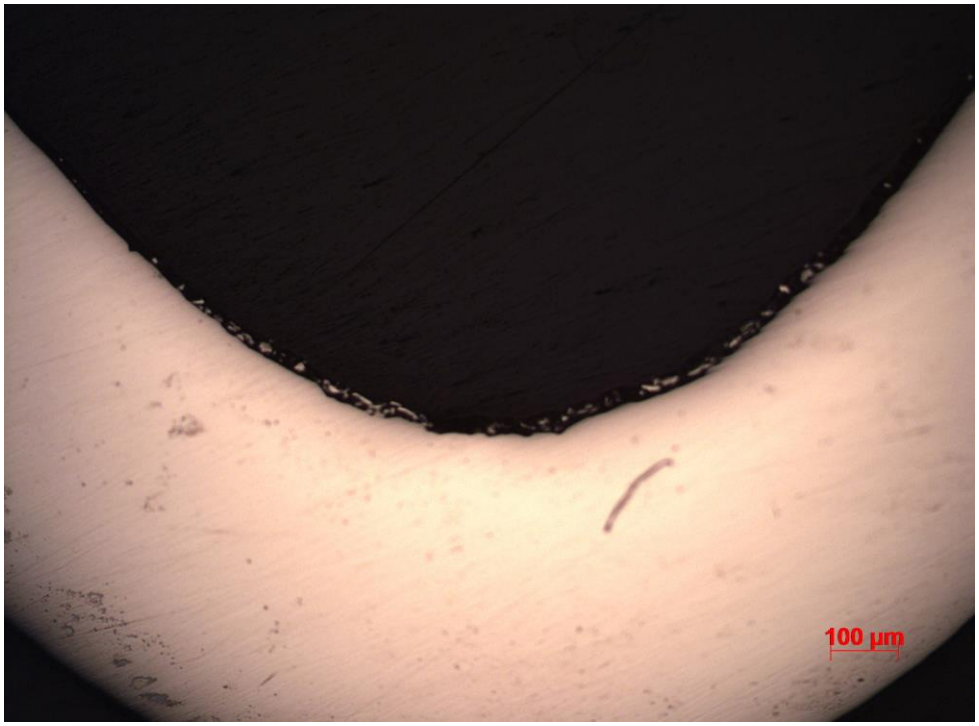

Figure 3 - Metallographic section: Case 13 (75x)

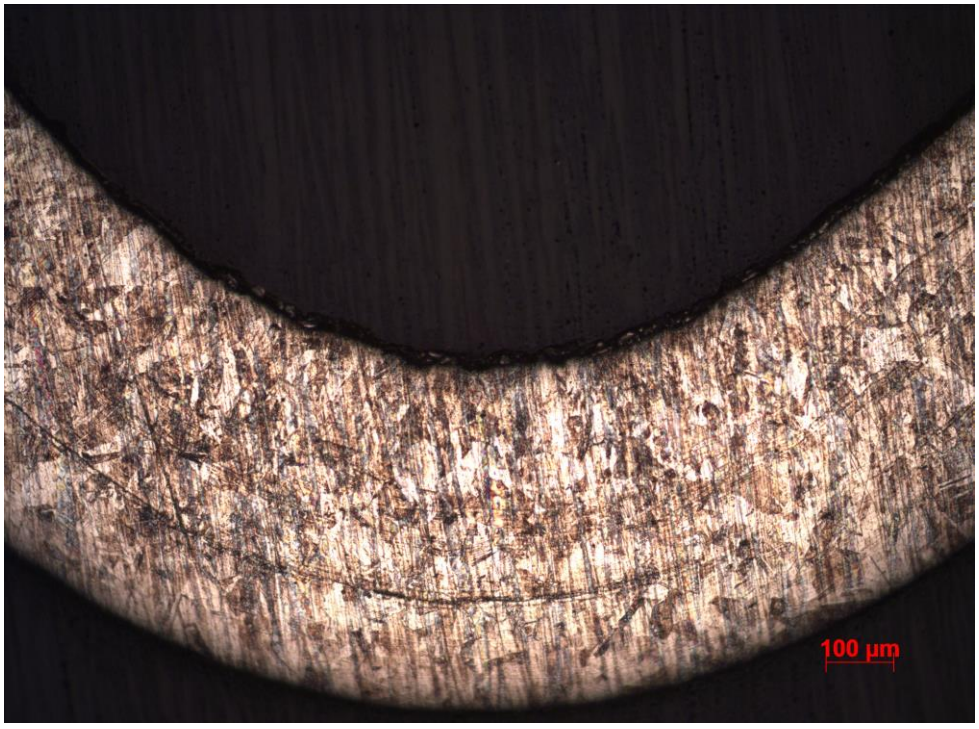

Figure 4 - Metallographic section: Case 13 (75x)

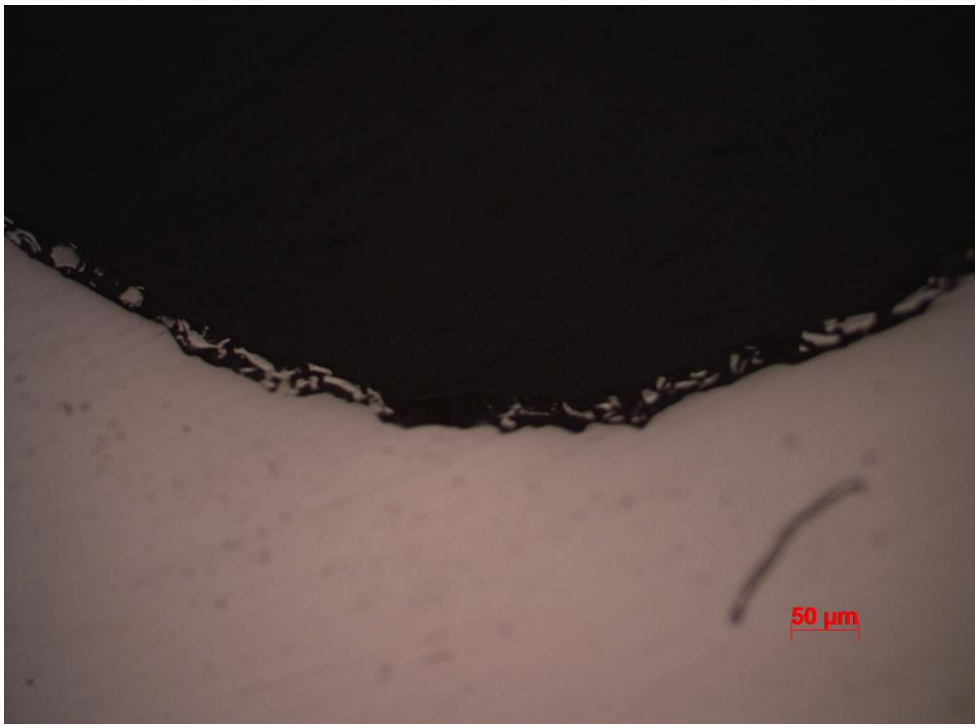

Figure 5 - Metallographic section: Case 13 (150x)

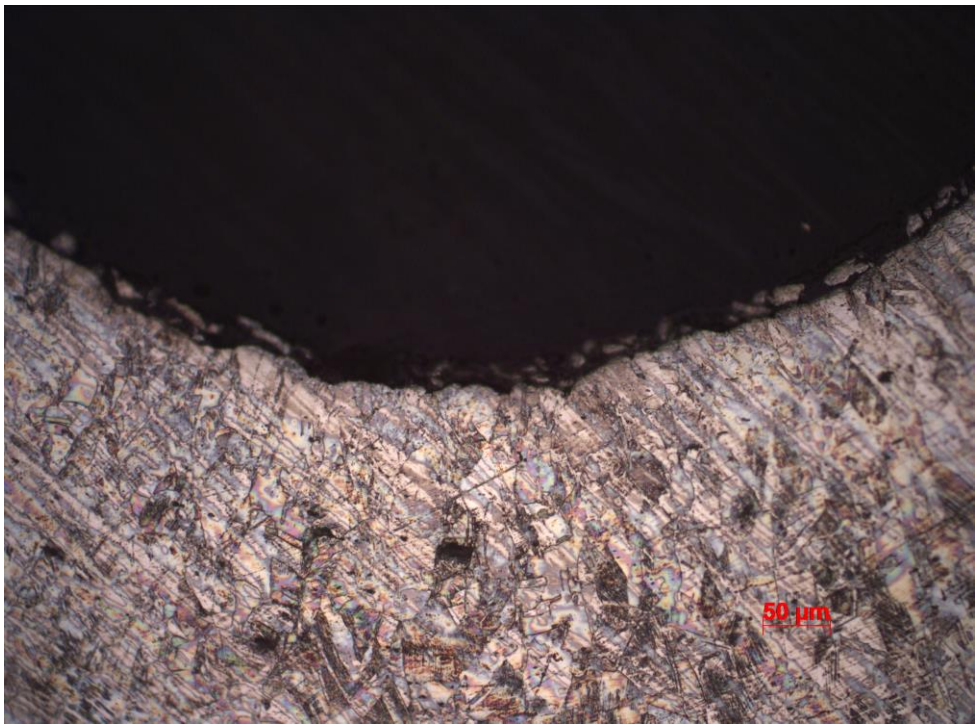

Figure 6 - Metallographic section: Case 13 (150x)

ANEXO D 2.3: Metallographic Sections – Case 16

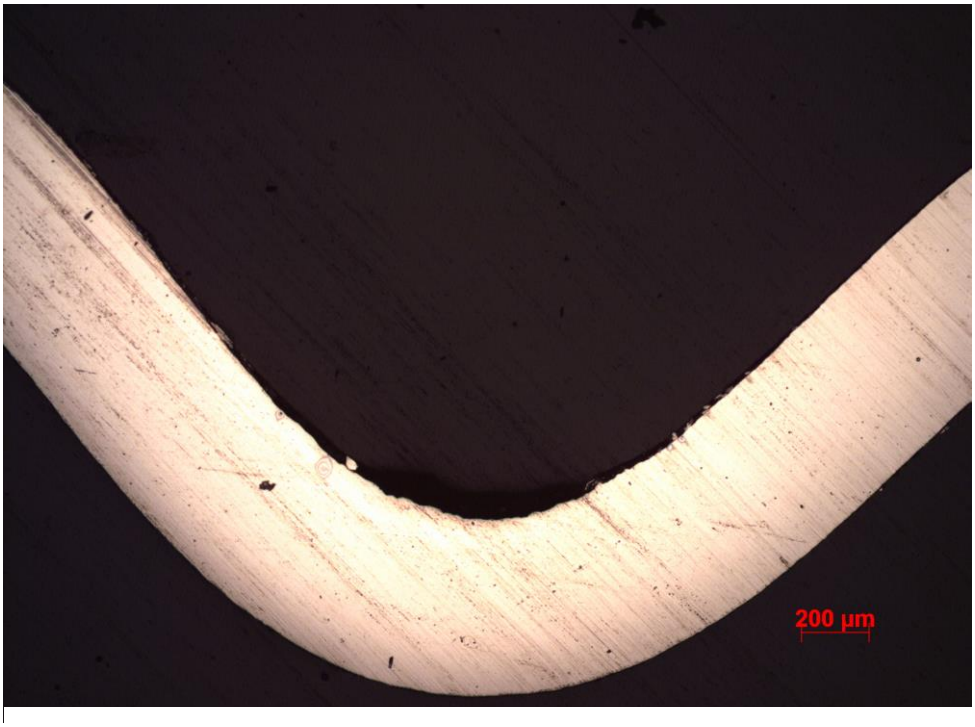

Figure 1 - Metallographic section: Case 16 (23x)

Figure 2 - Metallographic section: Case 16 (23x)

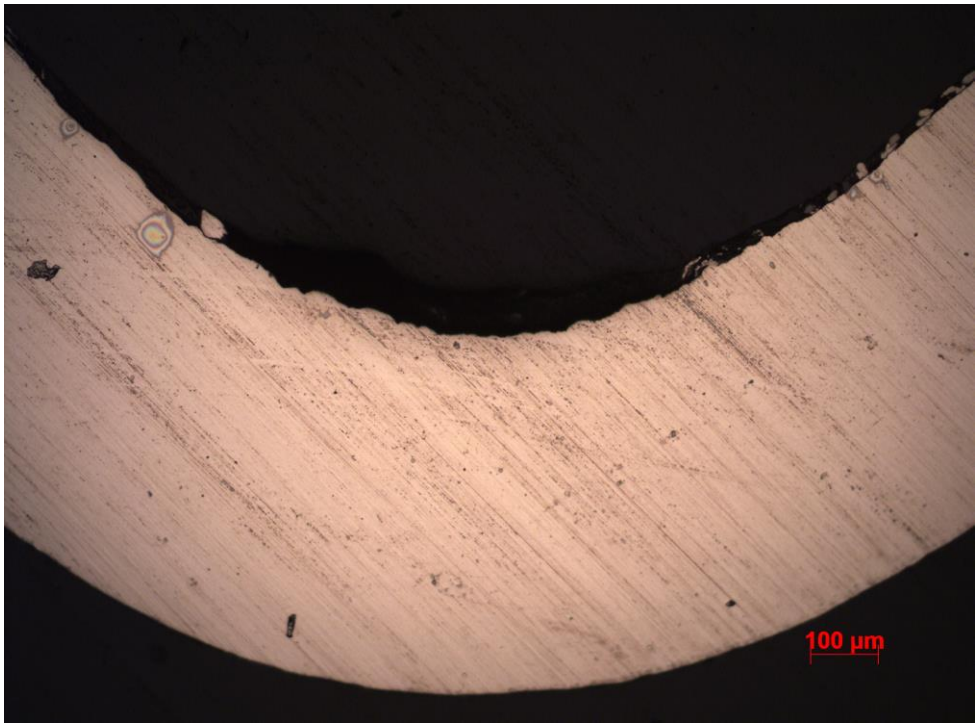

Figure 2 - Metallographic section: Case 16 (75x)

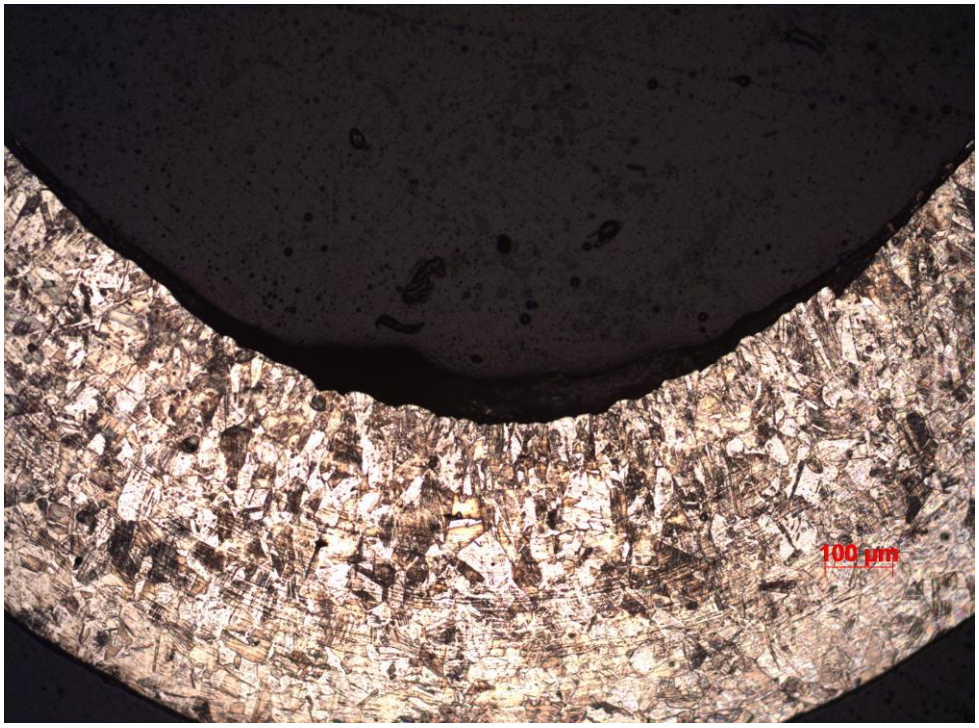

Figure 3 - Metallographic section: Case 16 (75x)

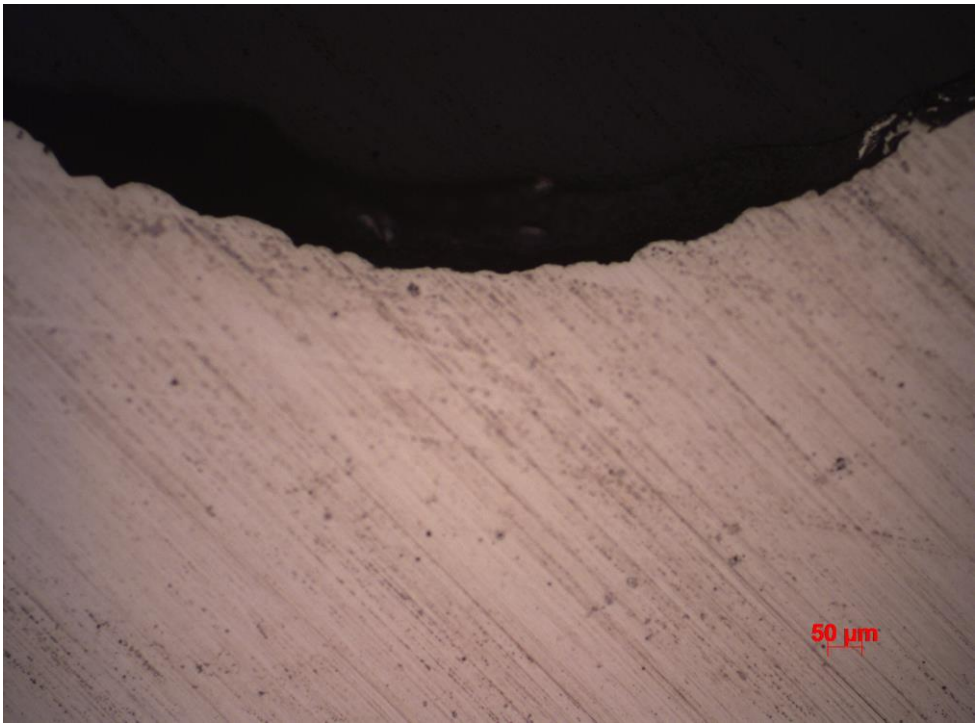

Figure 5 - Metallographic section: Case 16 (150x)

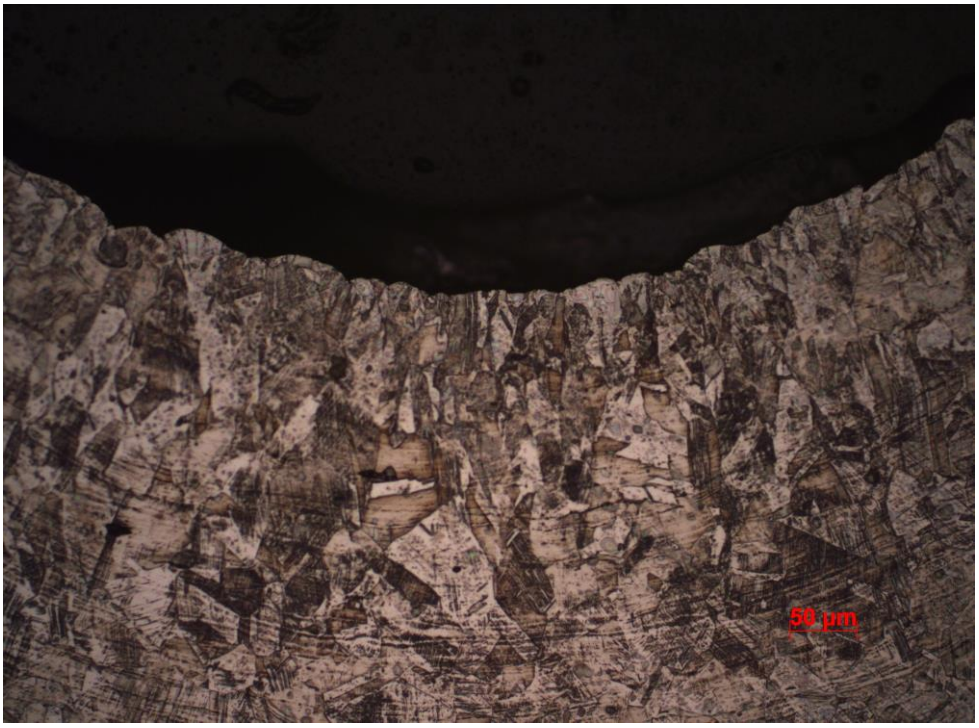

Figure 6 - Metallographic section: Case 16 (150x)

ANEXO D 2.4: Metallographic Sections – Case 17

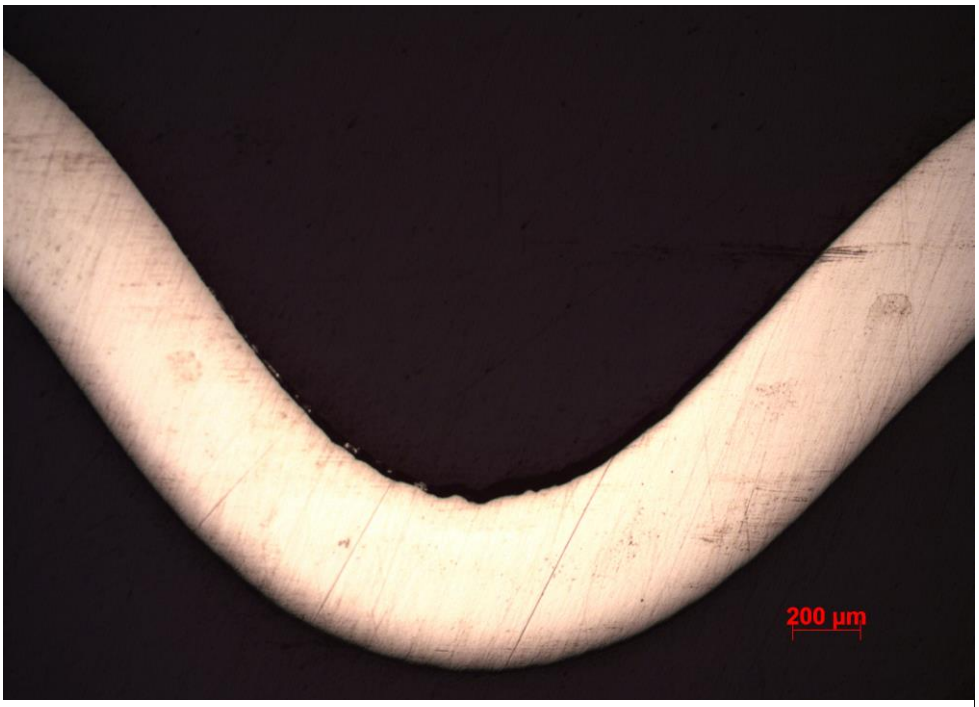

Figure 1 - Metallographic section: Case 17 (23x).

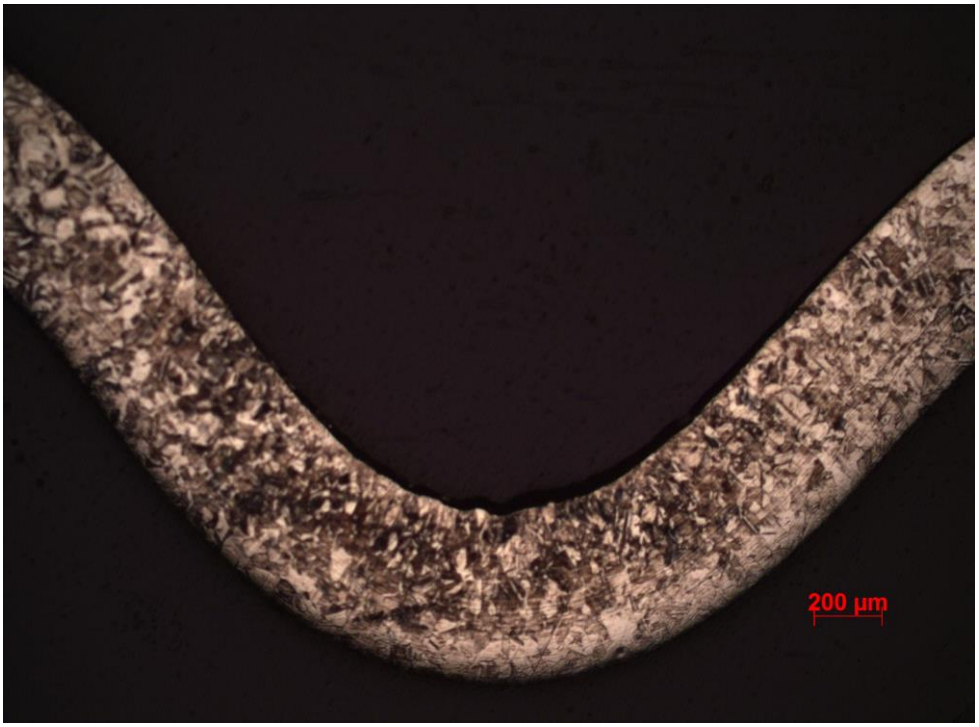

Figure 2 - Metallographic section: Case 17 (23x).

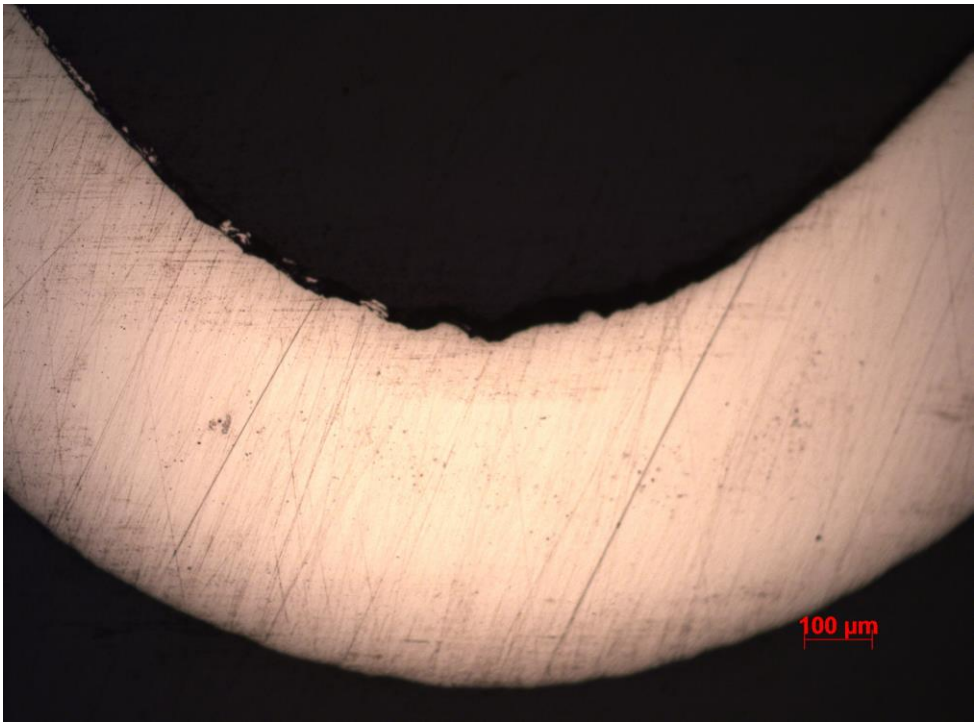

Figure 3 - Metallographic section: Case 17 (75x).

Figure 4 - Metallographic section: Case 17 (75x).

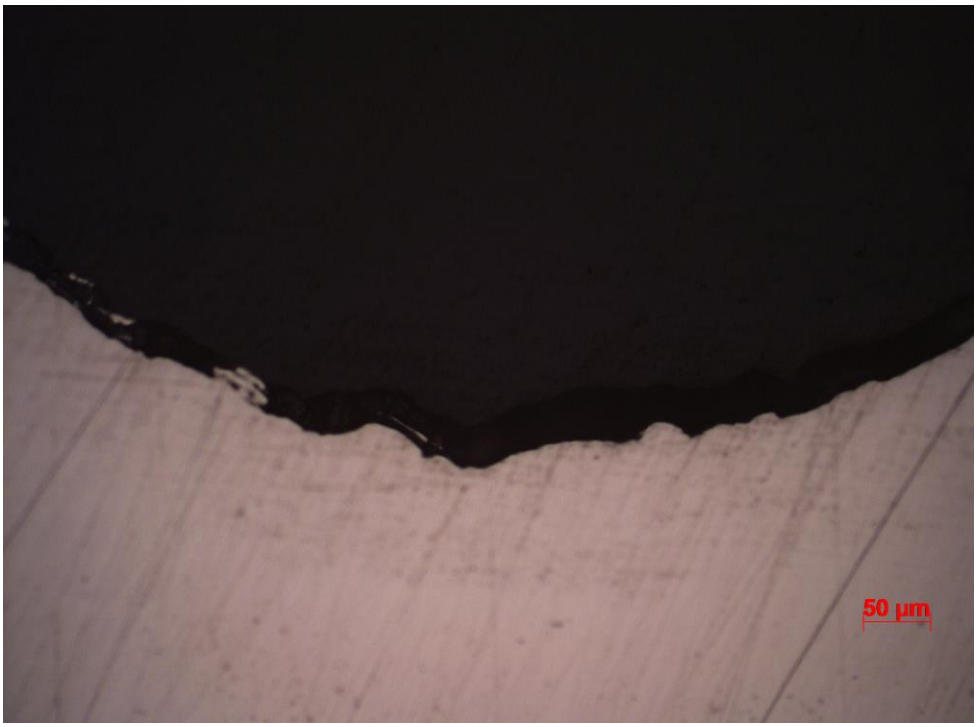

Figure 5 - Metallographic section: Case 17 (150x).

Figure 6 - Metallographic section: Case 17 (150x).

ANEXO E 1: Metallographic Sections – Reference E4

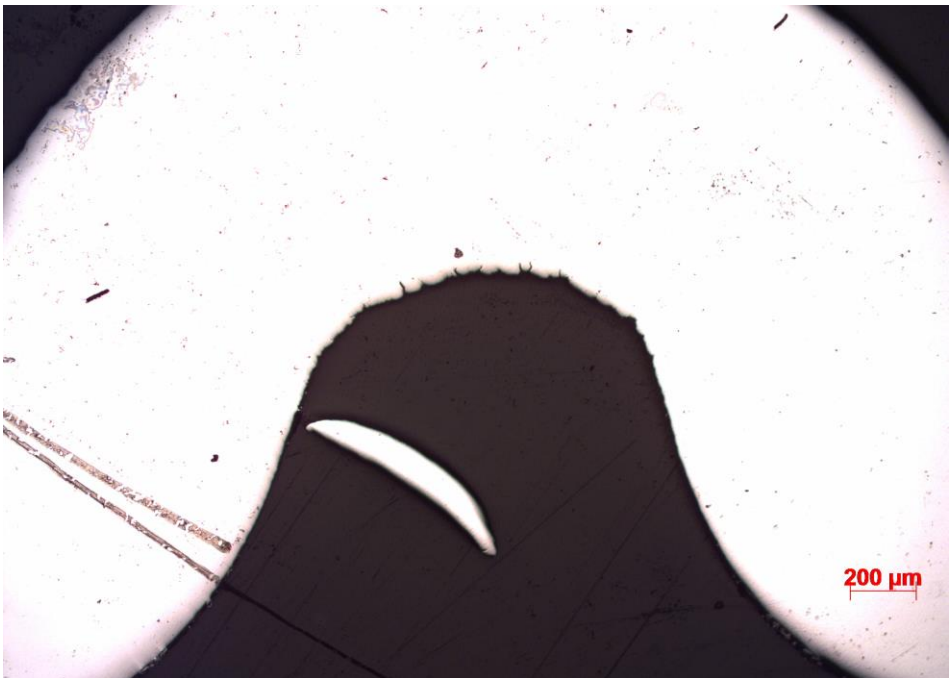

Figure 6 – Metallography reference E4 (23x)

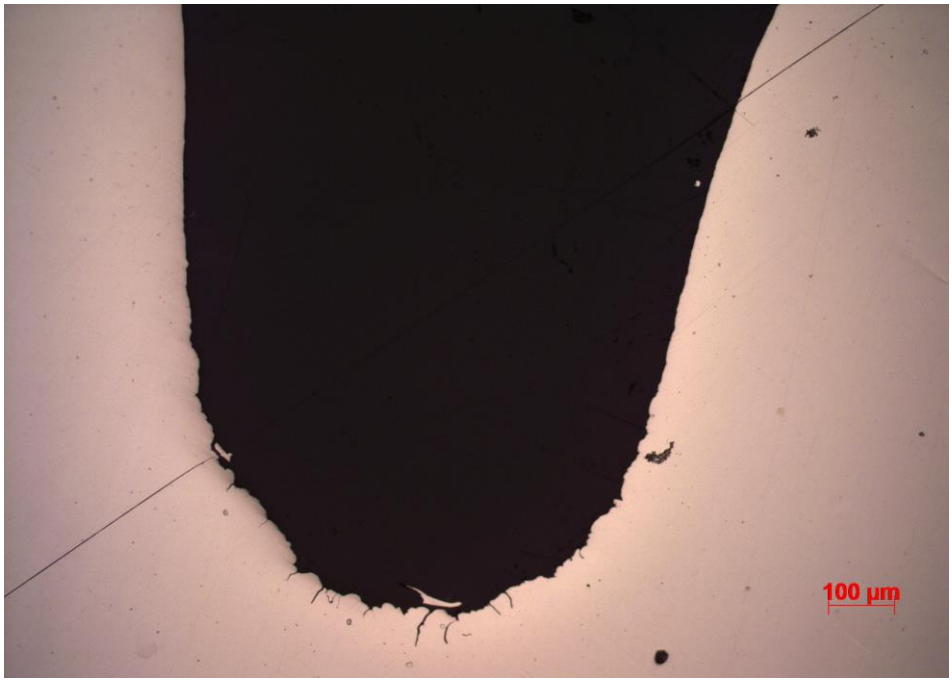

Figure 6 – Metallography reference E4 (75x)

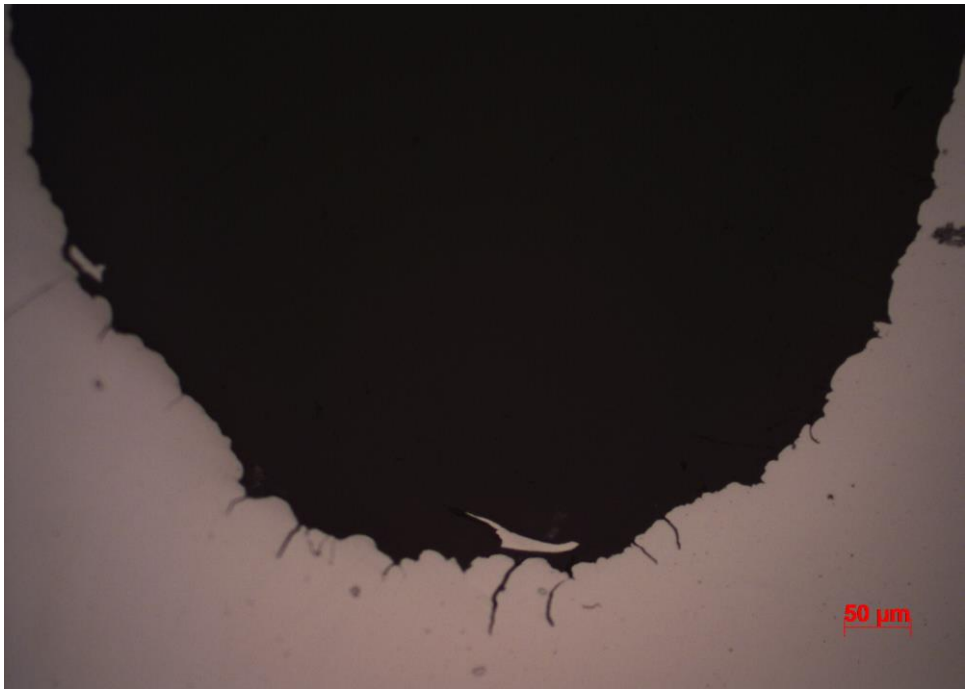

Figure 6 – Metallography reference E4 (150x)